Distributed Control of a Nanogrid Using DC Bus Signalling

John Karl Schönberger

A thesis presented for the degree of
Doctor of Philosophy
in
Electrical and Electronic Engineering
at the
University of Canterbury,
Christchurch, New Zealand.

May 2005

ABSTRACT

A nanogrid is a standalone hybrid renewable system that uses distributed renewable and non-renewable sources to supply power to local loads. The system is based on power electronics, with interface converters allowing the sources to supply power to the system and the loads to draw power from the system. The nanogrid is typically designed such that renewable sources supply the average load demand, while storage and non-renewable generation are used to ensure that the loads enjoy a continuous supply of power in the presence of the stochastic renewable sources.

To maintain the power balance in the system while maximising use of the renewable sources, all sources in the system are scheduled according to a supply-side control law. The renewable sources are used wherever possible and the storage is operated as a slack power bus. The storage is controlled to absorb any excess power from the renewable sources and release it to the system when necessary. The non-renewable generation is only brought online when the storage and renewable sources are incapable of balancing the load demand.

While the primary method for maintaining the power balance in the nanogrid is scheduling the sources according to a supply-side control law, a demand-side control law may also be used to help maintain the power balance in the system or protect the system from a complete collapse under overload conditions. A demand-side control strategy is implemented by shedding loads when the load exceeds the available generation, beginning with those loads having the lowest utilisation priority.

Hybrid renewable systems are typically designed and controlled in a similar manner to the traditional ac power system, operating at 50/60 Hz, and maintaining the power balance in the system using frequency droop for power sharing and central coordination for scheduling the sources. However a nanogrid has different components compared to the ac system, employing power electronic converters to interface the sources and loads to the system. The control flexibility afforded by the use of power electronic interface converters opens

the door to new transmission and control possibilities.

This thesis evaluates a number of transmission options ranging from dc to high frequency ac in order to determine an operating frequency that is suitable for this niche system. A number of control topologies are also investigated to find a low cost strategy for implementing a supply-side control law. DC is selected as the operating frequency of choice largely for its simpler source interface requirements. A novel control strategy, dc bus signalling (DBS), is proposed as a means of implementing a supply-side control law. Its distributed structure maintains the modularity inherent in the distributed structure of the nanogrid.

DBS uses the voltage level of the dc bus to convey system information. With a supply-side control law implemented using DBS, the source and storage interface converters operate autonomously based on the voltage level of the dc bus. The converters not only respond to the level of the dc bus, but they also change the level of the dc bus, automatically controlling other converters in the system. This thesis presents the theory of operation behind this control strategy and outlines a method for implementing a supply-side control law. A method for ensuring that the supply-side control law operates in a practical system where transmission line impedance affects the information conveyed by the dc bus is also given. For completeness, a method for implementing a demand-side control law using DBS is also presented.

A simulation model of a nanogrid is presented and results are obtained to demonstrate the operation of DBS. The design of a small experimental system is also presented, and results are obtained to verify the operation of this new control strategy in a practical system. The simulation and experimental results demonstrate the feasibility of implementing supply and demand-side control laws in a nanogrid using DBS, even in the presence of transmission line impedance.

ACKNOWLEDGEMENTS

I wish to take a moment to thank a number of people, without whom this work would not have been possible. Firstly, I would like to acknowledge my supervisor Richard Duke for the valuable guidance and input he has given me while undertaking this research work for the last three years. I also wish to acknowledge Simon Round for the input he provided during the first two years of this PhD research, and Alan Wood for the advice he provided while I was writing this thesis. A big thank you goes out to my family for their encouragement, and I would like to acknowledge the financial support I received from the Foundation for Research, Science, and Technology and the Todd Foundation. Without it, this research work would not have been possible. I extend my thanks to my colleagues in room 310 for their comments and discussions. Above all, I wish to give thanks to God for giving me the ability to do this work in the first place.

PUBLICATIONS ASSOCIATED WITH THIS THESIS

1. J. Bryan, R. Duke, and S. Round, Decentralised control of a nanogrid, *Australasian Universities Power Engineering Conference*, CD-ROM, September, 2003.

2. J. Bryan, R. Duke, and S. Round, Distributed generation - nanogrid transmission and control options, *International Power Engineering Conference*, 341-346, November, 2003.

3. J. Bryan, R. Duke, and S. Round, Decentralized generator scheduling in a nanogrid using DC bus signaling, *IEEE Power Engineering Society Summer Meeting*, 977 - 982, June, 2004.

4. J. Schönberger, R. Duke, and S. Round, Operation of a DC Nanogrid: Generator Scheduling and Practical Challenges at the *Electrical Engineers' Association (NZ) Conference*, CD-ROM, June, 2004.

5. J. Schönberger, R. Duke, and S. Round, Decentralised source scheduling in a model nanogrid using DC bus signalling, *Australasian Universities Power Engineering Conference*, CD-ROM, September, 2004.

6. J. Schönberger, R. Duke, and S. Round, DC Bus Signaling: A Distributed Control Strategy for a Hybrid Renewable Nanogrid, *IEEE Transactions on Industrial Electronics, Special Section on Renewable Energy and Distributed Generation Systems*, accepted for publication, April 2005. See Appendix B for full paper.

CONTENTS

Chapter 1

INTRODUCTION

1.1 GENERAL

The use of renewable sources in power systems is gaining popularity due to environmental concerns over burning fossil fuels to generate electricity. Environmental regulations such as carbon taxes under the Kyoto protocol are also hastening the use of renewable resources. Technological advances in power electronics have created opportunities for renewable sources to be harnessed at the distribution level. With the use of power electronic interface converters, renewable sources can be connected directly to a distribution network or combined with other local generators and loads to form an independent power system [1].

One such independent power system is a nanogrid. A nanogrid is similar to the microgrid concept proposed in [1]; however, the term nanogrid has been coined to describe the system in order to highlight the key differences between a nanogrid and the microgrid concept. A nanogrid is likely to be smaller in size than a microgrid, with a capacity in the order of 2-20 kW since its niche application is likely to be for remote area power supplies. Furthermore, a nanogrid operates at dc as opposed to 50/60 Hz and relies on power electronic converters to interface both sources and loads to the system. Step-up converters are employed to allow the low-voltage sources present in the nanogrid to provide power to the system, and step-down converters allow the loads to draw power from the nanogrid. Bidirectional converters allow the storage devices to charge from and discharge into the nanogrid.

Most hybrid renewable systems operate in a similar fashion to the conventional ac system. The operating frequency is typically 50/60 Hz for ease of interfacing the system with conventional loads and non-renewable sources, and the system is controlled using a combination of decentralised control and centralised control [2]. However, the ac system is

a legacy of the technology which the early power systems engineers used to build the original centralised ac systems. With the use of power electronic converters, new transmission and control options are possible.

A nanogrid may operate at a frequency lower or higher than 50/60 Hz if there are benefits to be gained in doing so. Furthermore, voltage deviations in the system may be used to convey control information since strict regulation of the system voltage is not as critical in a power electronic based system. The load interface converters can be controlled to maintain a constant output voltage over a wide range of disturbances in the system voltage, unlike transformers in a conventional system.

The main control issue in a nanogrid is one of maintaining the power balance in the system in the presence of fluctuating sources. The power supplied by the renewable sources varies considerably due to the stochastic nature of their renewable energy supply. Two approaches are available to ensure that the power injected into the system is always equal to the load demand: supply-side management and demand-side management. With supply-side management, the renewable sources are controlled to supply their maximum power to the system, while the storage and non-renewable sources are controlled to balance the load demand. With demand-side management, the renewable generation is left uncontrolled while the load profile is modified to balance the load demand. During power shortfalls, low-priority loads are tripped out to restore the power balance. In a nanogrid, using demand-side management alone to maintain the power balance in the system is problematic. The loads become dependent on the fluctuating output of the renewable sources.

Supply-side management is a better option for controlling this renewable based system, as the loads become independent from fluctuations in the renewable sources. In a nanogrid, supply-side management involves controlling the storage and non-renewable generation to balance the load since the output power of the renewable sources is variable. The storage performs the majority of the work, charging during periods of excess renewable power and discharging during power shortfalls. The non-renewable sources are only brought online during prolonged lulls in renewable power. Demand-side management may be included as an enhancement to this control strategy. For example, low-priority loads can be tripped out in a bid to reduce the peak load demand, preventing non-renewable generation from coming online to supply brief spikes in the load.

The traditional method of implementing a supply-side management scheme in a renewable based system is to use a central controller that schedules each source via a communications

link [3, 4, 5]. However, the system becomes dependent on the central controller and communications link. To ensure reliable operation of the system, redundant controllers must be included at an extra cost. A distributed control strategy improves the reliability of the system by distributing the control function throughout the system. However, the system is still dependent on a communications link for correct operation. To eliminate dependency on the communications link, the transmission network itself can be used to convey system information. Simulation results have shown the potential for using the voltage level of a dc transmission network to convey information for demand-side management in a system with an ideal transmission network [6, 7]. However the use of voltage levels to implement a supply-side management scheme in a dc system with a non-ideal transmission network has not yet been examined in detail. The key contribution of this thesis is the development and experimental verification of such a control strategy.

1.2 SCOPE OF THESIS

With advances in power electronics technology, new types of power systems are emerging. Various options are available for the utilisation of renewable sources, including nanogrids which are completely based on switching converters. However, little research has been conducted on techniques for implementing supply-side management schemes in such hybrid renewable systems. Conventional methods for controlling ac systems are generally adopted while most research effort focuses on the stability of the system and the design of efficient interface converters. This thesis examines the characteristics of a renewable-based nanogrid and proposes an efficient, cost-effective means of operating and controlling the system using new options made possible with the use of power electronics.

In Chapter 2, the characteristics of a nanogrid are described, and the electrical characteristics of the renewable sources likely to be present in a nanogrid are examined. Various transmission frequency options for a nanogrid are evaluated in Chapter 3 in order to determine the most suitable transmission frequency in terms of ease of interfacing renewable sources, efficiency, and safety. In Chapter 4, various topologies for controlling the renewable and non-renewable generation present in a nanogrid are evaluated to determine a control strategy that maintains the advantages present in the structure of a nanogrid. Chapter 5 proposes dc bus signalling (DBS) as a means of implementing a supply and demand-side control strategy for a nanogrid in a distributed fashion. The mechanism by which DBS operates is detailed, and a procedure for implementing supply and demand-

side control laws is given. A MATLAB/SIMULINK model of a nanogrid is presented in Chapter 6, and simulation results are included to demonstrate the operation of the supply and demand-side control laws that are implemented using DBS. In Chapter 7, the design of an experimental system is presented, and results are obtained to verify the practical operation of DBS. Chapter 8 addresses issues relevant to the operation of DBS in a real-life dc system based on switching converters. In particular, operation under fault conditions and small signal stability are discussed. Lastly, Chapter 9 summarises the thesis and points to areas of future research related to the use of DBS for controlling a nanogrid.

Chapter 2

BACKGROUND

2.1 INTRODUCTION

A nanogrid is a hybrid system which comprises a mix of renewable and non-renewable generation. Power electronics is the enabling technology of this system, being used to connect both sources and loads to the transmission network. This chapter presents the nanogrid concept in more detail, beginning with a description of the structure of the system. Niche applications for the system are highlighted because in the current electricity market, small renewable-based systems are not cost-competitive with the conventional ac system. The characteristics of the sources and loads present in the nanogrid are also explained since these impact the choice of operating frequency and control topology.

2.2 NANOGRID STRUCTURE

The structure of a nanogrid is shown in Figure 2.1. The primary building blocks of a nanogrid are power electronic interface converters. Step-up converters allow low voltage sources to supply power to the nanogrid, and step-down converters allow the loads to draw power from the nanogrid. Bidirectional converters allow storage nodes to charge from and discharge into the nanogrid.

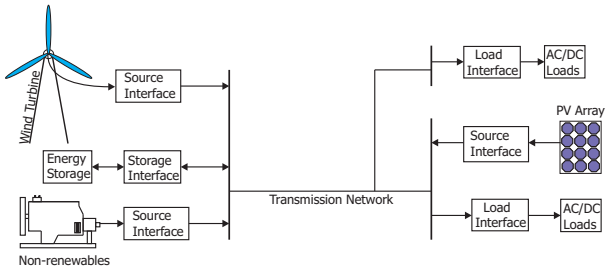

Figure 2.1 Structure of a standalone hybrid renewable nanogrid

Aside from the interface converters, a nanogrid comprises renewable sources, storage, non-renewable backup generation, loads, and a transmission network. Variable renewable sources supply the average load demand, and since the peak output of these sources is incapable of being controlled, energy storage devices are included in the system to act as an energy buffer, balancing differences between the source and load powers. Backup generation may be included to improve the system's reliability in the event of a long-term shortage of renewable energy.

Being a distributed system, a nanogrid has the advantages of increased redundancy and ease of expansion compared to a centralised power system. Generator failure in a centralised power system has a major impact on the system; however, in a distributed system, the system is not completely crippled by supply failure as additional supply nodes are still operating. The distributed structure of the nanogrid also lends itself well to modular construction and easy expansion. The need for initial investment is thus reduced since the system can be made small initially, then expanded as the load demand grows.

While there is no physical restriction on the size of a nanogrid in theory, efficiency and economics will largely dictate the size of a nanogrid in practice. For example, increasing the size of a nanogrid by including distant loads may improve the viability of the nanogrid due to the economies of scale that are gained in using larger generators. Other variable factors such as government subsidies, technological advances, and mass production will also affect the economic feasibility and hence size of a nanogrid. For the purposes of this thesis however, the size of a nanogrid that is considered is a cluster of 2-10 local loads that are located within 5 km of the sources. Assuming these loads are residential type loads, the power rating of such a system would be approximately 2-20 kW. High voltage transmission is not required for a system of this scale. Transmission voltages of several hundred volts are sufficient to provide efficient transmission of electrical energy in a localised system with these specifications. This will be demonstrated in Chapter 3.

2.3 NANOGRID NICHE

Regulatory changes to the electricity industry and environmental concerns over burning fossil fuels to generate electricity have heightened the interest in renewable energy systems. However, renewable-based nanogrids are restricted to niche applications for economic reasons. In the current market environment, the cost of electricity from small renewable sources tends to be more expensive than the cost of electricity from the ac network. The

only form of renewable generation that is cost competitive with conventional forms of generation is large-scale wind power generation [8, 9]. For this reason, the primary niche for nanogrids is currently found in applications such as remote area power supplies, where the cost of connecting to the conventional ac system is prohibitive.

In both industrialised and developing countries, it is generally uneconomic to connect remote loads to the existing electricity grid. The viability of using a nanogrid to supply electricity to local loads improves in these remote applications since the cost of connecting to the existing system outweighs the higher generation cost of the small-scale renewable sources present in the nanogrid.

Nanogrids may also be a viable option for rural electrification programs in developing countries. Using a multitude of small renewable based systems to supply widely dispersed villages decreases transmission line losses, and allows the system to be built with little initial capital investment. With a central power system, a large amount of capital is required to build the power station before the electrification process can commence.

In the future, nanogrids may find application in rural locations already serviced by an electricity network. The continuance of supply clause in New Zealand's Electricity Act states that on 31 March 2013, distribution companies will be released from the obligation to supply existing customers. The implication of this act is that customers in rural locations will begin to pay the true cost for their line-delivered electricity, which is currently subsidised. Forming a renewable-based system such as a nanogrid may become viable, especially if the system supplies a cluster of loads.

Forming a single hybrid power system to supply multiple customers in a local cluster is likely to be more economic than building a power system for each individual customer. The cost of electricity supplied by a hybrid system to a single house is significantly more expensive than the current cost of grid electricity; however, it has been shown that aggregating a number of loads improves the viability of standalone hybrid systems [10]. For example, the cost of supplying a cluster of twenty houses using a wind turbine and diesel generator is competitive with the existing cost of supply. This is due to an improvement in load factor and economies of scale present when purchasing generation.

Another future niche application for nanogrids, also to be found in rural locations, is parts of New Zealand's rural power system serviced by single wire earth return (SWER) systems. SWER systems are characterised by long feeders and high resistance lines. Consequently, the lines are limited by the voltage deviation at the receiving end of the line rather than

the current rating of the wires. Some of these systems are facing the need for an imminent upgrade since the system is operating at the limit of the acceptable voltage envelope. In addition, some of these feeders are nearing the end of their operational life. By deferring an upgrade, significant cost savings can be made. One means of deferring the upgrade is to install systems such as nanogrids to reduce the loading on the lines, or to help support the voltage at the end of the line.

It should also be mentioned that installing a nanogrid in rural locations may also benefit the end user. Customers in rural locations typically experience significant voltage deviations and frequent power outages. Forming a local system will improve the supply quality and increase the reliability of supply.

Over the next ten years, New Zealand's power system will continue to change, making it more viable for renewable energy systems to enter mainstream applications. The price of electrical energy will continue to increase due to increasing load demands, decreasing natural gas reserves and diminishing generation reserves. Carbon taxes under the Kyoto protocol and the continuance of supply clause affecting distribution companies may accelerate the price increase. At the same time, the cost of renewable energy systems will continue to decrease due to technological advances and mass production. As the price of conventional and renewable generation changes, the breakeven point will also shift, facilitating the movement of nanogrids from niche to mainstream applications.

2.4 GENERATION TECHNOLOGY

Power in the conventional ac system tends to come from large hydro or thermal power stations rated at 100 MW to 2 GW. At the heart of the power station is the synchronous generator which rotates at a fixed speed to produce 50/60 Hz ac, and has a controllable output power. In a nanogrid however, generation is primarily based on static renewable sources that produce a dc output. The peak output of the renewable sources is uncontrollable due to the stochastic nature of the renewable form of energy. As a result, storage and backup generation are required to maintain the power balance in the system in the presence of the fluctuating renewable sources.

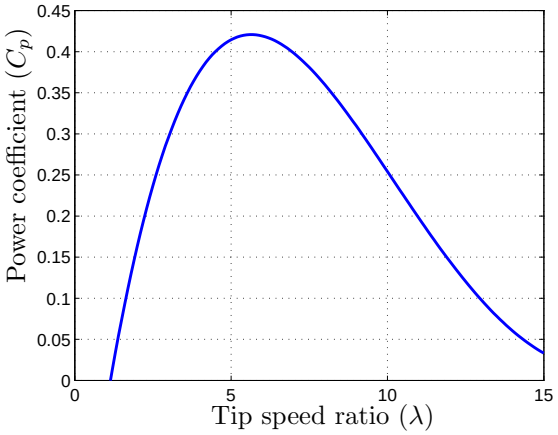

Figure 2.2 Typical power coefficient characteristic for a wind turbine

2.4.1 Wind turbine

Wind power has been the fastest growing energy technology in the world for the last decade [8, 9]. Due to economies of scale, large wind turbines are now cost competitive with large hydro and fossil fuel generators [8].

The peak output power available from a wind turbine is variable since it is largely dependent on the wind speed which is variable. The aerodynamic power of a wind turbine is given by

$$P = 0.5\rho A C_p v^3 \tag{2.1}$$

where ρ is the air density, A is the area swept by the turbine blades, v is the wind velocity, and C_p is the power coefficient of the turbine. The power coefficient of the wind turbine is a function of the tip speed ratio, λ, defined by

$$\lambda = \frac{\omega R}{v} \tag{2.2}$$

where ω is the rotational speed of the turbine, and R the turbine radius. A typical graph showing the relationship between the power coefficient and the tip speed ratio is shown in Figure 2.2. It can be seen that there is an optimal tip speed ratio, λ_{opt} that gives a maximum power coefficient. The wind turbine must therefore operate at a variable speed to ensure the optimum tip speed ratio is maintained as the wind speed varies. For example, as the wind speed increases, the rotational speed of the turbine must be increased to maintain the tip speed ratio at λ_{opt}.

Most large wind turbines such as those used in commercial wind farms employ induction or synchronous generators to produce electricity [11]. To permit variable speed operation, power electronic converters must be used to interface these generators to the ac grid [12]. Induction generators are also used in small wind turbines; however, permanent magnet generators are often employed. With this generator, there is no need for an external excitation source or a gearbox [13]. However a power electronic converter is still needed to permit power transfer between the permanent magnet generator and the power system.

For both small and large wind turbines, the power electronic interface not only has the task of interfacing the generator to the power system, but it also has the task of maximum power point tracking. To achieve this, the interface converter adjusts the power it injects into the system based on the wind speed. This control action controls the load torque and hence rotational speed, thus allowing the tip speed ratio to be maintained at λ_{opt}.

2.4.2 Photovoltaic Array

Photovoltaic (PV) arrays are another potential source of energy for nanogrids. They are reliable, produce no emissions, and require minimal maintenance. The drawback of solar arrays is their high initial cost. For example, the average cost of the PV modules in 625 residential grid-connected PV systems that were installed in United States between 1994 and 2000 was US$4.20/W [14]. However costs have been steadily decreasing since the inception of this technology due to ongoing research and mass production. The viability of photovoltaic systems can be improved by using the panels as building cladding [15], since this effectively reduces the installed cost of the panels.

The maximum theoretical efficiency of a silicon solar cell is 25%; however, the actual installed efficiency of modules ranges from 14-17% [14]. The maximum power point (MPP) of a PV array and its corresponding output voltage are variable, being a function of the sun's radiation and the temperature. Figure 2.3 shows the impact these two factors have on a typical PV array. It can be seen that increasing the temperature decreases the MPP, while increased radiation has the opposite effect.

The peak power available from a PV array is variable, being highly dependent on the sun's radiation. The radiation level varies according to the time of day and the season. Power is only produced during the daylight hours, and the peak power output is around midday. During the winter months, the angle of incidence between the sun and the earth effectively dilutes the intensity of the sun's rays reaching the array. Short-term fluctuations such as

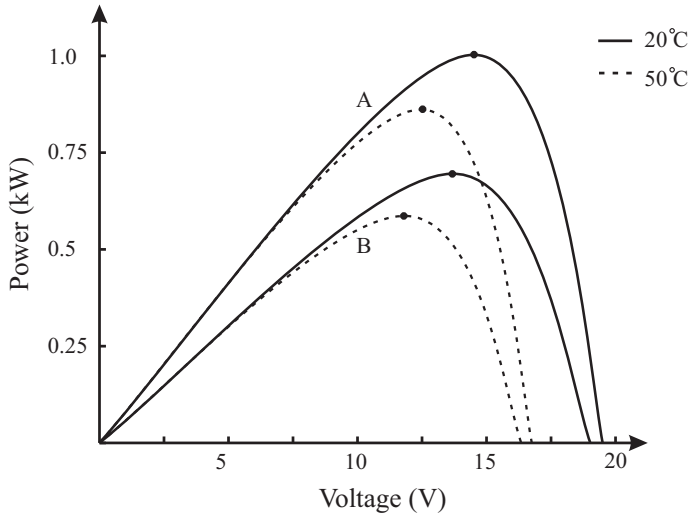

Figure 2.3 Effect of radiation and temperature on the MPP of a PV array. A. Radiation = 1 kW/m^2 B. Radiation = 0.7 kW/m^2

cloud cover also affect the output of the array.

A power electronic interface is required to interface PV arrays to an ac or dc power system. The interface must perform MPP tracking, and can take different forms, as explained in Section 3.4.1.

2.4.3 Fuel Cell

Fuel cells are well-suited for nanogrid applications as they provide a clean, controllable source of electricity. The major types of fuel cells are proton exchange membrane (PEMFC), direct methanol, solid oxide, phosphoric acid, and alkaline [16]. Although these fuel cells use different materials and forms of hydrogen fuel, they all operate according to the same principle. They convert hydrogen and oxygen into an electrical current through electrochemical oxidation and reduction. The only by-product of the reaction is water and heat.

Based on the operating temperature of a fuel cell, there are two broad categories of fuel cells: high temperature and low temperature. High temperature fuel cells operate at around $600 - 1000°C$ and are typically used for larger systems in the order of 200 kW. High temperature operation allows faster reaction rates and permits efficient generation of electricity by using the exhaust gas to drive turbines.

Low temperature fuel cells operate at temperatures from $50-200°C$ and are typically used for smaller systems up to several kW in size since there are cost advantages in reducing the operating temperature for smaller systems [16]. The fuel cells most likely to be used

in a nanogrid are low temperature fuel cells.

Fuel cells produce a variable voltage dc output that is dependent on the operating temperature and current supplied by the fuel cell. The output voltage of a single fuel cell is small, typically ranging from 0.7 to 1.2 V according to the operating conditions. To produce a more useful output voltage, a number of cells are connected in series to form a stack. The output voltage of a typical fuel cell stack is 22 to 41 Vdc [17].

The electrical efficiency of a fuel cell is around 40%, although the efficiency of the fuel cell system can be doubled by utilising the exhaust heat in cogeneration applications such as space and water heating [14]. An example of a fuel cell unit used for such cogeneration applications is the 1 kW NetGen unit produced by Ceramic Fuel Cells Limited [18]. The response time of a fuel cell depends on its construction. Low temperature fuel cells tend to have a fast response, while high temperature fuel cells used for baseload applications tend to respond more slowly [16].

2.4.4 Microhydro

Microhydro generation is generally classified as hydroelectric schemes that have an output power of less than 100 kW. This form of generation has significant potential for nanogrids due to the number of potential microhydro sites that exist. In developing countries, villages are typically built near streams and rivers, and microhydro is often used to supply a large portion of the village's electricity demands. In industrialised nations, although large-scale hydro developments are becoming more scarce due to environmental constraints and the lack of suitable locations, many sites suitable for micro-hydro schemes remain. In Japan for example, approximately 2400 such potential sites exist [19].

Microhydro can be a cost-effective method of supplying electricity to loads beyond the end of the electricity grid if a mechanical governor is not included in the system to regulate the flow of water through the turbine [20]. Another benefit of using microhydro is that power is usually available continuously. The flow of water in a stream or river is less variable than the wind speed or radiation from the sun. The water flow varies according to seasonal patterns whereas the wind speed and radiation fluctuate on an hourly or daily basis.

Most microhydro installations tend to operate on a run-of-the-river principle, generating electricity from the flow that the river provides [21]. Unlike large hydro plants, these smaller schemes operate from a lower head of water and a slower flow rate equivalent

to that of the river. Storage in the form of a dam reservoir is typically not included in the microhydro scheme to minimise the environmental impact of rising river and lake levels. Consequently, the output power of a microhydro plant is generally uncontrollable, dependent on the flow of water upstream.

Induction generators are generally preferred over synchronous generators for microhydro schemes due to their lower cost, smaller size, ruggedness, and ease of maintenance [22]. The induction generator can only be interfaced directly to a fixed-frequency power system if a mechanical governor or adjustable turbine blades are employed to ensure the turbine operates at a fixed speed. However, these mechanical solutions tend to be expensive. A cheaper solution is to use a turbine with fixed blades that operates at a variable speed [19]. As with variable-speed wind turbines, power electronic converters must be used to interface variable-speed microhydro turbines to a fixed-frequency power system.

2.4.5 Storage

Building a nanogrid based on renewable sources alone is fraught with difficulty as the renewable sources must be sized such that their minimum output is capable of supplying the peak load demand. Since this objective is costly to achieve, the renewable sources are sized such that their average output can supply the average load demand, and storage is included in the system to buffer the differences between supply and demand. The inclusion of storage improves the utilisation of the renewable energy sources [23]. The storage device acts as an energy buffer, storing excess renewable energy during periods of excess, and releasing the energy when the load exceeds the power available from the renewable sources. Energy storage systems can be provided using a range of technologies:

- Supercapacitors
- Superconducting magnetic energy storage
- Flywheel
- Batteries (old and new technologies)

These forms of storage typically produce a variable voltage dc output, and power electronic converters are required to allow bi-directional power flow between the storage device and the system.

Another form of storage that is worthy of mention in this section is discretionary space heating or water pumping. In the event that an excess of power from the renewable sources exists in the system and the conventional storage nodes are fully charged, the excess power can be put to use in this manner in order to maximise use of the renewable sources.

Storage can be classified as short term or long term. Short term storage has a full power time frame in the order of seconds to minutes, while long term storage can provide power to the system from hours to days. It is likely that a nanogrid will comprise a mix of both short and long term storage. Short term storage will be used to compensate for transient phenomena such as motor starting and the effects of wind turbulence, while long term storage will be used to smooth fluctuations in the output of the renewable generation.

However there is a limit to the amount of each form of storage that can be included in the system before the benefits it provides are outweighed by the incremental cost of increasing the size of the storage. For example, the cost of storage per kW-hr for most commonly used battery technologies increases significantly when the bank is sized to provide more than ten hours of reserve [23]. To provide backup for time periods longer than this, backup generation is typically more economical.

2.4.6 Backup Generation

Although it is possible to provide a continuous supply of power in a renewable based system with the addition of storage alone, including backup generation reduces the long-term storage requirements in the system. The storage bank does not have to be sized to cope for the worst-case lull in renewable energy. It has also been shown that the inclusion of backup generation in renewable based systems improves the supply reliability [24]. Although renewable sources have a lower operating cost, alone they can not provide an acceptable level of reliability due to their stochastic nature.

The most common form of backup generation is the diesel generator. Most backup diesel generators operate at a fixed speed to allow the alternator to be directly connected with the 50/60 Hz power system. However at low loads, fixed-speed generators are forced to operate outside their optimum fuel consumption envelope. For this reason, manufacturers of diesel generators typically stipulate a minimum loading of 40% to ensure economic operation and prevent combustion related maintenance problems [25]. However, operating the engine at a variable speed and using power electronics to interface the generator to

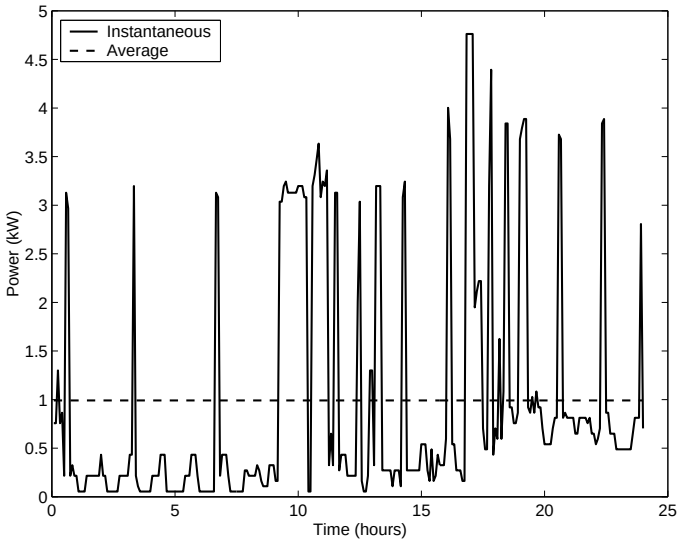

Figure 2.4 Load profile of a single house

the system can allow more efficient operation of the diesel generator [26]. Variable-speed operation allows the generator to run at its most efficient operating point as the load and ambient temperature change.

It is also worth noting that like fuel cells, backup generators may serve as combined heat and power (CHP) generators in a bid to increase their overall efficiency. An example of a diesel generator that has been specifically designed for a CHP application is the stirling engine-based generator produced by WhisperTech, which has an overall efficiency of up to 90% [27]. Such units are ideally suited for use in a nanogrid since the generation of heat is often handled by electricity, a valuable commodity in a small renewable-based system.

2.5 LOAD CHARACTERISTICS

Not only do the renewable sources in a nanogrid fluctuate, but the loads are also variable in nature. Figure 2.4 shows the load characteristics of a typical residential load in a rural location in New Zealand during the month of May.[1] The instantaneous load demand, sampled at five-minute intervals, varies significantly, and has a peak of nearly five times the average load demand.

There are benefits to be gained in combining loads, as shown by the aggregate load demand of three residential loads in Figure 2.5. Compared with the instantaneous load demand of an individual house, the combined instantaneous load demand is smoother, and the load factor, the ratio of peak to average load demand, is slightly smaller.

[1]Data courtesy Industrial Research Ltd, Christchurch, New Zealand.

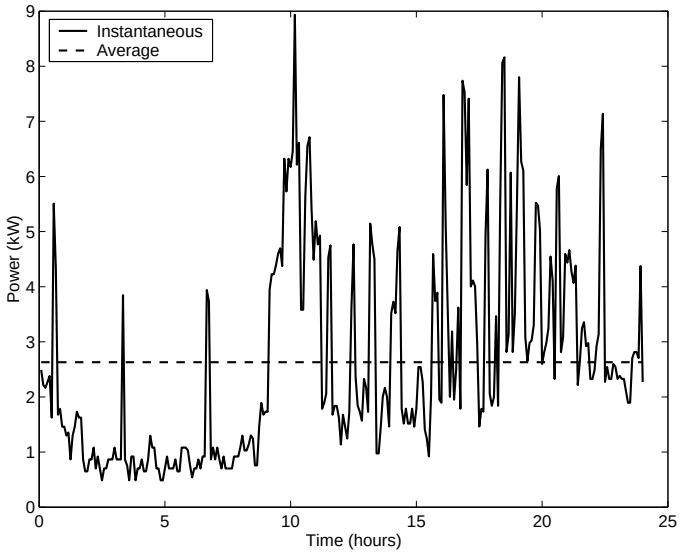

Figure 2.5 Load profile for three houses

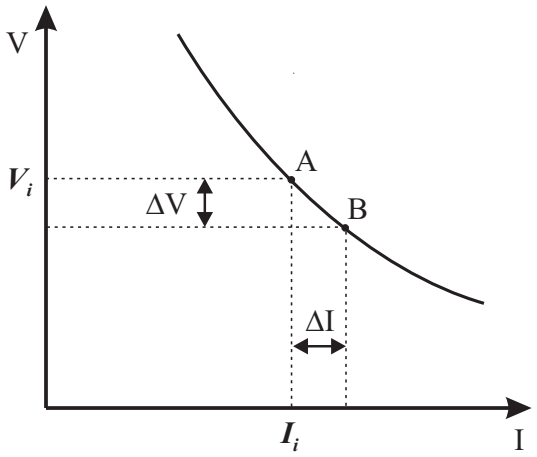

Figure 2.6 Negative impedance characteristic of constant power loads

The loads present in a nanogrid exhibit constant power characteristics since they are connected to the system using power electronic load interface converters. The output power of each load interface converter is constant due to regulation of the output voltage, hence the power drawn by the load interface converter from the system is also constant. This constant power characteristic causes the load interface converters to act as a negative input impedance on the system as shown in Figure 2.6.

With the load interface converter operating at point A, its nominal input voltage is V_i and its nominal current is I_i. The steady-state input impedance of the converter is therefore positive. When the input voltage decreases such that the system operates at point B, the input current increases in order to keep the load power constant. Thus it can be seen that the small signal impedance of the load interface converter, $\triangle V/\triangle I$, is negative.

2.6 SUMMARY

Primarily based on small renewable sources, electricity from a nanogrid is more expensive than grid electricity since these sources have a higher generation cost. Consequently, a nanogrid is currently restricted to niche applications such as remote power supplies for economic reasons. The size of a nanogrid that is considered in this thesis is in the order of 2-20 kW, with the loads located within 5 km of the sources.

A nanogrid not only includes renewable sources, but storage and backup generation are also included in the generation mix to smooth supply fluctuations and increase supply reliability. All these sources present in a nanogrid produce a variable voltage dc or a variable frequency ac output. Power electronic converters are therefore required to interface these sources to a fixed-frequency power system. Power electronic converters are also used to interface loads to the system. The load interface converters exhibit constant power characteristics, acting as a negative impedance on the system.

Chapter 3

NANOGRID TRANSMISSION OPTIONS

3.1 INTRODUCTION

A nanogrid has a different structure compared to the central ac power system. The ac system is based on large synchronous generators and uses transformers to connect generators and loads to the system, while a nanogrid is primarily based on static dc sources and uses power electronic converters to interface the sources and loads to the system. Since the source interface converters can be designed to produce an output frequency ranging from dc to high-frequency ac, the operating frequency for a nanogrid is not restricted to 50/60 Hz. In fact, operating a nanogrid at a frequency lower or higher than 50/60 Hz may be advantageous. The ideal operating frequency for the nanogrid should:

- Allow efficient transmission of power
- Have simple source and load interface requirements
- Present no major technical problems

This chapter begins by outlining the characteristics of all possible transmission frequency options for a nanogrid, ranging from dc to high ac frequencies. It then evaluates each option in light of the above criteria to determine the transmission frequency most suitable for the system.

3.2 TRANSMISSION FREQUENCY OPTIONS

3.2.1 DC

The first power systems operated at dc. Edison's original power system, developed in 1881, operated at 110 V, but its service area was limited due to its low voltage operation. The original dc systems were rapidly superseded by ac systems since ac was simpler to transform to high voltages for efficient transmission. With modern power electronics technology, dc transmission has become practical and has made a resurgence, finding niche applications.

The most common application for dc today is high voltage dc (HVdc) transmission. DC is the only means by which power can be transmitted efficiently at high voltages via cable. At 50 Hz, the significant dielectric losses in cable render high voltage transmission using this medium inefficient. Another advantage of dc operation is that there is no need for generator synchronisation. A dc link can therefore be used to provide a connection between asynchronous power systems.

Voltage source converters (VSC) are becoming attractive for HVdc transmission due to advances in power electronic devices such as insulated gate bipolar transistors (IGBT). HVdc schemes based on these converters are referred to as HVdc light [28]. Since VSCs are well-suited for parallel operation, multiterminal systems based on VSCs have been proposed for offshore windfarms [29]. Since the windfarms are 10-30 km offshore, operation at dc allows more efficient transmission of power to shore via underwater cable than mains frequency ac. Each windturbine is connected to an internal dc network using an ac-dc converter, while a dc-ac converter inverts the aggregated power into three phase ac to supply the central ac grid. A multiterminal VSC-based dc system has also been proposed for the distribution of power in urban areas of large cities [30]. The power electronic based dc system has performance advantages over the conventional ac system with regard to power quality under earth fault conditions.

DC is employed in other systems aside from HVdc. However, these systems tend to be niche systems such as telecommunications power supplies [31]. A DC system based on power electronic converters is also being considered to power the next generation of US Navy combat ships [32]. A number of reasons are cited for this choice of power system. The dc power system offers a reduction in size and weight since there is no need for intermediate distribution transformers. Another major benefit is that the generators are decoupled from

the distribution frequency. This allows the generators operate asynchronously, permitting operation at their most efficient speed. Furthermore, operational flexibility of the system is enhanced with the use of power converters to connect loads to the system. The converters not only provide power conversion, but they also have current-limiting features which help protect the system in the event of a fault.

In addition to the advantages dc offers in terms of high transmission efficiency and ease of connecting asynchronous systems, the effect of dc current on the human body is significantly less than that of mains frequency ac [33]. At 60 Hz, severe shock and muscular contractions occur at approximately 20 mA, while at dc this threshold is three times greater.

However, dc has one major technical problem. Interrupting dc current is more difficult than interrupting ac current since dc arcs are inherently non self-extinguishing. As a result, dc circuit breakers are more complicated and costly compared to their ac counterparts. This problem can be alleviated through the use of state-of-the-art technology such as hybrid circuit breakers. These circuit breakers comprise a solid-state switch to interrupt the fault and a mechanical switch in series to provide electrical isolation [34]. The issue of dc fault currents will be addressed in more detail in Chapter 8.

3.2.2 50/60 Hz

The conventional 50/60 Hz power system has been in existence for over 100 years. The first single phase ac system was installed in America in 1889, and for a short period of time, both ac and dc systems were used. However the invention of the transformer and Tesla's invention of the induction motor hastened the advance in the use of ac systems. Transformers allowed central power systems to service a large area whereas dc was restricted to small local power systems since generation of high voltage dc was impossible at the time. In addition, Tesla's ac induction motor proved to be superior to the dc machines of the era. The induction machines were simple and reliable, while the dc machines required frequent maintenance due to the use of brushes.

Since its inception, the main advantage of the 50/60 Hz power system has not changed. The ability to transform voltages in an efficient and reliable fashion with the use of a transformer is a major benefit even today. At 50/60 Hz, power transmission is fairly efficient with the use of overhead line, and switching and interrupting ac current is straightforward. However, the main drawback with operation at 50/60 Hz is the large size of the magnetic

components. Transformers and motors designed for operation at 50/60 Hz are significantly more bulky and costly than those designed for operation at higher frequencies.

3.2.3 400/500 Hz

Another transmission frequency for consideration is 400/500 Hz. Power systems for commercial aircraft tend to operate at 400 Hz as increasing the frequency allows a reduction in the size of the magnetic components [35]. In a nanogrid, not only would the reduction in the size and weight of the magnetic components be an advantage, but also the corresponding reduction in cost would improve the economic viability of such a system.

A drawback with operation at 400/500 Hz is that the line reactance is significantly greater than that at 50 Hz. Therefore reactive power support is likely to be necessary at this operating frequency. In addition, transmission at 400/500 Hz is less efficient due to skin effect and dielectric losses, although dielectric losses are only a significant factor with high voltage cable transmission.

It is also important to note that pulse width modulation (PWM) inverters designed to operate at 400 Hz have greater switching losses than those with a fundamental output of 50 Hz. To achieve the same frequency modulation ratio, the switching frequency of the inverter must be eight times greater than the switching frequency of a 50Hz inverter.

Aside from these factors, operating a nanogrid at this medium ac frequency offers the same advantages as operation at 50/60 Hz, namely simple voltage transformation using transformers, and ease of interrupting fault currents.

3.2.4 High-Frequency AC

High-frequency ac is not commonly used as as a transmission frequency for power systems. However, a high-frequency ac bus running at 20 kHz has been proposed as an alternative means of distributing power in buildings [36]. This system has merits such as very small magnetic components and inductive power transfer. However, Litz wire must be used to permit efficient power transmission at this frequency due to the skin effect. While this operating frequency may be a possibility for small transmission distances, the cost of the transmission line for any larger systems renders this option impractical. For this reason, high-frequency ac operation is precluded from consideration for a nanogrid.

3.3 TRANSMISSION LINE EFFICIENCY

An examination of the features of the various transmission frequency options show that dc, 50 Hz, and 500 Hz appear to be viable options in terms of efficiency and practicality. To determine the most suitable transmission frequency from these options, further analysis is performed. The effect of operating frequency on transmission line efficiency is evaluated. A transmission line and cable are modelled and simulated to determine the trend in efficiency as the frequency increases from dc to 500 Hz.

3.3.1 Transmission Line Model

The main parameters of a transmission line are resistance, inductance, and capacitance. These parameters can be calculated from the physical characteristics of the line, using standard formulae for two parallel uniform cylindrical conductors of radius r, spaced D meters apart. The loop resistance per unit length is given by

$$R = \frac{2\rho}{A} \quad \Omega/m \tag{3.1}$$

where ρ is the resistivity and A is the cross sectional area of each conductor. The inductance of a transmission line is made up of both internal and external inductance. The internal inductance of a single wire is given by

$$L_{int} = \frac{\mu_0}{8\pi} \quad H/m \tag{3.2}$$

where μ_0 is the permeability of free space. The external inductance of a single wire is given by

$$L_{ext} = 2 \times 10^{-7} ln\frac{D}{r} \quad H/m \tag{3.3}$$

As the frequency increases, the resistance tends to increase and the internal inductance tends to decrease due to the skin effect. The skin effect is accounted for by using Bessel functions to calculate the increase in resistance [33].

The capacitance per unit length for a pair of wires is given by

$$C = \frac{\pi\varepsilon_0\varepsilon_r}{\ln(\frac{D}{r})} \quad F/m \tag{3.4}$$

Table 3.1 Transmission Line Parameters at dc

Parameter	Transmission Line	Cable
Resistance (Ω/km)	0.2409	0.2409
Inductance (mH/km)	2.260	0.696
Capacitance (nF/km)	5.143	44.79

where ε_0 is the permittivity of free space, and ε_r is the relative permittivity. The dielectric losses in the cable are calculated using

$$P = V^2 \omega C \tan\delta \quad W \tag{3.5}$$

where V is the operating voltage, $\tan\delta$ is the loss coefficient, and ω is the operating frequency in radians/sec.

The transmission line parameters are calculated from the physical specifications of the line. For both lines, copper conductors with a radius of 7.137 mm are used. The transmission line conductors are 0.5 m apart while those of the cable are 1 cm apart, and separated by XLPE insulation. The characteristics of XLPE are $\varepsilon_r = 2.4$ and $\tan\delta = 0.5 \times 10^{-3}$. The parameters of the line are calculated assuming an operating temperature of $50°C$, and the results are shown in Table 3.1.

It is important to note that cable has a lower inductance and a higher capacitance than that of the transmission line, due to the closer spacing of the wires and the use of insulation. In addition, skin effect plays a small role when the frequency is increased from dc to 500 Hz. At 500 Hz, the skin effect causes the line resistance to increase by approximately 12%.

An equivalent PI model was used to represent the transmission line, since this model takes into account the travelling wave effect, which becomes significant as the frequency or length of the line increases [37]. The equivalent PI model is shown in Figure 3.1. The characteristic impedance is given by Z_c, the propagation constant is γ, and l is the length. The derivation of these constants from the transmission line resistance, inductance, capacitance, and operating frequency is not explained here, since this is adequately explained in technical literature [37].

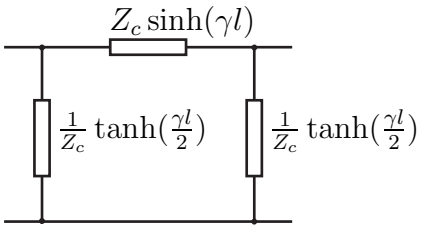

Figure 3.1 Equivalent PI model

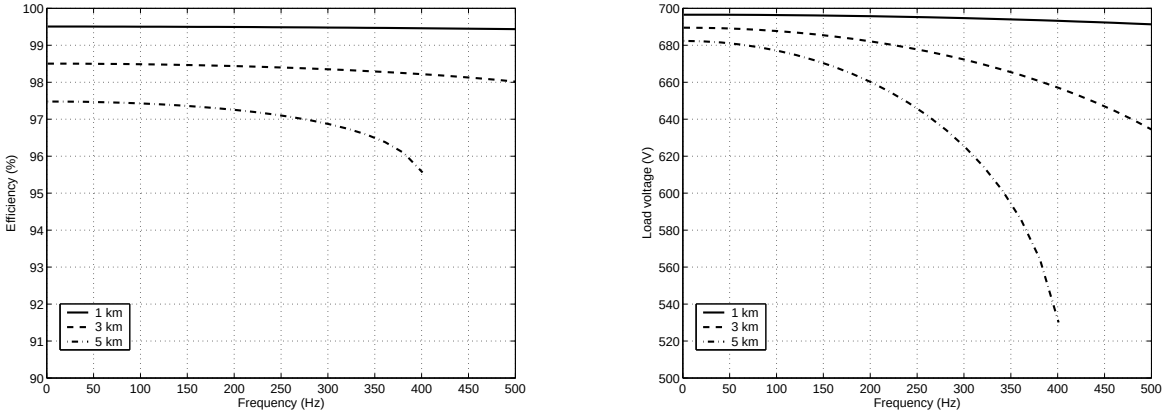

(a) Efficiency (b) Load voltage

Figure 3.2 Transmission line results

3.3.2 Simulation Results

The transmission line model was implemented in MATLAB, and a simulation was performed with a constant voltage source of 700 V supplying a constant power load of 10 kW at unity power factor. The source frequency was varied from dc to 500 Hz in increments of 20 Hz, and the efficiency and load voltage were monitored. The results are shown in Figures 3.2 and 3.3.

Figure 3.2 shows the effect of transmission frequency on line efficiency and load voltage for line lengths of 1, 3, and 5 km. The decrease in efficiency for the shorter line lengths is negligible. For line lengths of 1 and 3 km, the decrease in efficiency between dc and 500 Hz is less than 1% as shown in Figure 3.2(a).

However the decrease in load voltage for these line lengths is more pronounced, as shown in Figure 3.2(b). As the frequency increases, the reactance of the line increases, and the reactive voltage drop increases accordingly. This decreases the load voltage, since the load voltage is approximately the vector difference between the supply voltage and the reactive voltage drop.

The decrease in load voltage decreases the transmission line efficiency with the use of a constant power load. This decrease is especially noticeable with a line length of 5 km. As

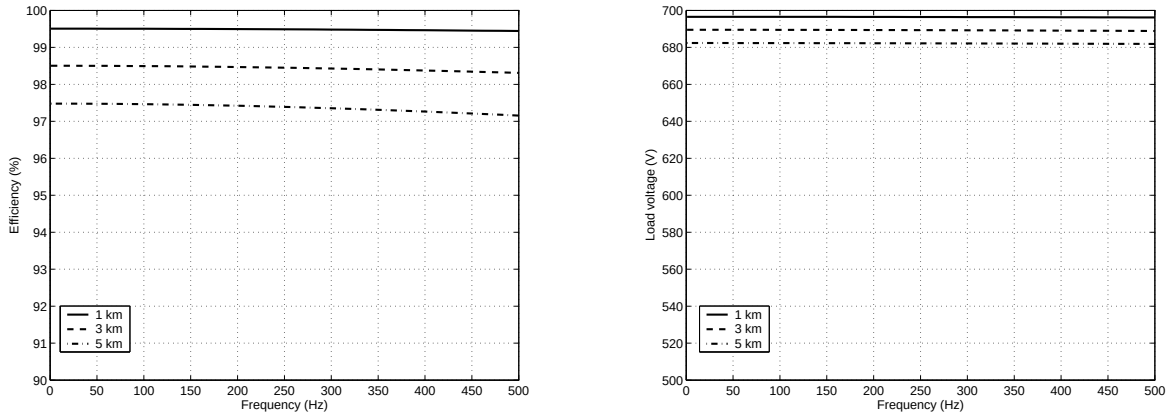

(a) Efficiency (b) Load voltage

Figure 3.3 Cable results

the load voltage decreases, the line current increases to supply the power demanded by the constant power load, and the resistive losses in the line increase accordingly. Eventually a point is reached at which the line is unable to supply the constant power load. In the simulation, this point is 400 Hz.

Figure 3.3 shows the effect of transmission line frequency on efficiency and load voltage with the use of cable. As with the transmission line, the efficiency and load voltage decrease as the frequency increases. However, the decrease in the load voltage is much less pronounced. As the frequency increases, the cable's voltage drop is smaller because of its lower inductance, and its higher capacitance providing a degree of reactive power support. A higher load voltage at 500 Hz in turn improves the efficiency of the line. The real power losses in the line are reduced as the current drawn by the constant power load does not increase due to a decrease in the load voltage.

In high voltage applications, cable transmission at ac frequencies is less efficient than overhead line transmission since the dielectric losses become significant. However in this simulation, cable is more efficient than overhead line transmission because the dielectric losses are insignificant. The dielectric losses are proportional to the voltage squared; therefore at low voltages, the dielectric losses are significantly reduced. For example, at 700 V, 5 km, and 500 Hz, the dielectric losses in the cable are calculated to be only 0.4 W.

The results indicate that dc and 50 Hz are the most efficient transmission options with the use of both overhead line and cable. Operation at 500 Hz may be feasible under the right operating conditions. With the use of cable, operation at 500 Hz is efficient since its reactive voltage drop is small and its dielectric losses are insignificant under low voltage operation. A transmission line can only be used at 500 Hz if reactive power support is

used to prevent the load voltage from collapsing.

Although operation at 500 Hz may be possible in a low voltage power system with the use of cable, operation at this frequency is ruled out from this point for the following reasons: Installing cable is generally more expensive than an overhead line system. On the other hand using an overhead line system is likely to require reactive voltage support to combat the increased line reactance at 500 Hz. Lastly, the power electronic converters are likely to be less efficient than those designed for operation at 50 Hz, since the switching frequency must be higher to achieve the same frequency modulation ratio.

3.4 INTERFACE REQUIREMENTS

The other major factor affecting the choice of operating frequency is the interface requirements. Ideally, the operating frequency of choice should permit a direct connection between the transmission system and the sources and loads most likely to be present in a nanogrid. In practice, the source and load characteristics do not match those of the system; therefore, source and load interface circuits are required. This section evaluates the interface requirements for connecting the sources and loads to dc and 50 Hz systems to determine which transmission frequency presents advantages in this area.

3.4.1 Source Interface

As pointed out in Section 2.4, the sources present in a nanogrid produce a variable voltage dc or a variable frequency ac output. However, the nanogrid operates at a higher voltage than the sources to achieve a high transmission efficiency, and its transmission frequency may be different from that of the sources. Consequently, the task of the source interface converter is two-fold. The source interface converter must raise the supply voltage and provide frequency matching between the source and the system. In addition, the source interface must provide galvanic isolation between the source and the transmission network for safety reasons. This section examines the interface requirements for the sources likely to be present in a nanogrid to ascertain whether dc or 50 Hz operation allows the use of simpler interfaces.

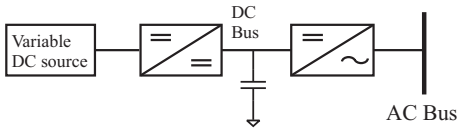

Figure 3.4 Interfacing a fuel cell to a 50 Hz network

Fuel Cell Interface

Since a fuel cell system typically produces an output voltage from 25-40 Vdc, a fuel cell interface must magnify the supply voltage and convert it into a 50 Hz voltage. This task can be achieved by connecting an inverter to a fuel cell to provide the 50 Hz voltage, and using a 50 Hz transformer to magnify the voltage. However, this method is not as popular as a two-stage approach because a low frequency ac transformer is bulky and expensive. A more common approach is to use a front-end dc-dc converter stage, followed by a dc-ac inverter [12]. Examples of this approach, portrayed in Figure 3.4, are given in [38, 17]. The front-end dc-dc converter provides voltage magnification and isolation while the inverter produces an ac voltage to allow connection with the system. A number of different topologies that can be employed in these converter stages are outlined in [12].

Another possible configuration for a fuel cell inverter is to use an isolated high-frequency dc-ac converter followed by a cycloconverter. This approach, outlined in [39], was proposed in a bid to reduce the rectifier and filter components required to produce an intermediate dc bus.

Interfacing a fuel cell to a dc network only requires one stage of conversion. A single dc-dc converter can be employed to provide both isolation and voltage magnification, allowing the fuel cell to be interfaced to the dc system. This converter is identical to the front-end stage shown in Figure 3.4. DC operation therefore has the advantage of eliminating the additional output conversion stage required for ac operation.

Photovoltaic Array Interface

A large number of topologies have been proposed for connecting photovoltaic arrays to an ac grid. A good overview of these topologies is given in [12]. A popular approach is to use a string inverter which comprises a number of PV arrays connected in series to provide a high input voltage, followed by an inverter to allow connection with an ac network. With this arrangement, galvanic isolation is achieved by using an isolated dc-dc converter at the input, or a mains frequency transformer at the output. Using an isolated front-end

dc-dc converter stage is preferred due to its smaller size and cost compared to the mains transformer.

Other power electronic interface converter topologies have been proposed. One topology is the multi-string converter where each string of PV arrays has a dc-dc converter that is connected to a common inverter [12]. Another approach that has been proposed is to use a single dc-dc converter per panel, and connect the dc-dc converters in series to form a high voltage dc bus that supplies an inverter [40]. This approach allows better utilisation of each panel and offers the potential for a lower implementation cost. To achieve isolation however, each dc-dc converter must incorporate a high-frequency transformer.

Although a number of options exist for connecting PV arrays to an ac system, in general, two stages are required to achieve galvanic isolation between the system and the source. A transformer based dc-dc converter is generally adopted as the front-end stage to provide the isolation. For this reason, interfacing PV arrays to a dc network in an isolated manner is simpler. Interfacing a PV array to a dc network can be achieved using a single isolated dc-dc converter, or a number of isolated dc-dc converters connected in a series string.

It should be noted that the source interface requirements for storage devices such as batteries are similar to the interface requirements for PV arrays. Batteries produce a low voltage dc output, and can be connected in series strings to provide a more useful operating voltage, as with PV arrays. Consequently, the interface circuits used for PV arrays are applicable to storage devices that exhibit similar electrical characteristics.

Interface for AC Sources

The ac sources likely to be present in a nanogrid are backup generators, microhydro generators, and wind turbines. These sources typically use permanent magnet or induction generators for the production of electricity. They operate at a variable speed since they are more efficient under these operating conditions as explained in Section 2.4. The method used for interfacing these asynchronous sources to an ac network is dependent on the type of generator used. For example, wind turbines that use induction generators can be interfaced to an ac system using partially or fully-rated power electronic converters [12]. A partially rated converter is more cost effective than converter with the same peak rating as the source itself, and reasonable performance can be achieved. For example, a doubly-fed induction generator in a wind turbine that uses a converter to control the rotor current allows the induction generator to vary its nominal synchronous operating

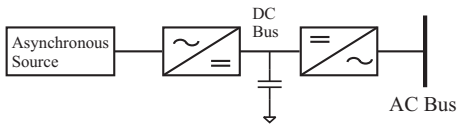

Figure 3.5 Interfacing an asynchronous source to a 50 Hz network

speed by 60% using a converter rated at only 30% of the generator's rating.

However, using a fully-rated converter to connect a wind turbine source to a 50 Hz network provides better performance, allowing more power to be captured from the wind. The typical method of using a fully-rated converter for connecting an asynchronous source such as a wind turbine to a 50 Hz system is shown in Figure 3.5. This conversion system, comprising back-to-back voltage source converters connected via a dc bus, is described in [41, 12]. The conversion system requires a 50 Hz transformer at the output of the dc-ac conversion stage to achieve isolation from the system.

Wind turbines that use permanent magnet generators can be interfaced to an ac system in a similar fashion, using a two voltage source converters to connect the asynchronous sources via a dc link [12]. However, another approach is to rectify the output of the converter and use a dc-dc stage followed by an inverter to connect the permanent magnet generator to the system [42]. To achieve isolation, a high-frequency transformer can be inserted in the dc-dc converter stage, eliminating the need for a bulky mains transformer at the inverter output.

As with the previous sources, the use of a dc network can simplify the source interface requirements for both induction and permanent magnet generators. The dc-ac output stage can be eliminated, as the front-end stage produces a dc bus by itself. To provide galvanic isolation with the use of dc, the front-end stage must be isolated. If this is not possible, an isolated dc-dc output stage must be substituted in place of the ac transformer would be present at the output of the equivalent ac interface.

In terms of source interface requirements, operating a nanogrid at dc presents advantages. DC operation generally eliminates the need for an extra inverter stage when connecting dc sources to a nanogrid. A single dc-dc converter is all that is needed to connect the source with the system, providing both voltage magnification and isolation. Similarly, dc operation simplifies the interface requirements for connecting ac sources such permanent magnet generators to the network. Under dc operation, the secondary dc-ac output stage can be eliminated. For both types of sources, the main reason dc offers simpler interface requirements is that the source interface converters typically comprise two stages linked

by an intermediate dc bus. The secondary stage can be eliminated and the dc bus used for direct connection with a dc system.

3.4.2 Load Interface

Small standalone renewable based power systems typically transmit power to the loads at 230 V 50 Hz, or 12 V dc in order to simplify interface requirements for common residential loads. However, operating a nanogrid at these utilisation level voltages is impractical. A nanogrid encompasses a larger area; therefore it must operate at a voltage that is typically greater than 230 V to achieve a high transmission efficiency. In addition, the transmission frequency may be different from the operating frequency of the loads. For these reasons, load interface circuits are required.

In a 50 Hz system, a step-down transformer typically interfaces 50 Hz loads to the transmission network, while a step-down ac-dc converter connects dc loads to the network. In a dc system, step-down type converters are needed to connect 50 Hz or dc loads to the transmission network.

In terms of interfacing conventional loads to a nanogrid, transmission at 50 Hz offers both advantages and disadvantages. Operation at 50 Hz permits the use of a transformer as the load interface, which is more simple and efficient than a power electronic based converter. However, it is bulky and expensive. In addition, a transformer does not buffer the loads from fluctuations in the system since its instantaneous output is uncontrollable. As a result, brief voltage anomalies in the ac system can affect the performance of critical loads.

In the conventional ac system, power electronic based equipment such as dynamic voltage restorers (DVR) are typically employed to improve the power quality for critical loads [43]. Based on electronics, the control bandwidth of the DVR is far greater than that of a rotating machine. This allows the DVR to mitigate brief fluctuations in the power system that would be detrimental to the performance of critical loads.

In a dc nanogrid, the use of step-down converters for the load interface also offers advantages and drawbacks. The load interface converters are less efficient than mains transformers. However a major advantage is that they can be controlled to provide high-quality power to the loads despite voltage fluctuations in the power system. The load interface converters can be controlled at a high bandwidth since they are based on high-speed switching converters.

Another advantage of using power electronic converters for the load interface is that voltage regulation is simple to achieve. In the ac system, online tap-changing transformers attempt to regulate the load voltage. These have a slow response and require additional control and tap-changing circuitry. On the other hand, voltage regulation can be achieved automatically with the use of a power electronic converter. A power electronic converter provides superior load regulation as it operates at a high speed. No additional control circuitry is required.

It should also be noted that while conventional loads are designed for operation at 230 V, 50 Hz, many of these loads operate internally at dc. For example, both computers and television sets contain ac-dc converters since they operate from dc. In addition most lighting and heating elements can operate at either dc or ac. Therefore in most cases, operating a system at dc does not increase the load interface requirements.

3.5 TRANSMISSION FREQUENCY SELECTION

The simulation results presented in Section 3.3.2 showed little difference between dc and 50 Hz in terms of transmission efficiency. An examination of the load interface requirements also showed little advantage in opting for dc or 50 Hz since they both have their relative merits and drawbacks. However an examination of the interface requirements has highlighted some significant differences between the two systems. Interfacing variable-voltage dc or variable-frequency ac sources to a dc network is simpler, requiring only one stage of power electronic conversion. In general, two stages of power electronic conversion are required to interface these sources to a 50 Hz network. An additional front-end stage is used to provide isolation and a stable dc bus for the 50 Hz inverter to operate from. For this reason, dc is selected as the operating frequency for a nanogrid.

Aside from having simpler source interface requirements, dc offers a number of other advantages. Transmission at dc is still the most efficient, and dc is intrinsically safer. The threshold for severe shock is approximately three times greater under dc operation. Although dc systems have issues with fault-current interruption, this issue is not a major problem in a power electronic based system since the source interface converters can be designed to limit the fault current. This issue will be addressed in Chapter 8.

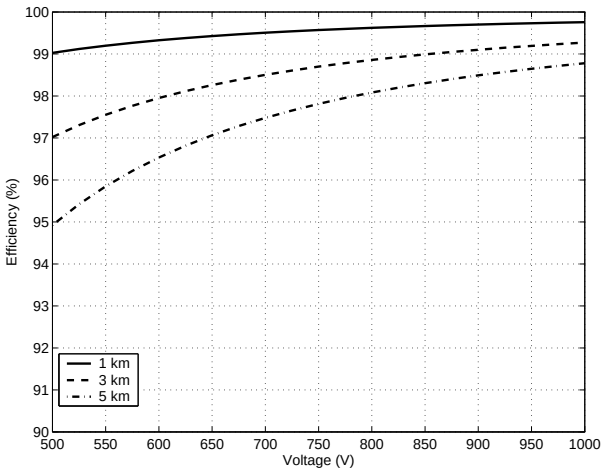

Figure 3.6 Effect of voltage on transmission line efficiency

3.6 TRANSMISSION VOLTAGE SELECTION

The selection of an appropriate transmission voltage, while not as critical as the choice of the transmission frequency, is nevertheless important, having a major impact on the efficiency of the transmission network. As the operating voltage increases, the line current decreases for a given load demand and the line conduction losses decrease accordingly. Figure 3.6 shows the effect of operating voltage on transmission line frequency for a constant voltage dc source supplying a constant power load of 10 kW. The line parameters are the same as those given in Table 3.1. It can be seen that the transmission line efficiency increases with an increase in operating voltage, although the rate of increase is less apparent as the operating voltage approaches 1000 V.

Ideally the transmission voltage should be selected such that the transmission line efficiency approaches 100%. However, this ideal figure is impractical to achieve, requiring an infinite operating voltage. A more practical figure is around 95%, similar to the efficiency of the source and load interface converters. In practice, resonant or soft-switching topologies would be used for these converters, providing conversion efficiencies of up to 95%. The benefits to be gained in increasing the transmission line efficiency to approach 100% are therefore negated by the conversion losses in the source and load interface converters.

A nanogrid operating voltage of 700 V is therefore selected to provide an efficiency of 97.5% with a line length of 5 km. It should be noted that in practice, transmission line efficiency is not the only factor influencing the choice of bus voltage. The choice of bus voltage also also impacts the design of the interface converters. These issues will be addressed in more detail in Section 8.3.

3.7 SUMMARY

The characteristics of a number of transmission frequency options, dc, 50 Hz, 500 Hz, and 20 kHz have been examined in this chapter in order to determine the operating frequency that is most suited to a nanogrid. Based on their operating characteristics, dc, 50 Hz, 500 Hz were identified as practical candidates for the transmission frequency. These frequencies were analysed to determine their transmission efficiency with overhead line and cable as the transmission medium. Operation at 500 Hz was consequently ruled out for use in a nanogrid since its transmission efficiency was significantly less than that of dc and 50 Hz with the use of overhead line. Although there was little difference between the efficiency of dc and 50 Hz, dc was selected largely due to its simpler source interface requirements. Interfacing variable-voltage dc or variable-frequency ac sources to a dc network typically requires only one stage of power electronic conversion. With a 50 Hz system, two stages of conversion are typically needed. Another benefit of dc operation is that the load interface converters required can provide better power quality to the loads than transformers in an ac system. Simulation results demonstrated that a suitable operating voltage for a nanogrid with a transmission line length of 5 km and a peak load demand of 10 kW is 700 V, assuming a line resistance of 0.24 Ω/km. While this operating voltage is dependent on a number of factors, it is primarily chosen such that the efficiency of the transmission network is comparable with the efficiency of the source and load interface converters.

Chapter 4

NANOGRID CONTROL OPTIONS

4.1 INTRODUCTION

As mentioned in Chapter 1, the main control issue in a nanogrid is one of maintaining the power balance in the system in the presence of stochastic sources and loads. A supply-side management scheme must be adopted as the primary means of maintaining the power balance in the system to prevent the loads from becoming susceptible to fluctuations in the output of the renewable sources. The purpose of the supply-side management scheme is to schedule the sources present in a nanogrid according to a supply-side control law which minimises the operating cost of the system. The supply-side control law ensures that use of the renewable sources is maximised since the cost of the fuel for these sources is negligible. The renewable sources supply the base load and any excess power is used to charge the storage devices. During shortages in renewable power, power is drawn from the storage devices. Backup generation is brought online when the storage is depleted due to a long-term shortage in renewable power.

A number of different control topologies are available for controlling the sources present in a nanogrid. The main criterion for choosing a control topology is its ability to permit source scheduling according to a supply-side control law. The control topology of choice should also maintain the reliability and modularity inherent in the distributed structure of the system. In addition, it should be inexpensive to implement in a reliable fashion to help improve the economic viability of the system. This chapter highlights the various control topologies that can be used for controlling a dc nanogrid and provides examples of where these control topologies are adopted in practical systems. Each option is then evaluated to determine the control topology most suitable for a nanogrid.

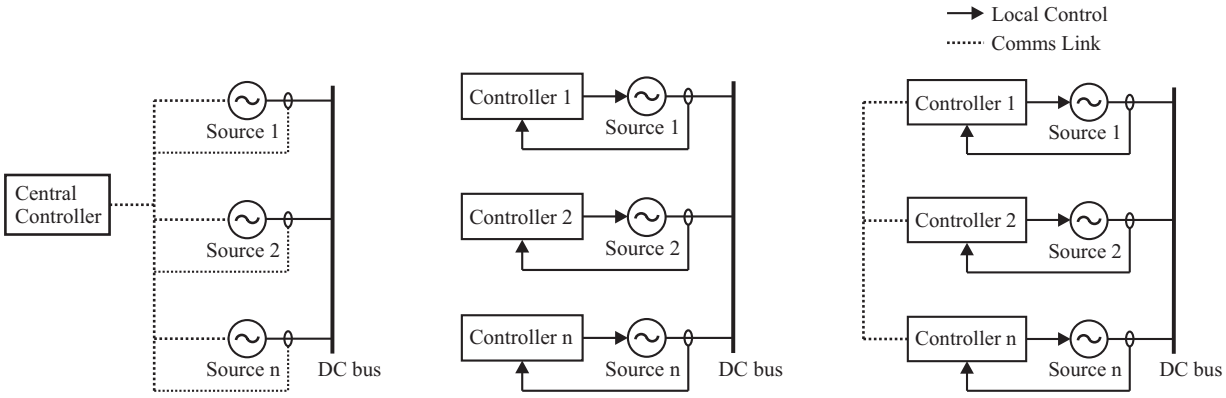

Figure 4.1 Nanogrid control topologies

4.2 CONTROL TOPOLOGIES

The three basic control topologies that can be used in a nanogrid are central, decentralised, and distributed control. These topologies are illustrated in Figure 4.1.

4.2.1 Central Control

The first control topology is central control, shown in Figure 4.1(a). A fast central controller controls each source in a real-time fashion by measuring parameters throughout the system, performing control calculations, then adjusting the output of each source to balance the load. Since all control action is performed in the central controller, a high-bandwidth communications link is required to convey the control information with minimum delay.

The main advantage with controlling the sources from a central point is that a supply-side control law can be implemented easily. Since the central controller is aware of each node in the system, the control law can be directly implemented in the central controller. Another benefit that arises from using a central controller is the ability to dynamically change the control law. This ability is important in commercial power systems to allow the central control system to alter the utilisation priority of the generators such that the most economic mix of generation supplies the load. In the traditional ac power system, this function is referred to as unit commitment and economic dispatch.

One of the main drawbacks with central control is that the reliability of the system is degraded. If either the central controller or communications link malfunction, the system will fail unless redundant controllers and communications links are included in the system.

Another major drawback is that real-time central control of a large multi-input/multi-output nonlinear system requires computing power far beyond that which is available today [44]. For these reasons, central control alone is not commonly used for the control of power systems. Typically, central control is combined with local decentralised control to ease the computational burden on the central controller. This is explained in Section 4.2.5.

4.2.2 Decentralised Control

With decentralised control, each source is independently controlled based on local quantities as shown in Figure 4.1(b). Characterised by the absence of a central controller and communications link, decentralised control is fast, and maintains the reliability inherent in the structure of the system. This control strategy is widely used to control the instantaneous power sharing between parallel-connected sources in both ac and dc systems.

In dc systems, decentralised power sharing between parallel-connected sources is typically implemented using voltage droop control [45, 46, 47]. Without voltage droop, the current supplied by each source to the system is governed by the interconnection impedance between the source itself and the load. Designing each source with a voltage droop characteristic allows the current supplied by each source to be controlled, even in the presence of interconnection impedance. Voltage droop is implemented by decreasing the output voltage of each source as its output current increases. This characteristic is given by

$$V_o = V_{ref} - k \cdot I \tag{4.1}$$

where V_{ref} is the nominal setpoint for the output voltage, k is the droop coefficient, and I is the output current of the module. An example of the use of voltage droop for current sharing between two parallel dc sources is shown in Figure 4.2. The proportion of load current supplied by each source is controlled by adjusting the droop coefficient for each source. The source with the largest droop coefficient supplies the greatest portion of current to the system. As shown in Figure 4.2, the droop coefficient of source 2, k_2, is set approximately half that of source 1 to ensure that it supplies twice as much current as source 1 at the given operating point, V_{bus}. It should be noted that the actual value of each droop coefficient is dependent on the interconnection impedance and the degree of current sharing accuracy required. In the presence of a large interconnection impedance, the droop coefficients must be increased to provide a high degree of current sharing accuracy [48].

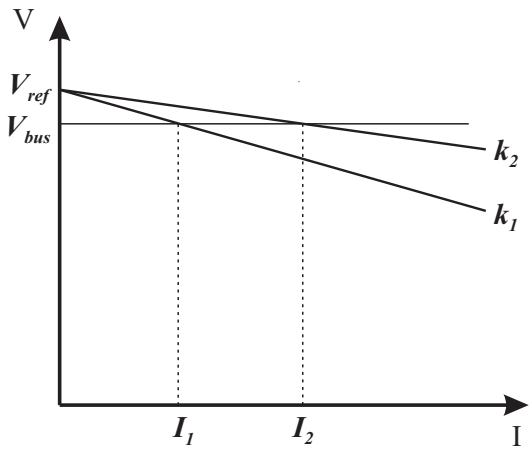

Figure 4.2 Voltage droop characteristics for two parallel dc supplies

In the ac system, another form of droop control is used to control the instantaneous sharing of real and reactive power between parallel connected generators. Frequency droop is used to permit real power sharing, and voltage droop is used to permit reactive power sharing [37].

In both dc and ac systems, the use of droop control results in steady-state error of the controlled quantity. This is evident from the voltage droop characteristics for two parallel dc supplies shown in Figure 4.2. For a total load current of $I_1 + I_2$, a steady-state error of $V_{ref} - V_{bus}$ exists. In dc systems demanding tight voltage regulation, this characteristic can be troublesome; however, a dynamic droop characteristic has been proposed to minimise the steady-state voltage error at high loads [49]. The droop coefficient is increased as the load is increased, reducing the steady-state error.

Although decentralised control is fast, reliable, and eliminates the dependency of the system on a single controller and communications link, it suffers from one major drawback. Implementation of a supply-side control law through independent control of each source is impossible since each source node is unaware of the other source nodes in the system. To implement a supply-side control law, each node must be aware of the other nodes that influence its operation. In a nanogrid for example, the storage node must charge when there is an excess of renewable energy, and discharge when the load exceeds the power from the renewables. Without knowledge of the renewable nodes, the storage node is incapable of obeying the supply-side control law.

4.2.3 Distributed Control

Distributed control, shown in Figure 4.1(c), exhibits characteristics present in both central and decentralised control topologies, having an external communications link but no central controller. As with central control, distributed control permits the implementation of a supply-side control law. The control law is implemented by embedding the portion of the control law related to the operation of each source in the source's local controller. Each source controller communicates with the other nodes that affect its operation in order to determine its own mode of operation. For example, the storage node communicates with the renewable nodes to establish whether they are operating at their MPP. If so, it begins discharging to provide the balance of load power.

A distributed control strategy for a hybrid wind-diesel system has been proposed in [50]. The distributed control strategy is implemented using the controller area network (CAN) system, a serial protocol that has traditionally been used for connecting electronic control units, sensors, and actuators in automotive and industrial applications. The CAN system has a bit speed of up to 1 Mb/s and the communications link is a twisted pair of wires.

The main advantage in adopting distributed control over central control is that the reliability of the system is improved since the system is independent of the central controller. With the control function distributed throughout the network, operation of the system is still possible when a control node malfunctions. However the system is still dependent on an external communications link for correct operation.

Although controlling a power system in a distributed fashion is possible, this control strategy is not widely used since it cannot match the performance and control flexibility a hybrid central/decentralised topology offers. Since the control law is embedded in each source, it can not be readily altered to permit dynamic operation. The control law remains static for all operating conditions.

4.2.4 Hybrid Topologies

The basic control topologies shown in Figure 4.1 can be combined to form hybrid control strategies that exhibit the advantages present in their constituent control strategies. Two such hybrid topologies, hybrid central control and hybrid distributed control, are shown in Figure 4.3.

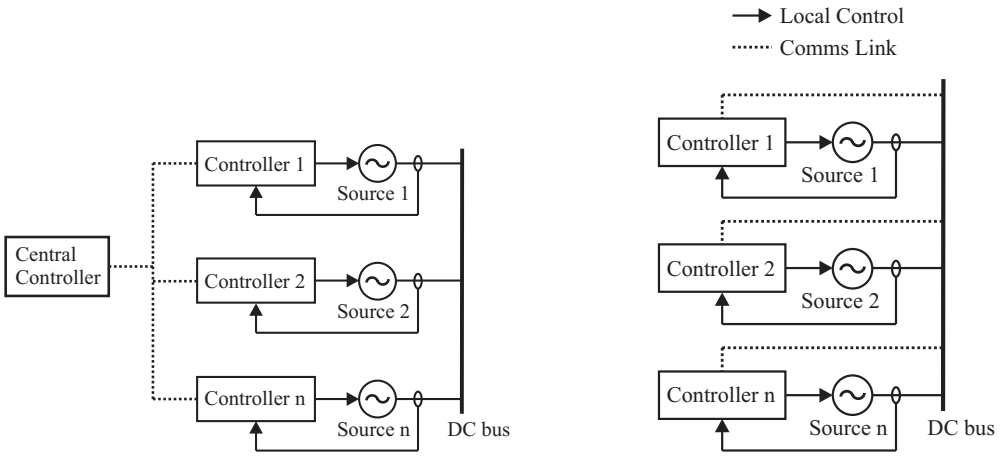

(a) Hybrid central control (b) Hybrid distributed control

Figure 4.3 Hybrid control topologies

4.2.5 Hybrid Central Control

Hybrid central control, a combination of central and decentralised control, is a hierarchial topology as shown in Figure 4.3(a). Decentralised control is used for instantaneous power sharing at the source level, relieving the control burden on the central controller. The task of the central controller becomes one of central coordination rather than real-time control of each node. Due to the inclusion of a central controller, a supply-side control law can be readily implemented.

Hybrid central control still retains the one of the major drawbacks present in central control: the system remains dependent on the central controller and communications link for correct operation. To improve the reliability of the control strategy, redundant controllers and communications links must be included at an extra cost. Nevertheless, hybrid central control generally offers the best compromise between performance and reliability, and this hierarchial topology is widely used for controlling the traditional 50/60 Hz ac system. Local decentralised control in the form of frequency and voltage droop performs instantaneous power sharing. Coordination and management of the system is accomplished using a supervisory control and data acquisition system and an automatic generation control program running on a central computer [2]. The central control system updates the setpoint of each generator, while control of each generator's power output is performed locally. This hierarchial approach, ideal for controlling the traditional ac power system, has also been carried over to the control of small renewable-based systems [51, 52]. However, other forms of hybrid control are capable of offering equal performance in these systems at a reduced cost.

4.2.6 Hybrid Distributed Control

Hybrid distributed control is a control strategy in which the control function is distributed among the source controllers as with distributed control. However, the communication between controllers takes place over the system power bus rather than an external communications link. Thus each source is effectively controlled using local variables as with decentralised control. The structure of a hybrid distributed control scheme is shown in Figure 4.3(b).

Hybrid distributed control combines the advantages of both distributed and decentralised control strategies. A supply-side control law can be implemented since communication exists between sources, and the system has the same reliability advantages as decentralised control since the system is independent of a central controller and external communications link. The lack of an external communications link also reduces the implementation cost of this control strategy. However, hybrid distributed control retains the same disadvantage as distributed control. A supply-side control law implemented using this strategy must be static for all operating conditions since it can not be readily altered.

Although hybrid distributed control is not as widely used in practice as hybrid central control, it is employed in certain niche applications. One of the applications in which this hybrid control strategy is adopted is industrial control schemes that rely on a power line carrier (PLC) system to provide communications between control nodes [53]. The main advantage a PLC scheme offers is that it eliminates the need for an external communications link and central controller. Communication occurs over the system power bus in the frequency range of 3 kHz to 148.5 kHz. However, additional control hardware is required at each node to allow for the modulation and demodulation of the control signals. There are also issues of signal attenuation and limited bandwidth to contend with due to the use of power line as the transmission medium. However, if these issues can be solved, PLC is a reliable method for controlling small systems of up to thirty nodes, where data is continuously exchanged between nodes [54].

Another application for which hybrid distributed control has been proposed is for implementing a demand-side management scheme in a dc network [6, 7]. The system, comprising controlled rectifiers feeding a superconducting dc bus, uses inverters to supply ac loads from the dc bus. The rectifiers are controlled with an active droop characteristic such that the bus voltage falls when there is a power shortage or system overload. Each inverter is then controlled based on the level of the dc bus. A voltage threshold is assigned

to each inverter, and if the dc bus decreases below this threshold, the inverter shuts down. The voltage thresholds are prioritised such that when the bus voltage decreases due to an overload, the loads having a low or medium utilisation priority are shut down first. This action restores the power balance in the system, allowing the high-priority loads to enjoy an uninterrupted supply of power.

It should be noted that using the voltage level of the dc bus to convey system information not only eliminates the need for an external control link and central controller, but also eliminates the need for additional control hardware compared with PLC control. Since the demand-side management scheme relies on the inherent behaviour of the controlled rectifiers and inverters to convey system information using the dc bus, control hardware is not needed to modulate and demodulate the control signals. The only major drawback with this scheme is that because it relies on voltage levels to convey system information, the presence of transmission line impedance has the potential to corrupt the information conveyed between sources.

4.2.7 Topology Selection

A summary of the control topologies presented in this chapter is given in Table 4.1. It can be seen that neither central, decentralised, nor distributed control exhibit all characteristics of the ideal control topology for a nanogrid. Central control potentially offers the best performance, but its implementation requirements render it impractical. Decentralised control has an excellent reliability and low implementation cost but does not lend itself to source scheduling according to a supply-side control law. Distributed control is a possible candidate for the supply-side control topology because it allows the implementation of a supply-side control law and offers improved reliability over central control. However this topology still requires an external communications link to successfully operate.

The two hybrid control strategies offer an improvement over the three basic control topologies. Hybrid central control offers similar advantages to central control at a greatly reduced cost since local decentralised control is employed for instantaneous power sharing. Although this strategy requires redundant controllers and communications links to ensure reliability, it is a definite option for controlling a nanogrid since it allows the implementation of a supply-side control law via a central supervisory controller.

Hybrid distributed control is also another possibility since it offers virtually the same benefits as hybrid central control without the need for a central controller or communications

Table 4.1 Summary of control topologies

Topology	**Advantages**	**Disadvantages**
Central	Potential to offer best performance	Impractical to implement
Decentralised	Simple and reliable. No external controller or communications link required	Cannot implement a supply-side control law
Distributed	Improved reliability over central control	Requires an external communications link
Hybrid central	Offers similar performance as central control at a reduced cost	System dependent on a central coordinator and communications link
Hybrid distributed	Simple and reliable. No external controller or communications link required	Limit to size of two-way line carrier systems. Transmission line impedance has potential to corrupt information

link. This strategy is inherently more reliable than hybrid central control because each node operates using terminal quantities measured from the dc bus. The implementation cost is consequently reduced because redundant controllers and communications links are not needed to maintain reliability.

Hybrid distributed control is therefore adopted since it meets the selection criteria and achieves a high degree of reliability without the need for redundant controllers or communications links. Although it does not have the ability to dynamically change a control law as those schemes using a central controller do, this capability is unnecessary in a nanogrid since the utilisation priority of the sources is unlikely to change as with sources in the central ac system.

Chapter 5

DC BUS SIGNALLING

5.1 INTRODUCTION

DC bus signalling (DBS) is the term used to describe the mechanism by which the source interface converters in a nanogrid are controlled to implement a supply-side management strategy using hybrid distributed control. DBS is implemented through control of the source/storage interface converters in a nanogrid. Each converter is assigned a voltage threshold to trigger the point at which it begins discharging into or charging from the system. The converters not only respond to the level of the dc bus, but they also change the level of the dc bus when their maximum power output is exceeded, thus automatically controlling other converters in the system.

DBS is a novel control strategy since the concept of using the level of the bus voltage to convey system information has only been proposed for demand-side management in a dc system having an ideal transmission network [6, 7]. This chapter explains the theory of operation behind DBS and describes a method for implementing a supply-side control law in a practical system that comprises transmission line impedance. To ensure that the supply-side control law operates accurately in the presence of transmission line impedance, a method for calculating the voltage thresholds is given. For completeness, a method for implementing a demand-side control law in a practical system using DBS is presented and the limitations of DBS are discussed.

5.2 MECHANISM OF DBS

The mechanism of DBS is based on controlling the source and storage interface converters to exhibit different modes of operation when discharging and charging. The operating

mode for each converter is dependent on two factors: the level of the dc bus in relation to its voltage threshold, and the maximum output power of the source.

5.2.1 Discharging

Discharging action occurs when a source/storage interface converter injects power into the nanogrid. When discharging, the interface converter exhibits three modes of operation: off, constant voltage with droop, and constant power. The converter remains off until the bus voltage decreases below its voltage threshold. At this point, the converter comes online, acting as a constant voltage source with a droop characteristic in a bid to regulate the dc bus at its voltage threshold.

When the power drawn from the converter exceeds the maximum power point (MPP) of the renewable source or the power rating of the interface converter, the converter enters constant power mode, limiting its output power to this maximum value. As load changes and variations in the MPP of the renewable source cause the converter to switch between constant voltage and constant power operation, the voltage level on the dc bus changes. These voltage level changes in turn affect the operation of other source/storage interface converters with different voltage thresholds.

The use of DBS to schedule interface converters discharging into a nanogrid is illustrated in Figure. 5.1. The example system, portrayed in Figure. 5.1(a), comprises a renewable source, a non-renewable source, and a constant power load. The control law for the system has two operating states to prioritise the utilisation of these sources. In state 1, only the renewable source is online, and in state 2, the non-renewable source comes online. The control law is implemented by assigning the renewable source to discharge at voltage threshold V_0, and the non-renewable source to discharge at voltage threshold V_1, as shown in Figure. 5.1(b).

With a load of PL1, the system operates at point A in Figure. 5.1(b). The renewable source interface converter alone is online since the load is less than the MPP of the renewable source, PS1. The converter operates in constant voltage mode, regulating the bus voltage to its voltage threshold, V_0. In constant voltage mode, the bus voltage decreases slightly as the load current increases due to the voltage droop characteristic of the converter.

When the load exceeds the MPP of the renewable source, increasing to PL2, the renewable source interface converter operates in constant power mode, limiting its output power to PS1. When the converter shifts operation to the constant power region, the bus voltage

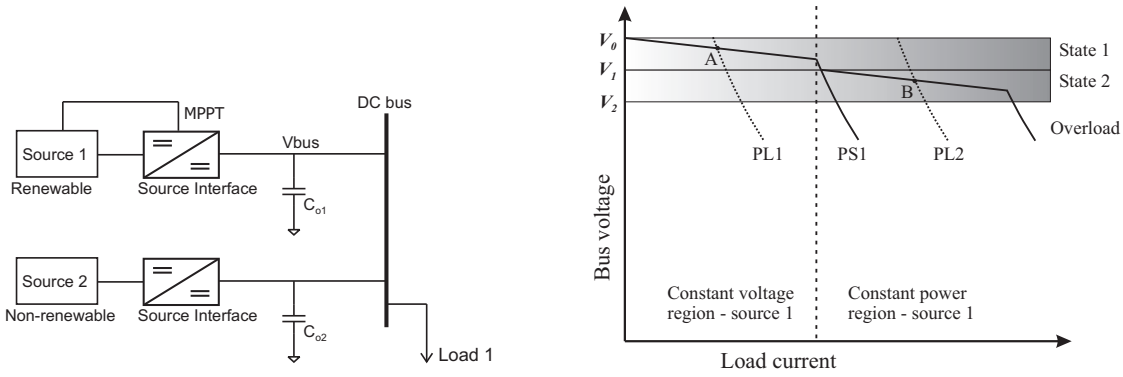

(a) System with discharge scheduling (b) DBS operation - discharge

Figure 5.1 Discharge scheduling with DBS

tends to collapse since the constant power load attempts to use more power than the system can provide. The converters' output capacitors temporarily support the dc bus; therefore the decrease in the bus voltage is given by

$$V_{bus}(t) = \sqrt{\frac{2}{C_{bus}} \int_0^t \left(P_{S1}(t) - P_{L2}(t)\right) dt} \tag{5.1}$$

When the bus voltage decreases to threshold V_1, the non-renewable source interface converter comes online to supply the balance of power. The system now operates at point B.

It should be noted that with DBS, the operating point of the system is not only dependent on the load, but also on the MPP of the renewable source. For example, at operating point A, if the MPP of the renewable source decreases below PL1, the bus voltage collapses to threshold V_1, bringing the non-renewable source online earlier than before. Thus DBS maintains the power balance in the system in the presence of both load and supply changes.

Another point worthy of mention is that the discharging mechanism of DBS only functions correctly if each source comes online the instant the bus voltage decreases to its voltage threshold. For storage nodes, this requirement presents no problems; however, for nodes such as fuel cells and backup generators, a finite startup time or ramp up time prevents the source from immediately supplying the sudden power demand increase. Consequently, the bus voltage will tend to collapse due to the power shortfall. As the bus voltage decreases, sources with a lower priority that can respond instantly will come online or loads will be shed in accordance with the demand-side control law which explained in Section 5.5. In the interest of maintaining a seamless supply of power to the system, other measures can be implemented. A transient overload capability can be added to the storage interface

converters or short-term storage can be combined with a fuel cell or generator to idealise its startup response. These solutions will be discussed further in Section 8.6.

5.2.2 Charging

The charge mechanism of the storage interface converter is similar to the discharge mechanism of the source/storage interface converters. The storage interface converter has two voltage thresholds, one for discharging, and another for charging. With just a single storage node in the system, these voltage thresholds may be identical; however, with multiple storage nodes in the system, each voltage threshold must be calculated using the procedure outlined in Section 5.4.

When charging, the storage interface converter exhibits three modes of operation: off, constant voltage, and constant power. These operational modes are determined by the level of the bus voltage in relation to the storage interface converter's voltage threshold for charging. Compared with discharging, the operational modes are triggered by a rising bus voltage rather than a falling bus voltage since charging tends to collapse the dc bus rather than support it.

The storage interface converter remains off while the bus voltage is below its voltage threshold for charging. When the bus voltage rises above this voltage threshold, indicating excess renewable power in the system, the converter begins charging the storage device by operating in constant voltage mode. The converter draws power from the system in a bid to regulate the dc bus at its voltage threshold. It should be noted that a droop characteristic may be added to the converter in constant voltage mode to allow it to share power with any other storage nodes that are present in the system. When operating in constant voltage mode, the storage interface converter may limit the power it draws from the system to prevent the storage device from charging at a dangerously high rate. This mode of operation is known as constant power limit.

The use of DBS to schedule the charging action of storage interface converters is illustrated in Figure 5.2. The example system comprises a renewable source, a constant power load, a low-priority storage node, and a high-priority storage node as shown in Figure 5.2(a). The high-priority storage node is short-term storage and the low-priority node is long-term storage. The storage nodes are assigned in this fashion such that the short-term storage is used in preference to the long-term storage. The storage nodes do not exhibit a voltage droop characteristic since the nodes take different utilisation priorities. Power

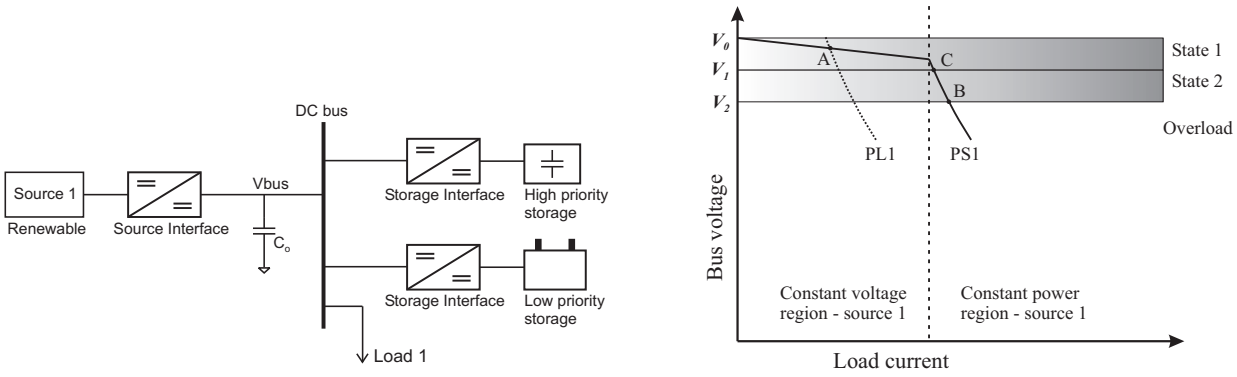

(a) System with charge scheduling (b) DBS operation - charge

Figure 5.2 Charge scheduling with DBS

sharing between the storage nodes is not required.

The control law requires two operating states to prioritise the charging of the storage nodes. In state 1, both storage nodes are charging, while in state 2, only the high-priority storage node is charging. To implement the control law, the low-priority storage is assigned a voltage threshold of V_1, while the high-priority storage has a lower voltage threshold of V_2 as shown in Figure 5.2(b).

Initially the load on the system is PL1, and both storage nodes are off. The system therefore operates at point A as shown in Figure 5.2(b). When the storage nodes are brought online, both storage nodes attempt to charge since the bus voltage is above their voltage thresholds. However, the storage assigned to state 2 takes precedence since it has the lower voltage threshold. The high-priority storage acts as a slack bus, drawing the balance of power from the system in order to regulate the bus at its voltage threshold, V_2. The system therefore operates at point B. The power transferred to the storage device is the difference between the MPPT of the source and the load power, PS1 - PL1.

When the high-priority storage has completed charging, the bus voltage rises, allowing the low-priority storage to begin charging. The low-priority storage interface draws power from the system in order to regulate the bus voltage at its voltage threshold, V_1. The system therefore operates at point C. When the low-priority storage has finished charging, the system resumes operation at point A.

It is important to note that the voltage thresholds for charging are set in the maximum power region of the renewable sources to ensure that the storage interface extracts maximum power from the source while charging. If the voltage thresholds are set in the constant voltage region, the storage interface converters are unable to extract maximum excess power from the renewable sources.

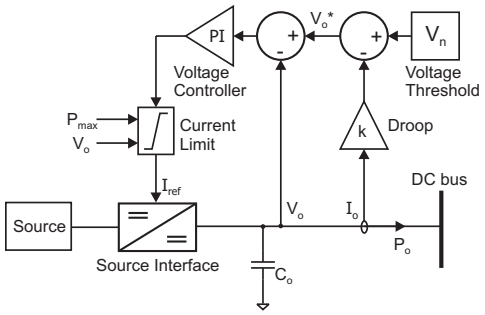

Figure 5.3 Discharge controller

5.3 CONVERTER CONTROL STRUCTURE

The previous section outlined the mechanism by which DBS operates. This section describes the control structure required for the source/storage interface converters such that they exhibit different modes of operation based on the dc bus voltage and the converter's voltage threshold for discharging or charging. It will be shown that a voltage controller with a droop characteristic implements constant voltage mode, and a dynamic current limit implements off and constant power modes of operation.

5.3.1 Discharge Controller

The control structure required to implement the three discharge modes of operation is shown in Figure 5.3. The control structure is two-tiered, comprising a fast inner current control loop and a slower outer PI voltage control loop. The current loop controls the converter's output current; however, for simplicity it is not shown since it is an order of magnitude faster than the voltage loop. A dynamic current limit is included between the voltage and current loops to allow the output power of the converter to be limited.

In constant voltage mode, the PI controller regulates the output voltage of the converter to its voltage threshold by providing a reference current to the inner loop. A voltage droop characteristic is included in this mode to permit sharing of the load current between other source/storage interface converters assigned to the same voltage threshold. With voltage droop, the setpoint for the output voltage is given by

$$V_o^* = V_n - k \cdot I_o \tag{5.2}$$

where V_n is the voltage threshold of the converter, I_o is the output current of the converter, and k is the droop coefficient.

The dynamic current limit is used to implement off and constant power modes. When the bus voltage is above the voltage threshold, the converter must be off as converters with a higher utilisation priority are capable of supplying the load. Under these conditions, the PI voltage controller attempts to provide a negative reference current to the inner loop. Therefore imposing a lower limit of zero on the reference current deactivates the converter when the bus voltage rises above the converter's voltage threshold for discharging.

Constant power mode is implemented by dynamically adjusting the upper limit for the reference current to

$$I_{ref\ max} = P_{max}/V_o \tag{5.3}$$

where P_{max} is the MPP of the renewable source or the peak discharge rating of the storage device, and V_o is the bus voltage. Thus as P_{max} or V_o change, the reference current limit is altered such that the peak output power of the converter tracks P_{max}.

5.3.2 Charge Controller

The control structure required to implement the three charge modes of operation takes the same form as the discharge controller shown in Figure 5.3. However, since the power flow is reversed in charge mode, the operation of the charge controller has subtle differences compared to the discharge controller.

The PI control gains are different because the dynamics of the system change when the power flow is reversed. The control gains are calculated taking into account the dynamics of other storage interface converters supplying power to the system. This will be explained in more detail in Section 7.3. In addition, the PI controller supplies a negative reference current to the storage interface converter, allowing the three modes of operation to be triggered by a rising bus voltage.

The converter remains off while the bus voltage is below its voltage threshold for charging. Under this operating condition, the charge controller attempts to supply a positive current to the storage interface to increase the bus voltage. Since the limit for the minimum charge current is zero, the converter effectively remains off.

When the bus voltage rises above the voltage threshold for charging, the converter begins charging the storage device by operating in constant voltage mode. The charge controller regulates the dc bus at its voltage threshold by drawing power from the system. In

constant voltage mode, the reference voltage for the bus voltage exhibits a voltage droop characteristic as given by Equation (5.2). It should be noted that the droop relationship causes the bus voltage to increase as the charging current increases because I_o is negative under charging conditions. This increase in bus voltage permits power sharing between other storage devices having the same voltage threshold.

As with the discharge controller, a power limit is imposed on the interface converter by dynamically adjusting its current limit to P_{max}/V_o. With the storage charger, the purpose of the power limit is to prevent the storage from charging at a dangerously high rate. The charge limit is set by calculating P_{max} as follows:

$$P_{max} = (I_{charge\ max} \cdot V_{storage})/\eta \tag{5.4}$$

where $I_{charge\ max}$ is the peak charge current, $V_{storage}$ is the operating voltage of the storage device, and η is the efficiency of the storage interface converter.

5.4 IMPLEMENTATION OF A SUPPLY-SIDE CONTROL LAW

In a hybrid renewable nanogrid, the sources must be consumed in a prioritised fashion to maximise use of the renewable sources. The utilisation priority for the sources is defined by a supply-side control law, which consists of a number of operating states. The control law is implemented using DBS by prioritising the voltage thresholds for the interface converters. To ensure correct operation of the system, the voltage thresholds must be calculated to ensure that each converter can accurately determine the current operating state.

To prioritise the sources that discharge into the system, the sources that take the higher priority operating states are assigned to come online at higher voltage thresholds than the lower priority sources. Since the voltage level of the dc bus decreases when a group of sources reach their MPP, those sources with the higher voltage thresholds come online first.

Prioritising the charging of storage nodes is accomplished in the opposite fashion, since charging tends to decrease the bus voltage rather than support it. The storage devices with the highest charging priority are assigned the lowest voltage thresholds.

The voltage thresholds are calculated beginning with the highest threshold. Each successive threshold is calculated to ensure that when the sources assigned to the previous

threshold are online, voltage drop in the system, caused by transmission line resistance and voltage droop, does not prematurely activate sources assigned to the next threshold. In general, the first voltage threshold, V_0, is set to the nominal operating voltage of the system. Each successive voltage threshold, V_n, is calculated by subtracting the voltage drop and a margin of error from the preceding threshold:

$$V_n \leq V_{n-1} - Vd_n - V_e \tag{5.5}$$

where

- V_{n-1} is the preceding threshold, corresponding to operating state $n-1$.
- Vd_n is the maximum voltage drop that occurs with the system operating in the state $n-1$
- V_e is a margin of error that accounts for measurement inaccuracies and voltage ripple on the dc bus.

A dc load flow of the system is performed to determine the worst-case voltage drop, Vd_n, in (5.5). The dc load flow is similar to conventional ac load flow algorithms based on the iterative Newton Raphson technique. The dc load flow calculates the power generated or absorbed at each bus using

$$P_i = \sum_{j=1}^{k} V_i \ (V_i - V_j) \ g_{ij} \tag{5.6}$$

where V_i is the bus voltage, V_j is the voltage of an adjacent bus, and g_{ij} is the conductance between bus i and bus j. To solve the power flow equation, the voltage at each bus is incremented each iteration using the Newton Raphson technique until the mismatch between the calculated and scheduled powers for each bus is negligible.

The dc load flow is performed with the system operating in state $n-1$ for all permutations of generation and loading conditions. The worst-case voltage drop is the difference between threshold V_{n-1} and the minimum voltage at the point where any source assigned to threshold V_n is connected with the system.

It should be noted that a typical nanogrid comprises only three operating states. The renewable sources are assigned to the first operating state, and the storage and backup generator are assigned to the second and third operating states. This means that only three separate load flows need to be performed.

5.5 DEMAND-SIDE MANAGEMENT

This chapter has thus far focussed on the implementation of a supply-side control law since this control strategy was chosen as the primary means of maintaining the power balance in the nanogrid. Nevertheless, including demand-side management in the overall system control strategy provides two major benefits to a nanogrid. Firstly, demand-side management in the form of load shedding reduces the peak load demand. With supply-side management alone, a nanogrid must be designed to meet the peak load demand. In a standalone system, the peak load demand can often be as high as five times the average load, as shown in Figure 2.4. Load shedding reduces the peak demand, lowering the cost of the system.

Load shedding also prevents the dc bus from collapsing under overload conditions, ensuring that critical loads enjoy an uninterrupted supply of power. As the bus voltage begins to collapse due to a shortfall in power or excessive load, low priority loads are tripped out to restore the power balance and prevent the dc bus from collapsing.

5.5.1 Mechanism

Research has shown that prioritised load shedding can be accomplished in power electronic based dc systems by shutting down the load converters based on the voltage level of the dc bus [6, 7]. Each load converter is assigned a shutdown threshold according to the utilisation priority of the load it supplies. When the dc bus voltage decreases below the load interface converter's shutdown threshold, the converter reduces its output current to zero, effectively shedding the load. By prioritising the shutdown thresholds, low-priority loads are shed first under overload conditions, ensuring that power is maintained to the high-priority loads.

This same technique can easily be applied to a nanogrid by adding a shutdown mode to the load interface converters and setting the shutdown thresholds for the converters in a prioritised fashion. A graph showing the control mechanism used to implement prioritised load shedding in a nanogrid for two loads of different priority is shown in Figure 5.4.

Figure 5.4(a) shows the load interface converter control characteristic for the low priority load. Under normal operating conditions, the load interface converter acts as a constant power load on the system. However, when the bus voltage decreases below the load interface converter's shutdown threshold, Vs_0, the converter turns the load off. Compared

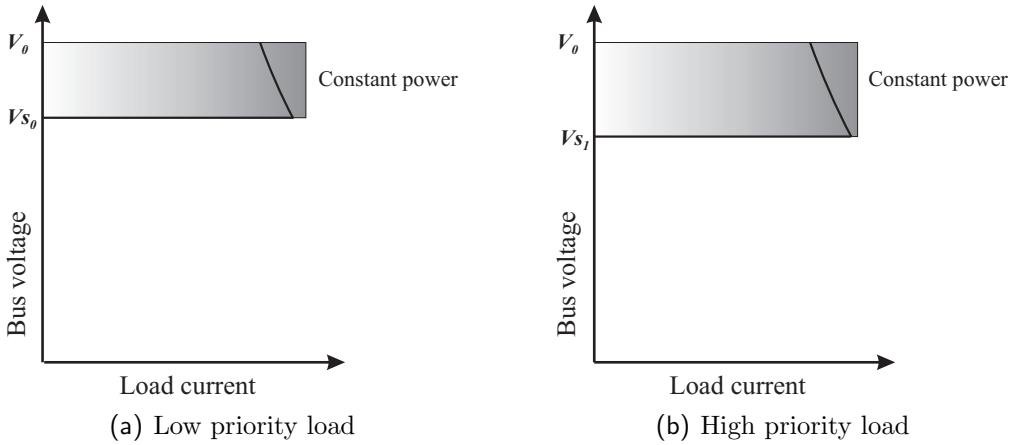

Figure 5.4 Load shedding through control of load interface converters

with the load shedding mechanism in [6, 7], the load interface converter reduces its output current to zero immediately rather than entering a voltage dependent current limit (VDCL) mode. This prevents sensitive loads from experiencing half their nominal rated voltage while the converter is shutting down.

The load interface converter connecting the high-priority load to the system is controlled in a similar fashion. However the threshold at which the converter shuts down, Vs_1, is set lower than the shutdown threshold for the low priority load as shown in Figure 5.4(b). This ensures that during supply shortfalls, the low-priority load is tripped out first.

5.5.2 Calculating the shutdown thresholds

The effect of transmission line impedance on the load shedding mechanism presented in [6, 7] was not considered as it was assumed the transmission network uses superconducting cable to minimise resistive losses. In a nanogrid however, the transmission network is non-ideal therefore the effect of transmission line impedance must be considered in order for the load shedding to operate successfully. The shutdown thresholds must be calculated such that the shutdown priority of the loads remains unaffected by the unequal propagation of the dc bus voltage throughout the system.

The shutdown threshold for the lowest priority load is calculated first as follows:

$$Vs_0 = V_n - Vd_n - V_e \tag{5.7}$$

where V_n is the lowest voltage threshold, Vd_n is the worst-case voltage drop that occurs in the system with the system operating in state n, and V_e is a margin of error to account

for ripple on the dc bus and measurement tolerances. A dc load flow program similar to that outlined in Section 5.4 is used to calculate the voltage drop, Vd_n. The voltage drop is found by analysing the system for all possible loading conditions in state n. It is the difference between V_n and the lowest voltage at the connection point of a load assigned to shutdown threshold Vs_0 with the system.

Each successive shutdown threshold is calculated using

$$Vs_n = Vs_{n-1} - Vd_n - V_e \tag{5.8}$$

where Vs_{n-1} is the previous shutdown threshold. In other words, each successive threshold is calculated by subtracting for the maximum steady-state difference in the bus voltage between the load interface converters assigned to adjacent shutdown thresholds.

5.6 LIMITATIONS OF DC BUS SIGNALLING

While DBS is ideal for controlling sources in hybrid renewable systems, the limitations that arise as a result of using distributed control preclude it from use in more mainstream applications such as a control of a free-market power system. With the use of DBS, the power sharing between sources assigned to the same voltage threshold can not be as precisely controlled as with central control. Furthermore, the supply-side control law is static.

5.6.1 Power Sharing Between Sources

With central control, the power supplied by each source to the network is set by the central controller. The central controller, aware of each node in the system, dispatches the power to be supplied by each node. With DBS however, the power supplied by each source is not so precisely controlled.

When multiple sources are assigned to the same voltage threshold, they may not come online at exactly the same instant. This phenomenon is the result of transmission line impedance causing the dc bus voltage to propagate unequally through the system. Sources assigned to the same threshold experience different voltages if they are connected to different points of the transmission network.

This indeterminate behaviour may be insignificant when the interconnection impedance between a group of sources assigned to the same voltage threshold is small. However, with a large interconnection impedance, such as in the case of two sources with the same voltage threshold being connected to the two extremes of a network, the behaviour may be significant. Droop is used in a bid to minimise this effect and to maintain power sharing between sources of the same priority at to a predetermined ratio. Even with the inclusion of droop, the transmission line impedance still impacts on the power sharing between sources more so than with central control.

It should be mentioned that indeterminate triggering of the sources due to transmission line impedance is not a problem in a nanogrid provided the thresholds have been calculated correctly. By accounting for the worst-case voltage drop across the transmission line, premature triggering of sources assigned to a lower voltage threshold is prevented. In a free-market system however, indeterminate triggering of the sources may be a problem. In this type of system, the point at which the sources come online should be set by a central controller to allow economic dispatch rather than being determined by the operating point of the system.

5.6.2 Static Control Law

Another reason why DBS is unsuitable for application to a free-market system is that a supply-side control law implemented using DBS is static, determined by the voltage threshold to which each source is assigned. In a free-market system, a dynamic control law is needed since the utilisation priority of each source changes as generation prices fluctuate.

To allow power dispatch based on bidding, a more advanced control system, such as a hybrid central control system, is needed. The control system must change the utilisation priority of the generators in the system as the generation cost changes. This more complicated operation of the generators is not possible in a system that uses DBS, as the control law is static, fixed by the voltage threshold to which each node is set.

Although DBS does not permit a dynamic control law, this type of control law is unnecessary in a system that is primarily based on uncontrollable renewable sources because a different set of operating conditions prevail. The system is sized such that the renewable sources supply the average load demand, and optimal economical operation is achieved by maximising use of the renewable sources. The use of the controllable sources, the storage

and backup generation, is kept to a minimum. These are only brought online to maintain the power balance in the system. With such an arrangement, a fixed control law is all that is necessary to manage the sources because the utilisation priority of the sources remains fixed. However, the main point to note is that DBS is unsuitable for application to a deregulated power system where the utilisation priority of generation changes in accordance with the fluctuating supply cost.

5.7 SUMMARY

DBS is a novel hybrid distributed control strategy that relies on voltage level changes on the dc bus to convey information used for implementing supply and demand-side control laws. DBS is made possible with the use of power electronic converters to interface sources and loads to a dc system. The mechanism of DBS relies on each source/storage interface converter exhibiting different modes of operation based on the voltage level of the dc bus in relation to the voltage threshold of each converter. In discharge mode, the converter is off while the bus voltage is above the voltage threshold. When the bus voltage decreases below the voltage threshold of the converter, the converter comes online, acting as a constant voltage source with a constant power limit. Charge mode works in the opposite fashion, being triggered by a rising bus voltage, since the power flow is reversed.

A supply-side control law is implemented using DBS by setting the voltage thresholds for the source/storage interface converters in the sequence defined by the control law. The thresholds must be calculated to prevent voltage drop in the system from prematurely activating a source in the next state.

DBS has a number of significant advantages in small renewable based systems such as nanogrids:

- Using DBS minimises the control hardware requirements compared to the traditional hybrid central control strategy. A dedicated communications link and central controller are not required since communication occurs as a result of the source/storage interface converters changing operating modes, thereby inducing voltage level changes on the dc bus.

- DBS maintains the reliability present in the distributed structure of a nanogrid as each node is effectively controlled using terminal quantities.

- DBS also maintains the modularity of the system by allowing each node to operate independently. The control technique allows plug-and-play operation of the system, facilitating easy modification and expansion. Nodes can be added to the system by simply setting the voltage threshold for that node. Reconfiguration of the central controller and extending the communications network is not required.

DBS is well-suited for application to a nanogrid because in such a system where uncontrollable renewable sources supply the average load demand, the primary control focus is on maximising use of the uncontrollable renewable sources. However DBS falls short in free-market systems where dynamic control laws are needed to allow more flexible operation. A more complicated control system is needed to permit system-wide operations such as bidding, unit commitment, and economic dispatch.

Chapter 6

MODELLING AND SIMULATION RESULTS

6.1 INTRODUCTION

This chapter presents a nanogrid model from which simulation results are obtained to verify the operation of DBS. Generic models for each nanogrid component are presented and these models are combined to form an overall nanogrid model that is based on an example system.

The means by which supply and demand-side control laws are implemented using DBS is illustrated by developing these control laws for the nanogrid model. The procedure for ensuring these control laws operate successfully in the presence of transmission line impedance is also delineated. A dc load flow is performed for the nanogrid model to determine the propagation of the dc bus voltage throughout the system, allowing the voltage and shutdown thresholds for the source and load interface converters to be set accordingly. The simulation results demonstrate the effectiveness of the supply and demand-side control laws. The supply-side control law maintains the power balance in the system in the presence of supply and load changes by scheduling the sources. Under overload conditions, the demand-side control law maintains a supply of power to high-priority loads by shutting down lower priority loads.

6.2 NANOGRID MODELLING

The nanogrid was modelled in a modular fashion to allow the structure of the nanogrid model to be easily modified. The nanogrid model was implemented using MATLAB since this package is well-suited for implementing complex control functions such as the different control modes present in the source interface converter. Each module was implemented

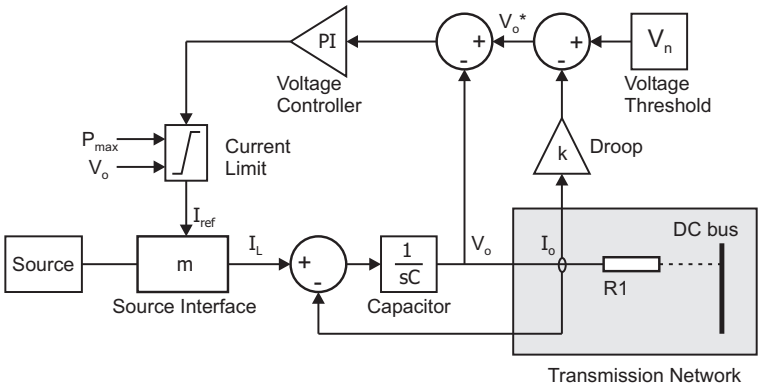

Figure 6.1 Source interface model

using MATLAB functions, and the MATLAB functions were combined in the SIMULINK environment to form the complete model.

A major drawback with using MATLAB to simulate a system of power electronic converters is its slow simulation time. To circumvent this problem, simplified models of the nanogrid components were implemented. High-frequency phenomena such as converter switching dynamics were ignored to speed up the simulation time. In addition, the time constant of the loads was increased to allow a complete simulation to be performed over a shorter time scale than in a real-life system. Although these simplifications impacted the accuracy of the transient response of the system, it should be noted that the purpose of the simulation model was to verify the operation of DBS for implementing supply and demand-side control laws, not to analyse the transient response of the system.

6.2.1 Source Interface

As explained in Section 5.3.1, the source interface is a current-controlled converter, using a fast inner current loop to regulate the inductor current and a slower outer voltage loop based on a PI controller to regulate the output voltage of the converter. The model for the source interface converter, shown in Figure 6.1, includes the PI controller, the voltage droop characteristic of the converter, and the converter's output capacitance. The high frequency switching dynamics of the converter are ignored by modelling the converter as an ideal current loop. The current loop is represented by a gain, m, which is the gain of the current loop, I_L/I_{ref}. This simplification assumes that the inductor current tracks the reference current instantaneously. The simplification is valid since the bandwidth of the current loop is an order of magnitude faster than that of the voltage loop.

Changes in the MPP of the renewable source supplying the source interface converter are

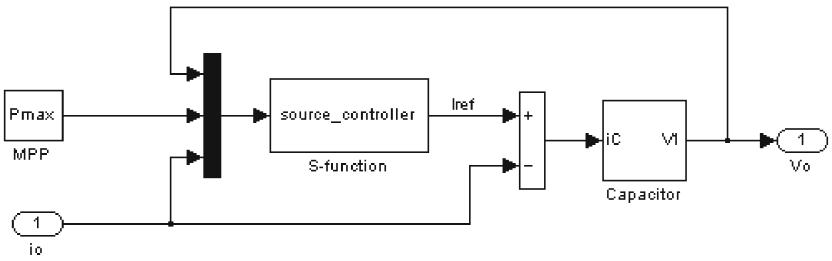

Figure 6.2 SIMULINK implementation of source interface

also included in the source interface model since these fluctuations affect the converter's output power. These changes in the MPP are modelled by varying P_{max}, the maximum power limit signal. This signal controls the maximum output current of the converter, as the peak value of I_{ref} is given by P_{max}/V_o. Consequently, the MPP is modelled as a varying current limit. Since the non-renewable sources do not have a MPP characteristic, P_{max} is held constant for the source interface converters that are supplied by these non-variable sources.

The implementation of a generic source interface converter model in the SIMULINK environment is shown in Figure 6.2. The dynamics of the PI controller and current limit are implemented as a custom MATLAB s-function and the capacitor is modelled using an integrator block. The generic converter model is customised to represent a specific source interface converter by adjusting the parameters that characterise its operation. These parameters, portrayed in Figure 6.1, are V_n, P_{max}, C, k_p, and k_i, where k_p and k_i are the gains of the PI controller.

6.2.2 Load Interface

In practice, the load interface is a dc-dc or dc-ac switching converter. For simulation purposes however, the switching dynamics of the load interface converter are ignored and the converter is modelled as a constant power load. As explained in Section 2.5, the load interface converter exhibits constant power characteristics because the power it draws from the system is constant up to the bandwidth of the voltage control loop. The dynamics of the constant power load, P_L, are represented using

$$\dot{P}_L = \tau(P_L^* - P_L) \tag{6.1}$$

where P_L^* is the setpoint of the load and τ is the time constant of the load.

Each constant power load is included in the simulation model as a resistor in the transmission network. For each timestep of the simulation, the dynamics of each constant power load are converted to a resistance, R_L, as follows:

$$P_{L,k+1} = P_{L,k} + \tau \cdot h(P_L^* - P_{L,k}) \tag{6.2}$$

$$R_{L,k+1} = V_L^2 / P_{L,k+1} \tag{6.3}$$

where V_L is the load voltage, and h is the timestep of the simulation.

In situations where a demand side control law is used, a load shedding capability is added to the constant power load model by setting P_L^* to zero when the bus voltage decreases below the load's shutdown threshold.

6.2.3 Storage Interface

In practice, the storage interface converter is bidirectional, allowing the storage device to both charge from and discharge into the system. The storage interface converter model is almost identical to the source interface converter model shown in Figure 6.1. In discharge mode, the PI controller provides a positive reference current to the idealised current loop to model power flow from the storage device to the system. In charge mode, the parameters of the PI controller, current limit, and voltage threshold are simply altered. This allows the PI controller to supply a negative reference current to the inner current loop to model charging action.

6.2.4 Transmission Line

Although a practical transmission line has resistance, inductance, and capacitance, the transmission line model only includes the effect of resistance. Inductance and capacitance are ignored since these parasitic components only affect the high-frequency dynamics of the system. The transmission system is therefore modelled as a resistive network. Represented by a matrix, the branch currents are solved at each time step using the known node voltages.

6.3 CASE STUDY

6.3.1 System Characteristics

The simulation model is based on a case study that encompasses two generation/load buses that are located 1 km apart as shown in Figure 6.3. The primary sources of generation for the nanogrid are a wind turbine and photovoltaic array. A battery bank and backup diesel generator are included to maintain a continuous supply of power in the presence of the stochastic sources and loads. The nominal operating voltage of the system is 700 V, and the transmission line is an overhead network that has a dc resistance of 1 Ω/km. A droop coefficient of 1 V/A is used to permit power sharing between the renewable sources when they are online simultaneously.

The system is sized such that the average output from the renewable sources exceeds the average load demand. The average combined load is 2 kW and the peak load is 8 kW. The peak output power of the PV array is 2 kW, and the peak output of the wind turbine is 3 kW. Due to the stochastic nature of these sources, the average combined output of the PV array and wind turbine is significantly less than 5 kW. The PV array only produces power during daylight hours, and the wind speed experienced by the wind turbine is often less than the full rated wind speed. Assuming five peak daylight hours per day and a wind turbine capacity factor of 60%, the average combined output of the renewables is 2.2 kW.

The battery bank and backup generator are sized to meet the average load demand during an absence of renewable energy. The charge/discharge rating of the storage device is 2 kW, and the generator is also rated at 2 kW. It should be noted that although it is possible to optimally size the generation present in a hybrid system using linear programming techniques [5], this analysis has not been performed on the case study. The purpose of the simulation is to test the operation of DBS in the presence of fluctuating sources and

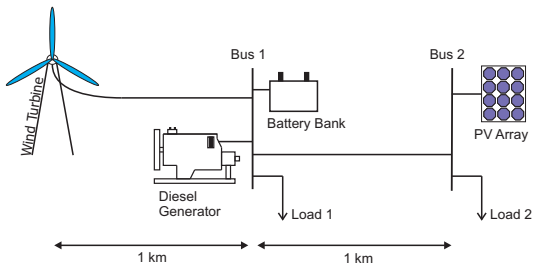

Figure 6.3 Case study

Table 6.1 Parameters of nanogrid components

Source Interfaces	P_{max}: 0-3 kW C: 2.2 μF k_p: 0.02 k_i: 200
Storage Interface	P_{max}: 2 kW C: 2.2 μF k_p (charge): 0.02 k_i (charge): 200
Loads	P_{max}: 5 kW τ: 200 s

loads, not to precisely size the generation in the most economical fashion.

6.3.2 Implementing the Nanogrid Model

Implementing a nanogrid model to represent the case study is a three-stage process. Firstly, source and storage interface modules are created to have the same characteristics as the sources in the case study. Because the nanogrid is modelled in a modular fashion, this process simply involves adjusting the parameters of generic converter models such that the converters represent the sources and loads in the case study. The parameters of the source, storage and load converter models are given in Table 6.1. The time constant of the load is selected to be 200 s to allow load changes to occur in under 5 ms, allowing for a rapid simulation.

In order to design the PI controller for the source interface, the open loop transfer function of the voltage loop for the source interface converter was first derived. A bode plot was then drawn using a value of 1 kΩ for the load resistance. A crossover frequency of 1 kHz was selected in order to provide a good transient response. Using these parameters, the proportional and integral gains, k_p and k_i, were calculated to be 0.02 and 200 respectively. The transfer function of the system and design procedure are explained in detail for the experimental system in Section 7.3.1. The PI control gains for the storage interface were designed using a similar procedure which is also detailed in Section 7.3.1.

Next, the equation for the transmission network is derived using the schematic of the case study, shown in Figure 6.4. In the schematic, V1 represents the wind turbine, V2 the PV array, V5 the storage, and V6 the backup generator. The constant power loads, denoted by

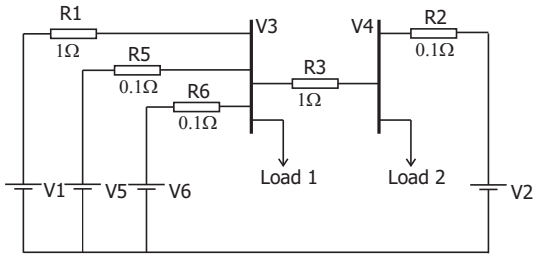

Figure 6.4 Schematic of case study

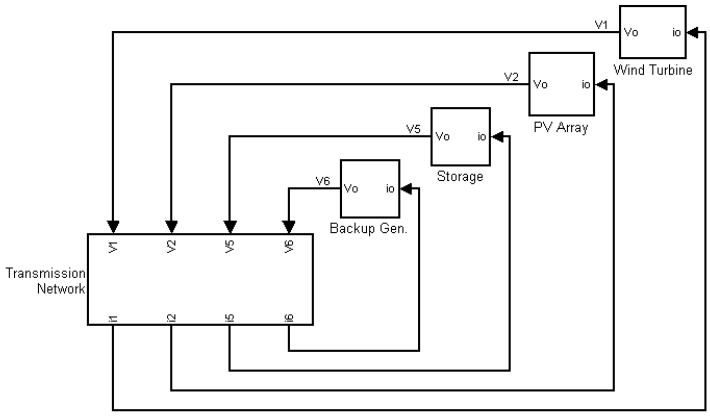

Figure 6.5 Top-level Simulink representation

Load 1 and Load 2, are included in the transmission network model as dynamic resistances, which are modelled using Equation (6.3). Finally, each converter model is connected to the transmission line model in the SIMULINK environment as shown in Figure 6.5. The output voltage of each converter is connected to the appropriate input port of the transmission line model. Each time step, the transmission line model calculates the branch currents, which are used by the converter models to calculate the output voltage for the next time step.

6.3.3 Control Law for Supply-side Management

Formulation

The supply-side control law, having the objective of minimising the operating cost of the system, is designed such that use of the renewable sources is maximised and use of the backup generator is minimised. The control law is formed by prioritising all possible operating conditions for the sources into states, as shown in Table 6.2. State 1 is the highest priority state in which the renewable sources are online, acting as constant voltage sources, while the storage charges using any excess power. The system operates in this

Table 6.2 Supply-side Control Law

State	Renewables	Storage	Generator
1	Const. voltage	Charge	Off
2	Const. power	Const. voltage	Off
3	Const. power	Const. power	Const. voltage

state when the load is less than the maximum power available from the renewable sources. The system enters state 2 when the load exceeds the output from the renewables. In this state, the renewable sources supply their peak output to the system, acting as constant power sources, while the storage node acts as a constant voltage source, supplying the remaining power demanded by the load. The generator comes online in state 3, the lowest priority operating state, acting as a slack bus, or constant voltage source. In this state, the remaining sources supply their maximum output power to the system.

Although the generator normally operates in state 3, a startup mode of operation is added to the generator to prevent rapid on/off cycling. When the generator initially comes online, it takes the same utilisation priority as the renewable sources for a minimum cycle time. This prevents the generator from turning off immediately when the system is operating at the boundary of states 2 and 3.

Implementation

As explained in Section 5.4, implementation of a supply-side control law is achieved by prioritising the voltage thresholds for the source and storage interface converters. Implementation of the supply-side control law for the case study is achieved by prioritising the voltage thresholds, $V_0 - V_3$, as shown in Figure 6.6. It should be noted that the thresholds $V_{s1} - V_{s3}$ are used for implementing the demand-side control law. Implementation of the demand-side control law will be addressed in Section 6.3.4.

The renewable sources take the highest priority and are therefore assigned to the highest voltage threshold, V_0. Because the storage node charges from any excess renewable power, its voltage threshold for charging, V_1, is set at the point where the renewable sources have just switched from constant voltage operation to constant power operation.

The storage node takes next discharge priority after the renewable sources. It is therefore assigned to discharge at the next lower voltage threshold, V_2. The backup generator takes the lowest priority, and is therefore assigned to the lowest voltage threshold, V_3. With the

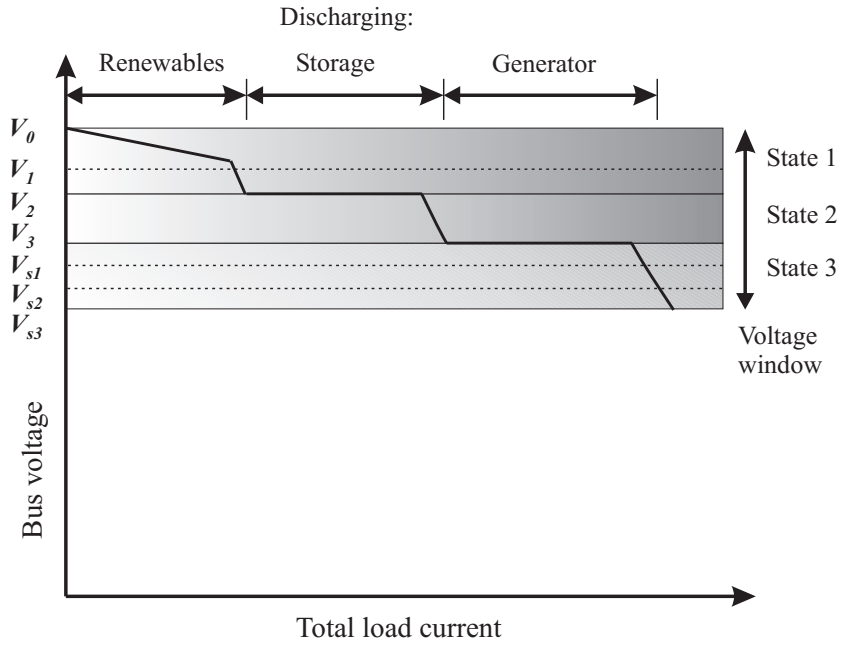

Figure 6.6 Supply and demand-side control law implementation

voltage thresholds prioritised, the exact voltage level for each threshold is calculated to ensure that the supply-side control law operates correctly despite the effect of transmission line impedance.

DC Load Flow

With the voltage thresholds prioritised, the spacing between adjacent thresholds is calculated to prevent parasitic voltage drop in the system from prematurely activating sources assigned to lower voltage thresholds. Each voltage threshold below the first is calculated by subtracting the maximum voltage drop and a margin of error from the previous voltage threshold. The worst-case voltage drop is obtained by performing a dc load flow in each operating state. The details of the dc load flow required to calculate the exact spacing of the voltage thresholds are explained in Section 5.4.

To apply this technique to the case study, the voltage threshold for the renewable sources, V_0, is set to the nominal operating voltage of the system, 700 V. The next lower voltage threshold is obtained by using a dc load flow to determine the lowest voltage at the point where a source assigned to the next operating state is connected to the system. The procedure is then repeated in the next operating state using this new voltage threshold until all voltage thresholds have been calculated. The schematics that represent the dc load flows for each operating state are shown in Figure 6.7, with the line impedance and droop coefficients expressed as conductances. The results and worst-case operating

Table 6.3 Voltage thresholds

Threshold	Value (V)	Worst-case conditions
V_0	700	-
V_1	690	$P_{L1} = 4\ kW, P_{L2} = 0, P_R = 5\ kW, P_S = -1\ kW$
V_2	688	-
V_3	687	$P_{L1} = 3\ kW, P_{L2} = 4\ kW, P_R = 5\ kW, P_S = 2\ kW$

conditions used to obtain the results are given in Table 6.3. In the table, the operating conditions used for the threshold calculations are denoted as follows: P_R is the power from the renewable sources, P_S is the output from the storage, P_{L1} represents the power absorbed by load 1, and P_{L2} represents load 2.

The voltage threshold for charging of the storage node, V_1, is calculated with the system operating in state 1. In this state, the renewable sources, V1 and V2, act as constant voltage sources with a constant power limit. They regulate the bus voltage to V_0, while supply nodes V5 and V6 are inactive.

Voltage threshold V_1 is set below the lowest voltage that appears at bus V3, the connection point of the storage node with the system. The worst-case operating conditions used to calculate V_1 occur when both renewable sources operate at their maximum values, PL1 is operating at its peak value of 4 kW, and the storage is charging at a rate of -1 kW. Under these conditions, the lowest voltage at bus V3 is 691.3 V. Therefore allowing a margin of error of approximately 1 V, and applying Equation (5.5), V_1 is set to 690 V.

A load flow is not needed to calculate the voltage threshold, V_2, the voltage at which the storage node begins discharging. Because only one storage node is present in the system, the voltage drop between multiple storage nodes does not need to be accounted for. The voltage threshold is simply found by subtracting a margin of error of 2 V from voltage threshold V_1. Voltage threshold V_2 is therefore set to 688 V.

To calculate voltage threshold V_3, the point at which the backup generator begins discharging, a load flow based on the schematic shown in Figure 6.7(b) is first performed to determine the voltage drop with the system bus being regulated at voltage threshold V_2. Under these conditions, the renewable sources act as constant power sources while the storage node acts as a constant voltage supply, regulating the bus voltage to V_2. Under worst-case operating conditions, the maximum voltage drop at bus V3, the connection point of the backup generator with the system, is 0.8 V. Voltage threshold V_3 is therefore set below this value, to 687 V.

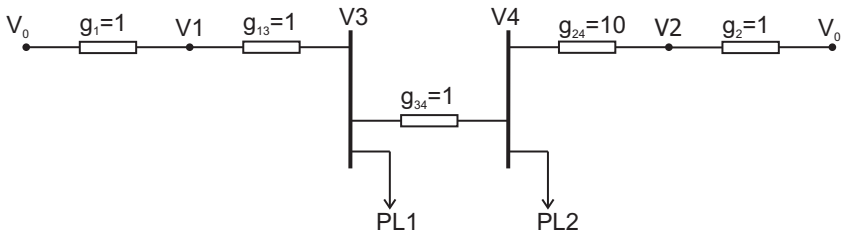

(a) Voltage threshold V_1

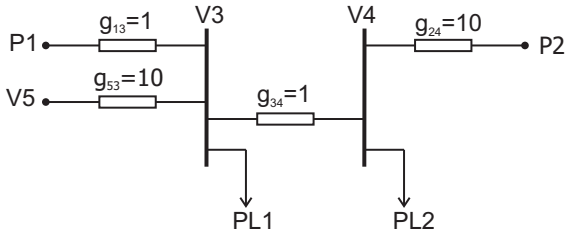

(b) Voltage threshold V_3

Figure 6.7 DC load flows used for voltage threshold calculations

6.3.4 Control Law for Demand-side Management

The objective of the demand-side control strategy adopted for the model nanogrid is straightforward. Its purpose is to maintain power to the high-priority loads under overload conditions. To achieve this, all loads present in the system are divided into three priorities: low, medium, and high. Under overload conditions, the low-priority loads are taken offline, followed by the medium-priority loads, in a bid to restore the power balance in the system. The high-priority loads are only taken offline if the system still remains in danger of a voltage collapse after the loads with a lower utilisation priority have been shed.

The load shedding mechanism relies on each load coming offline when the bus voltage decreases below its specific shutdown threshold, as explained in Section 5.5. To implement the demand-side control law, the shutdown thresholds are first prioritised. The shutdown threshold for the low-priority loads is assigned to a higher value than the shutdown thresholds for the medium and high-priority loads to ensure that these loads are taken offline first as the bus voltage decreases under overload conditions. This prioritisation is shown in Figure 6.6. The shutdown threshold for the low-priority loads, V_{s1}, is set at the point where the backup generator has just entered constant power mode. The shutdown thresholds for the medium and high-priority loads, V_{s2} and V_{s3}, are subsequently set below this first shutdown threshold.

As with the supply-side control law, the spacing between the shutdown thresholds is calculated to compensate for the voltage droop introduced in the system by transmission

Table 6.4 Shutdown thresholds

Threshold	Value (V)	Worst-case conditions
V_{s1}	683	$P_{L1} = 2\ kW, P_6 = 2\ kW$
V_{s2}	679	$P_{L1} = 2\ kW, P_6 = 2\ kW$
V_{s3}	675	$P_{L1} = 2\ kW, P_6 = 2\ kW$

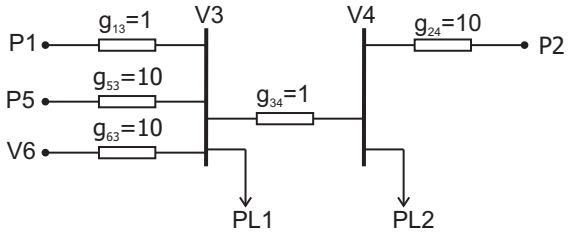

Figure 6.8 DC load flows for shutdown threshold calculations

line impedance. The first shutdown threshold, V_{s1}, is calculated by operating the system in state 3 with the bus being regulated at voltage threshold V_3. A dc load flow is then performed to determine the minimum voltage in the system under the worst-case operating conditions. This voltage is then used for V_{s1}. The subsequent shutdown thresholds are calculated by repeating the above procedure, using the previous shutdown threshold in place of V_3. This procedure was explained in detail in Section 5.5.

The worst-case operating conditions used to calculate these shutdown thresholds are given in Table 6.4, and the circuit used for the dc load flow is shown in Figure 6.8. It should be noted that the generation and loading conditions used for calculating the shutdown thresholds are different from those used to calculate the voltage thresholds. Since the maximum available generation in state 3 is 2 kW, the system is operated with a load of this value for all shutdown threshold calculations.

6.4 RESULTS

This section presents simulation results that verify the operation of the supply and demand-side control laws. The supply-side control law is verified by applying changes to the MPP of the renewable sources and by adjusting the load demand. Under these operating conditions, the supply-side control law maintains the power balance in the model nanogrid by scheduling the storage and backup generation. The demand-side control law is verified by monitoring the response of the loads to overload conditions. Overload conditions are created by reducing the available generation or increasing the load such that

the total load demand exceeds the maximum generation capability of the system. The demand-side control law begins shedding loads according to their utilisation priority in a bid to maintain a constant supply of power to the high-priority loads.

6.4.1 Verification of Supply-Side Control Law

System Response to Load Changes

The supply-side control law maintains the power balance in the system in the presence of load changes and fluctuations in the MPP of the renewable sources. Figure 6.9 demonstrates the effect of load changes on the system. For the duration of the simulation, the MPP of the renewable sources is held constant. The output power of the wind turbine and photovoltaic array are kept at 2 kW and 1 kW respectively while the load is varied.

Initially load 1 is 0.5 kW and load 2 is 1 kW. Since the renewable sources are capable of supplying the load, the system operates in state 1. The storage node extracts the excess power from the renewable sources up to their MPP by regulating the bus voltage at its voltage threshold for charging. The power it draws from the system is approximately -1.5 kW.

At 5 ms, load 1 is increased to 1 kW and load 2 to 1.5 kW. Despite these load changes, the system still operates in state 1 since the renewable sources are able to meet the load demand. However, the storage charges at a lower rate of -0.5 kW as shown in Figure 6.9(b) because of a reduction in the excess renewable power.

At 12 ms, load 2 is increased to 3 kW. The system now operates in state 2 since the load exceeds the power available from the renewable sources. The storage node begins discharging, supplying 1 kW to the system in order to maintain the power balance. It can be seen from Figure 6.9(c) that the voltage at bus V1 drops to the level of the storage node's discharge voltage threshold.

At 20 ms, load 1 is also increased to 3 kW. The storage attempts to supply the power balance, briefly operating at its maximum power limit of 2 kW. However, since the load exceeds the maximum combined output of the renewable sources and storage, the bus voltage decreases below the voltage threshold of the backup generator, bringing it online. The generator begins injecting power into the system, taking the same priority as the renewable sources. Since the storage is still required to supply power to the system to balance the load, the bus voltage remains at the storage node's discharge voltage threshold.

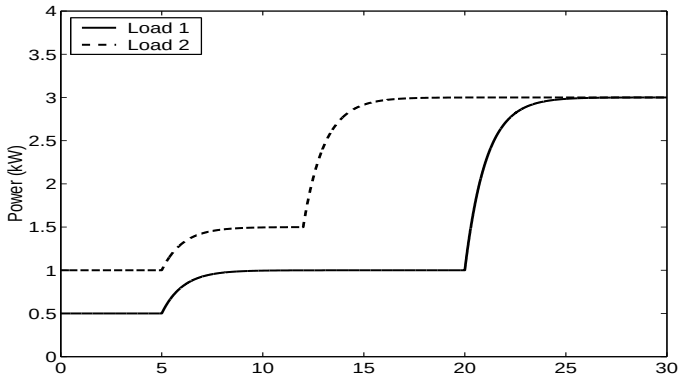

(a) Load powers

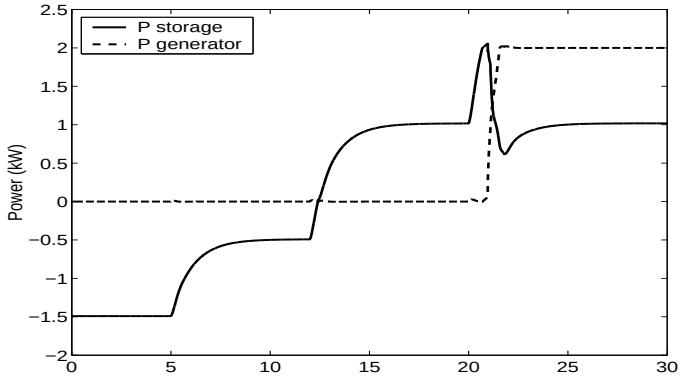

(b) Storage and generator output powers

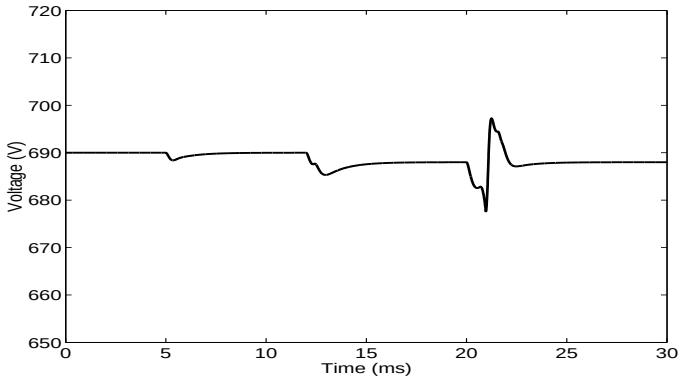

(c) Voltage at bus V1

Figure 6.9 Effect of load changes

System Response to Supply Changes

The supply-side control law is further verified by monitoring the response of the system as changes in the MPP of the renewable sources are made to upset the power balance in the system. Figure 6.10 demonstrates the effect these supply changes have on the system. Figure 6.10(a) shows the variations in the output of the renewable sources. The source powers are changed in order to cycle the system through its operating states. The power drawn from the storage and backup generator nodes in order to maintain the power balance is shown in Figure 6.10(b), and the voltage level at bus V1 is portrayed in Figure 6.10(c). For the duration of the simulation, load 1 is 1 kW, and load 2 is 2 kW.

Initially excess renewable power is available, hence the system operates in state 1, charging from the excess renewable power. At 5 ms, the MPP of the wind turbine is reduced from 3 kW to 1.5 kW. This change reduces the excess renewable power, hence the charging rate of the storage is reduced from -2 kW to -0.5 kW. It should be noted that this supply change is not instantaneous, but has a similar time constant to the constant power loads since the source interface converter buffers the supply from the system.

At 12 ms, another change in renewable power forces the storage to begin discharging in order to balance the load. Finally, at 20 ms, the diesel generator is triggered online since the storage is incapable of supplying the balance of load power alone.

6.4.2 Verification of Demand-Side Control Law

The demand-side control law is verified by simulating the model nanogrid under overload conditions. Supply and load changes are applied to the system to create operating conditions where the load demand exceeds the peak available generation. Under these operating conditions, the only means by which the power balance can be maintained is for load shedding to occur. Figure 6.11 depicts the changes in the bus voltage that occur under overload conditions, and the corresponding effect the bus voltage has on the load shedding strategy.

Initially, the total load on the system is 3.5 kW. Load 1 contributes 2 kW to this total demand in both low and medium-priority loads. Another 1.5 kW of the total demand comes from load 2, which comprises 1 kW of medium-priority load and 0.5 kW of high-priority load. The system operates in state 3, with the storage providing its maximum output of 2 kW to the system, and the backup generator providing the balance.

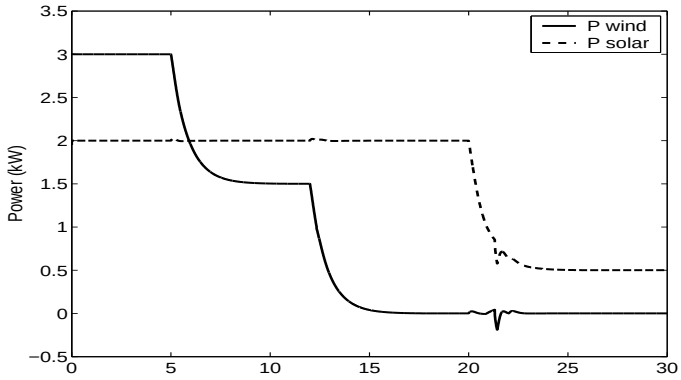

(a) Renewable source powers

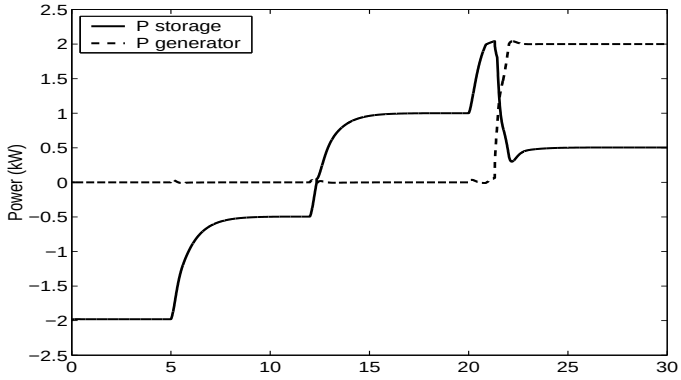

(b) Storage and generator output powers

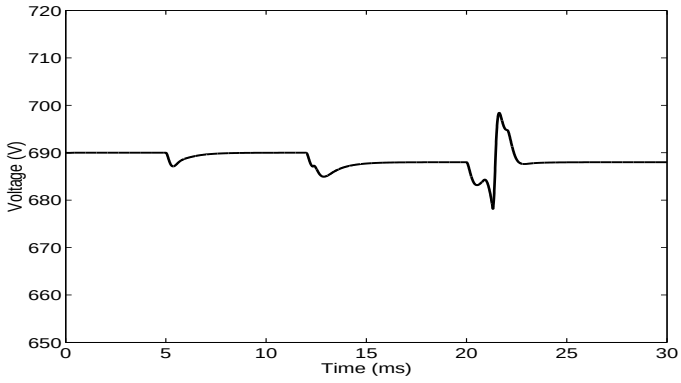

(c) Voltage at bus V1

Figure 6.10 Effect of renewable supply changes

At 5 ms, the high-priority load increases from 0.5 kW to 1.5 kW as shown in Figure 6.11(b). An overload condition is created since the maximum generation is exceeded, and consequently, the bus voltage decreases. When the bus voltage decreases below the shutdown threshold 1 for the low-priority load, V_{s1}, the low-priority load is taken offline as shown in Figure 6.11(a). This action restores the power balance in the system.

At 13 ms, another overload condition is created by taking the storage offline. The available generation is reduced to 2 kW, while the load on the system initially remains at 3.5 kW. When the bus voltage decreases to the shutdown threshold of the medium-priority loads, these loads are shed, restoring the power balance in the system.

6.4.3 Discussion

The results have shown that implementing supply and demand-side control laws in a nanogrid using DBS is possible provided the voltage and shutdown thresholds are calculated to compensate for the unequal propagation of the dc bus voltage throughout the transmission network. The simulation results showed that the supply-side control law successfully maintained the power balance in the system in the presence of supply and load changes. The power imbalance created as a result of these changes introduced steady-state changes in the voltage level of the dc bus that signalled the additional supplies, the storage and backup generation, to come online. Similarly, the demand-side control law prevented the bus voltage from collapsing under overload conditions. When the voltage level of the dc bus indicated the system was in danger of overload, loads were shed according to their utilisation priority in order to maintain a continuous supply of power to the high-priority loads.

Although the simulation results have indicated the successful operation of DBS for supply and demand-side management purposes, it should be noted that the transient response of the simulation model is not an exact representation of a practical system. The response of the constant power loads have been deliberately sped up, and high-frequency phenomena have been ignored to allow for a rapid simulation. However, the experimental results presented in the next chapter will provide a more accurate representation of the transient response of a practical system.

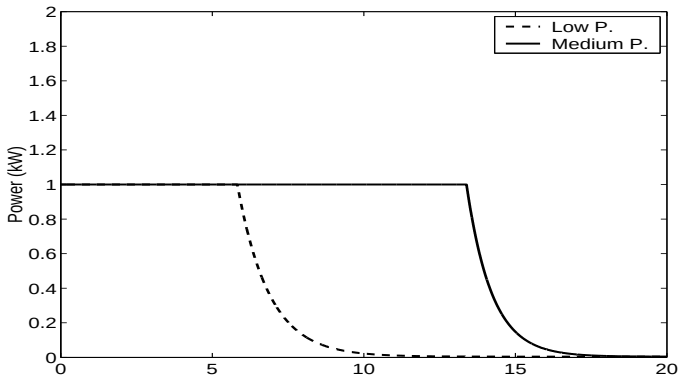

(a) Load 1

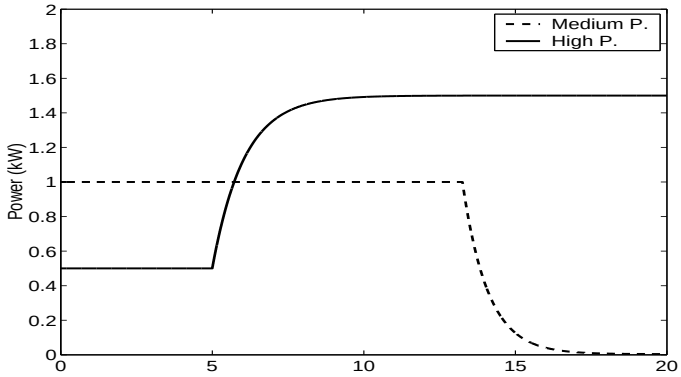

(b) Load 2

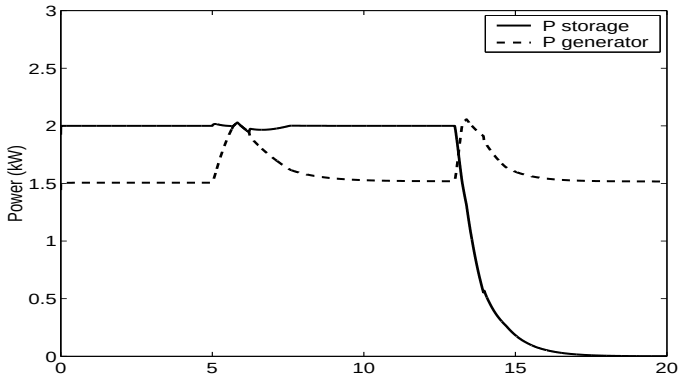

(c) Storage and generator output powers

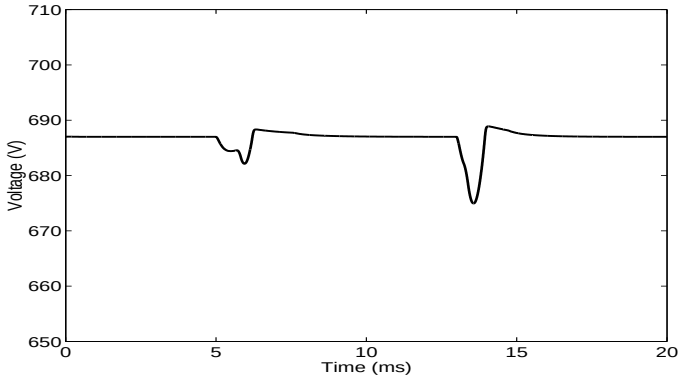

(d) Voltage at bus V1

Figure 6.11 Load shedding results

Chapter 7

EXPERIMENTAL RESULTS

7.1 INTRODUCTION

An experimental nanogrid was constructed in the laboratory to demonstrate the practicality of implementing supply and demand-side control laws using DBS. The system was designed to represent the model nanogrid presented in the previous chapter; however, for ease of construction, the power and voltage rating of the experimental system was scaled down by a factor of ten. The experimental system was designed with a nominal operating voltage of 70 V and an average load of 200 W. This chapter explains the design of each hardware module present in the experimental system, in particular describing the design of the source interface current and voltage control loops. Experimental results are presented to demonstrate the practical operation of DBS.

7.2 SYSTEM OVERVIEW

The experimental system was designed to represent the nanogrid model presented in Section 6.3. A block diagram of the experimental system is shown in Figure 7.1, and the key parameters of the system modules are summarised in Table 7.1. This section outlines the design of each hardware module present in the experimental system. The hardware modules consist of sources, loads, interface converters, a transmission network, and a load controller.

For simplicity, 12 V laboratory power supplies are used in place of actual renewable and non-renewable sources. Since the supplies do not have a MPP characteristic, this characteristic which is present in the renewable sources is accounted for by controlling the peak output power of the converters. The means by which a source interface converter is controlled to emulate the behaviour of a renewable source is explained in Section 7.3.3.

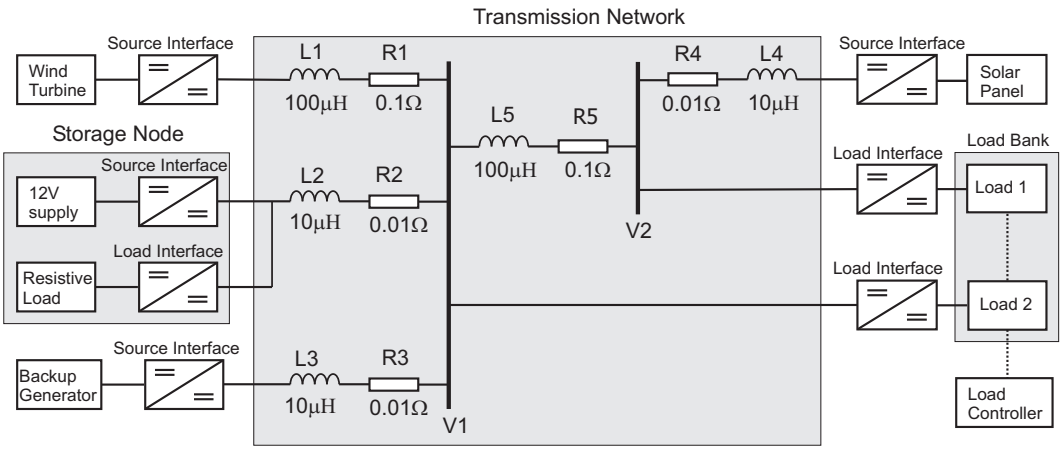

Figure 7.1 Experimental system

The main building block of the experimental system is the source interface converter. A step-up dc-dc converter rated at 100 W, the source interface boosts the supply voltage from 12 V to 70 V to allow the source to be connected to the system. Based on a full bridge topology, the source interface employs PWM hard switching and uses a high-frequency transformer to achieve the large voltage transformation ratio. A full bridge topology is employed since it reduces the current and voltage stress on the switches when compared to topologies such as the push-pull and half bridge, and a PWM hard switching scheme is adopted for its simplicity. It should be noted that in a full-scale system, a zero voltage switching or resonant topology may be used in a bid to reduce switching losses.

The other primary building block, the load interface, is constructed in a similar fashion to the source interface. The load interface is based on a full bridge hard switched topology, but unlike the source interface, the load interface is a step-down converter, allowing the 12 V loads to draw power from the system. Its rating is also higher, at 200 W. The load interface converter is designed to operate over an input voltage range from 58-70 V to prevent any variations in the bus voltage within this voltage window from causing the converter to lose regulation of the loads.

Both load nodes, load 1 and load 2, are constructed using a bank of incandescent lights. Each load bank consists of six 12 V lights rated at 25 W. The load banks can be controlled in discrete steps of 25 W up to a peak of 150 W with the aid of the load controller. The load controller controls the load bank by using MOSFET switches.

For simplicity, the storage interface is constructed by connecting a source and load interface converter in parallel. The load interface converter connects the nanogrid to a resistive load to allow charging action to take place, while a source interface converter and 12 V

Table 7.1 System Parameters

Source	Vout: 12 V
Source Interface	Vin: 10-15 V Vout: 70 V Pmax: 100 W Efficiency: 83 %
Load Interface	Vin: 58-70 V Vout: 12 V Pmax: 200 W Efficiency: 88 %
Load Bank	Resolution: 25 W Pmax: 200 W
Transmission Network	Resistance: 0.1 Ω/km Inductance: 0.1 mH/km

supply allow the storage node to discharge into the nanogrid. It should be noted that in practice, a bidirectional converter would be used in place of two separate converters to minimise the components count and the construction cost. However in the interests of minimising design effort, the simpler approach of using two separate converters was adopted.

The transmission line module in the experimental system is constructed to accurately represent a practical transmission line, including inductance in addition to resistance. Line capacitance is neglected since this parasitic component is negligible compared to the output capacitance of the source interface converters. The resistance is calculated such that it has the same per-unit resistance as the simulation model. Its value is consequently 0.1 Ω/km, one-tenth the line resistance used in the simulation model. The line inductance is calculated in a similar fashion. As shown in Section 3.3.1, the inductance of overhead line or cable is in the order of 1 mH/km. For the experimental model, the inductance used is equivalent to this value scaled down by a factor of ten.

7.3 SOURCE INTERFACE CONVERTER CONTROL DESIGN

This section details the design of the current and voltage control loops present in the source interface converter. The design procedure for the two control loops is explained, and the design of the digital control board used for the voltage loop is presented. The means by which the functionality of the voltage loop is implemented in software is given.

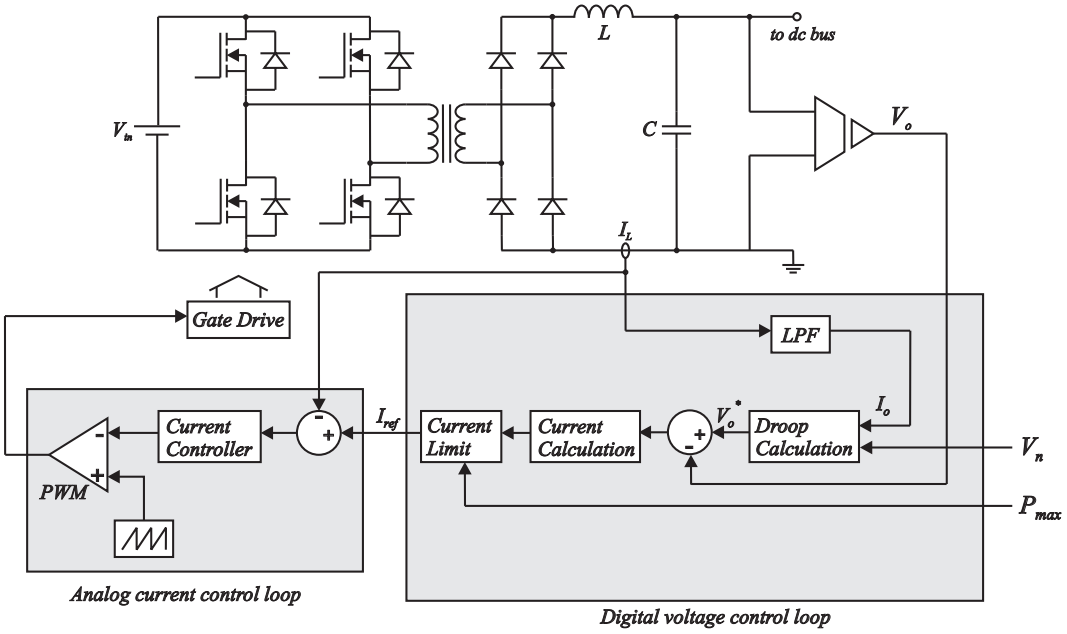

Figure 7.2 Control hardware for source interface converter

Lastly, the differences between the design of the storage charge controller and the source interface controller are highlighted.

7.3.1 Control Loop Design

The control strategy for the source interface converter is based on a two-tiered structure. An inner current loop regulates the inductor current, and an outer voltage loop regulates the output voltage of the converter. The current loop is implemented in an analogue fashion for high speed, while the voltage loop is implemented using a digital controller for control flexibility. Figure 7.2 shows the configuration of these control loops.

Current Loop

Two types of current mode control are commonly used for the control of switching converters, peak current mode control and average current mode control (ACMC). ACMC is chosen to control the current loop of the source and load interface converters due to its superior characteristics. ACMC exhibits better noise immunity, does not require slope compensation, and does not have peak to average current error [55]. However, the loop gain at the switching frequency must be limited in order to achieve stable operation.

The ACMC loop is implemented using an analogue controller as shown in Figure 7.3. The controller is a type 2 compensator, with a low-frequency pole at the origin of the s-plane,

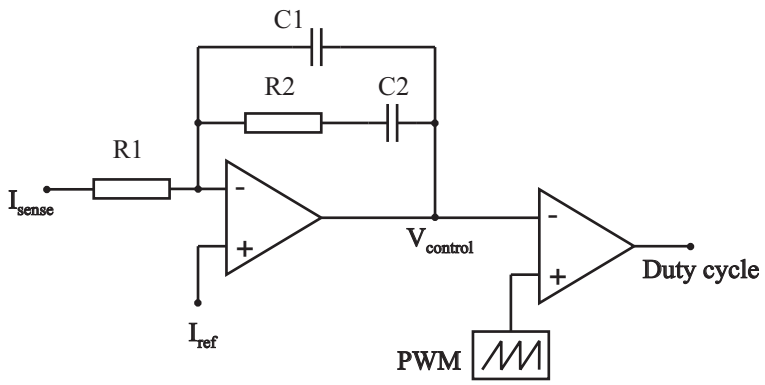

Figure 7.3 Implementation of current loop based on ACMC

a zero at $f_s/10$, and a high-frequency pole at f_s. The compensator is designed using the method outlined in [55]. The gain of the compensator at f_s is calculated such that the slope of the amplified inductor current, $V_{control}$ does not exceed the slope of the PWM sawtooth waveform. A high-frequency pole caused by R2,C1 is placed at f_s to eliminate noise spikes on the current waveform, the nemesis of peak current mode control. The zero caused by R2, C2 is placed at approximately one-tenth the switching frequency to boost the low-frequency gain, allowing rapid tracking of the reference current. Because the circuit is powered by a 5 V supply, an integrator antiwindup mechanism is inherent in the design as the integrator output will never exceed this value.

Voltage Loop

A proportional plus integral (PI) controller is used for the voltage loop of the source interface converter because it is less susceptible to noise on the dc bus voltage signal than a proportional plus integral plus derivative (PID) controller. Although more advanced control strategies such as H∞ control can be implemented, PI control was selected because it provides adequate performance and is simple to implement in the digital domain.

To design the PI controller, a transfer function of the converter is first derived. Because the converter employs current mode control, the transfer function is simplified. The system can be reduced to a simple first order system by idealising the current loop with a gain, m, as shown in Figure 7.4. The simplified model has a resistive load and omits the output capacitor's equivalent series resistance (ESR) since this has little effect at the frequencies of interest for designing the voltage loop.

The open loop transfer function of the voltage loop obtained from the model is given by:

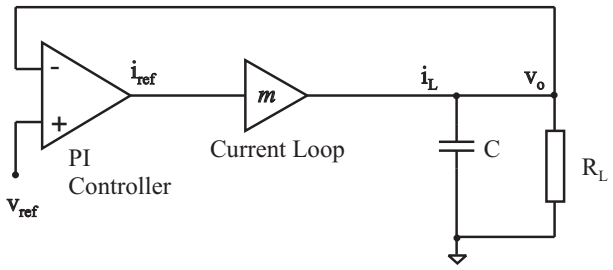

Figure 7.4 Simplified converter model

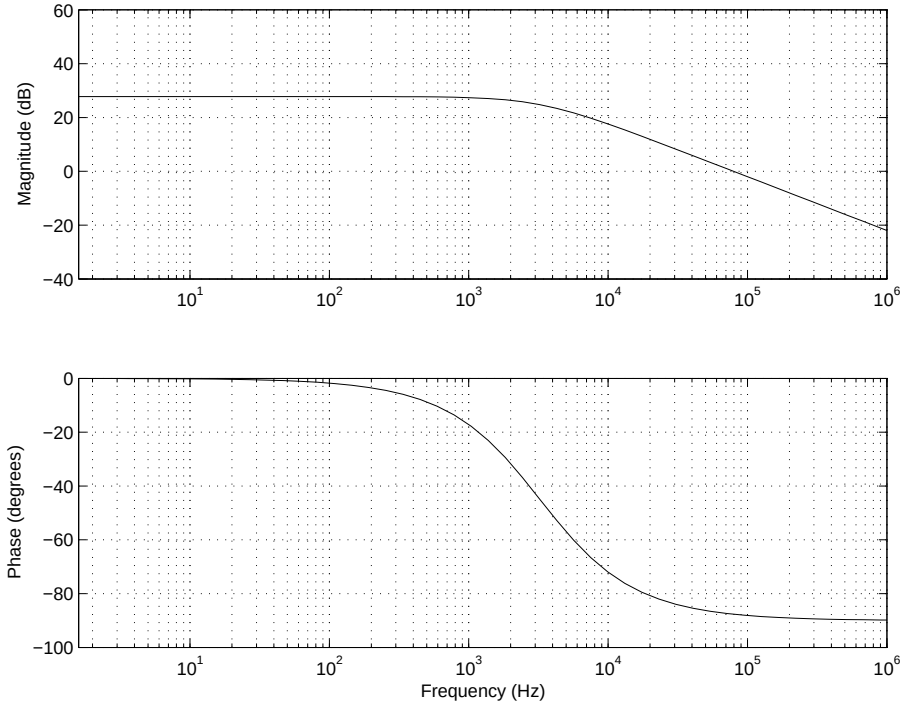

Figure 7.5 Open loop Bode plot of voltage loop

$$\frac{v_o}{i_{ref}} = \frac{mR_L}{sR_LC + 1} \tag{7.1}$$

The PI controller is designed in the frequency domain with the aid of the Bode plot shown in Figure 7.5. The design is translated to the digital domain through emulation of the analogue design. The parameters used to obtain the Bode plot are: $R_L = 490\ \Omega$, $C = 1\ \mu$F, and $m = 0.5$. A crossover frequency of 1 kHz was selected to provide a good transient response, and the zero in the PI controller was also placed at 700 Hz to ensure a good dc gain under closed loop operation. Using these parameters, the proportional gain k_p, and integral gain, k_i, were calculated to be 0.0316 and 139 respectively.

The voltage loop for the load interface was designed in a similar fashion to that of the storage interface. The same simplified model and transfer function were used since the

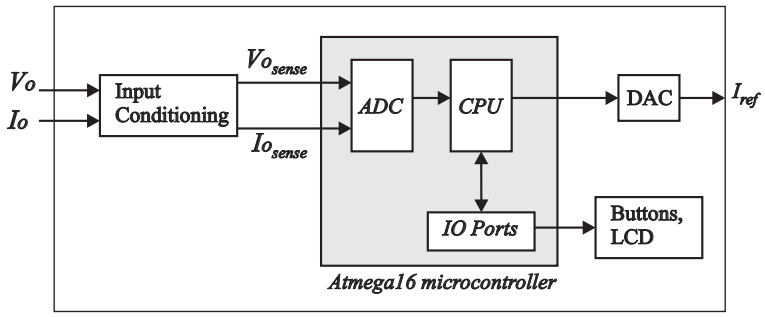

Figure 7.6 Microcontroller-based digital control board

converter topology of the load interface is identical to that of the source interface. The PI controller was designed with a bandwidth of 50 Hz. At this bandwidth, the PI gains were calculated to be 0.0562 and 17.7 respectively.

The storage charge node, based on a load interface converter, was designed using a different transfer function since it has a different control structure. The charge node regulates the input voltage of the converter rather than the output voltage. Consequently, the dynamics of the source interface and transmission line must be included in the transfer function since these affect the input voltage. A simplified model of the storage charger and corresponding transfer function are given in Appendix 1.

7.3.2 Digital Control Board

The voltage control loop was implemented in a digital fashion using a microcontroller. A block diagram of the microcontroller-based digital control board that was designed to implement the voltage control loop is shown in Figure 7.6.

A microcontroller was used as opposed to a DSP since implementation of the PI control law does not require a large number of multiplications or other complex instructions. An ATmega16 microcontroller was selected as it provides good performance for the selected application, having an operating speed approaching 16 MIPS and an onboard hardware multiplier. The microcontroller uses a RISC based architecture and is flash based, having 16K words of program memory.

The ADC on the microcontroller is used for measuring the output voltage and current. The ADC has 10-bit resolution and a conversion time of approximately 5 μs when running at full speed. Since the microcontroller has no means of directly controlling the reference current for the inner loop, an external DAC is used for this purpose. The DAC, a MAX5541, has a resolution of 16 bits and an operating speed of up to 1 MHz.

Input conditioning is required to interface the control inputs directly to the ADC module on the microcontroller. A differential amplifier interfaces the bus voltage, Vo, to the microcontroller by reducing the input voltage by a factor of 5/90. The differential amplifier also performs low pass filtering to eliminate switching noise and to prevent aliasing. The output current is not directly measured from the full bridge circuit, but is derived from the inductor current. Since, the average inductor current is equivalent to the output current, the output current is obtained by using a first-order low pass filter to extract the average value from the inductor current waveform.

7.3.3 Software Design

The actual functionality of the outer control loop for the source interface is implemented in software. This section explains how the PI control law and constant power limit are implemented by programming the microcontroller on the digital control board.

Program Structure

The code required to implement the PI control law and constant power limit is time critical, and is therefore implemented using a timer interrupt service routine (ISR) that is executed at regular intervals. The response of peripheral devices on the other hand is not so critical, therefore the peripherals are serviced by a main routine that executes in the time available between servicing the timer interrupts. The program flow of the timer ISR is divided into five steps, A-E, as shown in Figure 7.7.

The first step in the timer ISR involves performing preliminary calculations, namely reading the output voltage and calculating the error and integral error values. Limits are imposed on the integral action to prevent unsigned integer overflow and integrator windup. The next step involves calculating the PI control action, or reference current. A dynamic current limit function is then executed to implement the constant power limit. Finally the droop action is calculated and the reference current is written to the DAC. The execution time for the each function executed inside the timer ISR is shown in Figure 7.8.

The timer interrupt is set to 80 μs, fast enough to allow accurate emulation of the analogue control law, yet slow enough to allow servicing of the peripheral devices once the voltage loop calculations have been completed. The voltage loop calculations take 53 μs, allowing 27 μs for the main routine to service the peripheral devices. With an interrupt of 80 μs, the sampling frequency is effectively 12.5 kHz. Since the bandwidth of the voltage loop is

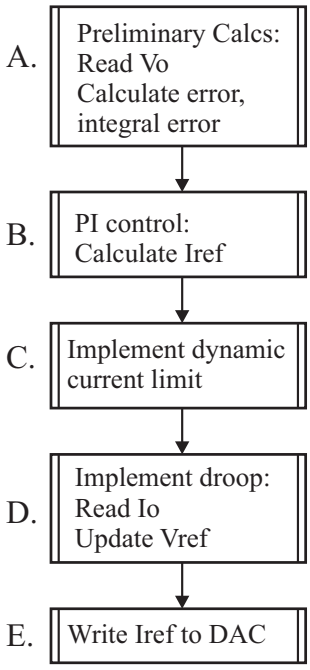

Figure 7.7 Program flow of timer ISR

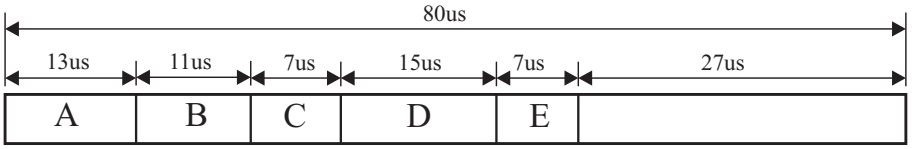

Figure 7.8 Timer ISR timing

1 kHz, the sampling frequency is more than ten times greater than the control bandwidth, ensuring that the digital PI controller accurately emulates the analogue PI controller design.

Implementation of PI Control Law

The key function of the voltage control loop is the implementation of the PI control function. In the analogue domain, the PI control law is given by

$$u(t) = e(t)(k_p + \frac{k_i}{s}) \tag{7.2}$$

where $e(t)$ is the error. This PI control law is translated to the digital domain by using trapezoidal numerical integration to approximate the integral term, k_i/s. In the digital domain, the PI control law is given as follows:

$$e_k = V_{ref} - V_k \tag{7.3}$$

$$i_{k+1} = i_k + \frac{h}{2}(e_{k+1} + e_k) \tag{7.4}$$

$$u_k = k_p \cdot e_k + k_i \cdot i_k \tag{7.5}$$

where V_k is the output voltage, e_k is the error, i_{k+1} is the integral error, h is the sampling period, and u_k is the control output value.

To ensure the digital PI control law is an accurate representation of the analogue PI controller given in Equation (7.2), the proportional and integral gains, k_p and k_i, are first adjusted to account for the scaling introduced by the digital control board. The scaling process involves adjusting the PI control gains to account for the gain of the ADC, the differential amplifier, and the DAC. Without scaling, the first of these three hardware elements cause the error and integral error to be calculated incorrectly. Similarly, the gain of the DAC distorts the reference current, u_k, when this value is output to the inner current loop.

To speed up the execution of the PI control law in the microcontroller, the PI gains are further scaled to allow the use of 16-bit fixed point math. Without this additional scaling, implementation of the PI control law requires multiplication of floating point numbers. In an 8-bit microcontroller, floating point calculations take considerably longer than fixed point multiplication. This final scaling process therefore involves scaling the control gains, k_p and k_i, such that they become fixed point numbers.

Implementation of the dynamic current limit

Aside from the PI control law, the other major function implemented in the timer ISR of the microcontroller is the dynamic current limit. The dynamic current limit function implements the constant power mode of operation by adjusting the upper limit for the reference current to

$$I_{ref\ max} = P_{max}/V_o \tag{7.6}$$

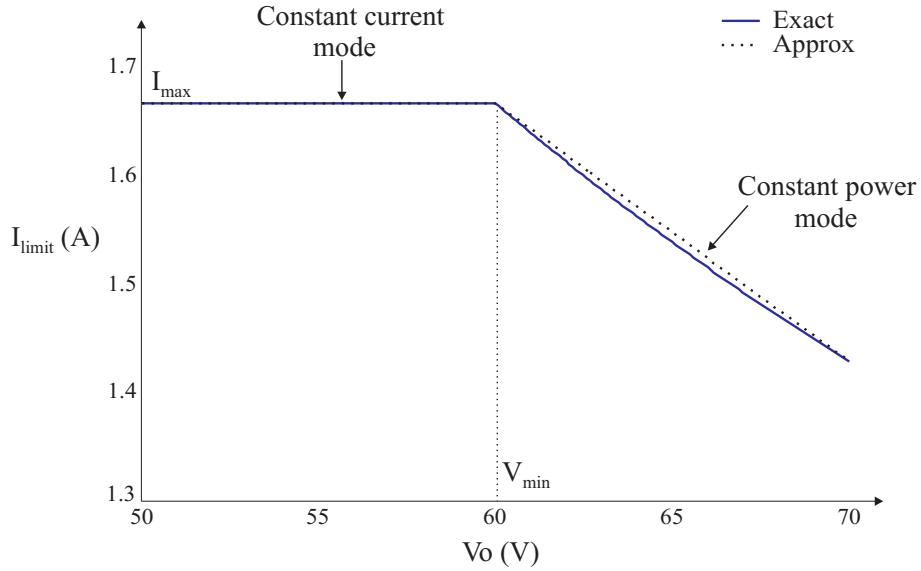

Figure 7.9 Dynamic current limit

where P_{max} the input value to the function that represents the instantaneous peak power available from the renewable source, and V_o is the measured bus voltage. Thus as P_{max} or V_o change, the reference current limit is altered to ensure that the output power of the converter never exceeds P_{max}. The operation of the dynamic current limit was explained in detail in Section 5.3.1.

Because the dynamic current limit function effectively limits the output power of the source interface converter to P_{max}, the MPP characteristic of the renewable sources can be emulated simply by varying P_{max}. This feature is important for testing the operation of the control laws since the laboratory power supplies used in the experimental system do not have a variable MPP characteristic or a MPP tracking circuit.

The dynamic current limit function can be implemented in an exact fashion by calculating the source interface converter's current limit in the constant power region in accordance with Equation (7.6). This exact calculation of the dynamic current limit results in a current limit characteristic delineated by the solid line in Figure 7.9. The graph was obtained with the aid of MATLAB for a MPP of 100 W. The only drawback with this exact calculation is that implementing the division operation P_{max}/V_o in the microcontroller takes significantly longer than the other operations in the timer ISR. The division operation takes approximately 60 μs because it involves dividing a 32-bit number by a 16-bit number.

An approximation of Equation (7.6) is therefore used to speed the execution time to 5 μs.

The current limit is approximated in the constant power region by a straight line:

$$I_{limit} = I_{max} - m(V_o - V_{min}). \tag{7.7}$$

where m is the slope of the current limit line. The characteristic of the approximate dynamic current limit is shown by the dotted line in Figure 7.9. It can be seen that the approximation is a close representation of the exact current limit. The reason for this good correlation is that the slope of exact current limit graph in the constant power region is nearly constant.

Although this approximation of Equation (7.6) speeds the execution time in the microcontroller, the variable MPP characteristic of renewable sources must be emulated in a slightly different fashion. Instead of varying P_{max}, I_{max} and m are varied since these parameters dictate the behaviour of the constant power limit.

7.4 STABILISING THE SYSTEM

When the source and load interface converters in a dc system are designed in a standalone fashion, there exists a potential for instability when the modules are integrated into a system. Interaction can occur between the source and load interface converters [56, 57], resulting in oscillations on the dc bus. To ensure stable operation of the system, the ratio of the small signal output impedance of the source interface converters to the input impedance of the load interface converters, Z_o/Z_i, must be kept from encircling (-1,0) on the s-plane. This is explained in Section 8.4.

Figure 7.10(a) shows the transient response of the experimental system before the system was stabilised. The system was operated with the wind turbine's source interface supplying load 2 since this operating condition presents the largest interconnection impedance, increasing the likelihood of Z_o/Z_i being unstable. Figure 7.10(a) shows the voltage at bus V1 when load 2 is increased from 25 W to 50 W. It can be seen that the system response, while not unstable, is significantly underdamped.

To improve the system response, the control bandwidth of the load interface converters was reduced, damping was added to the system, and the bus capacitance was increased. These techniques have been shown to be successful in stabilising a power electronic based dc system [57]. In the original design of the system, the load interface converters were designed with a bandwidth of 1 kHz at 10% load, no input filters with damping were used,

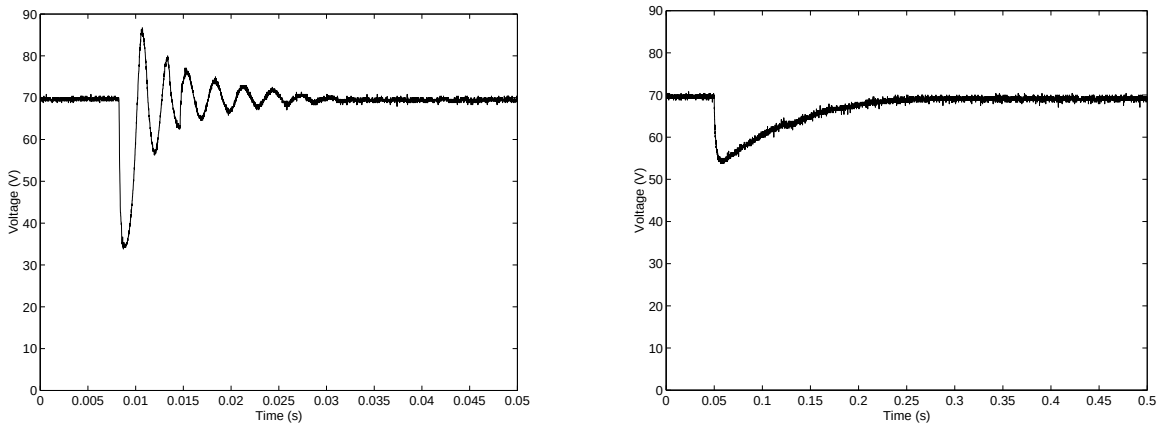

(a) Before stabilising (b) After stabilising

Figure 7.10 Transient response of system

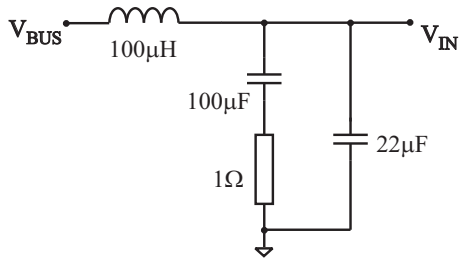

Figure 7.11 Parallel-damped input filter

and the only capacitance present on the dc bus was the 2.2 μF input capacitors of the load interface converters. To stabilise the transient response, the control bandwidth of the load interface converters was reduced to 50 Hz and an input filter with a 1 Ω damping resistor was added to the load interface. The bus capacitance was also increased to 100 μF. The input filter, a parallel-damped low pass filter with a cutoff frequency of 5 kHz, is shown in Figure 7.11.

The new transient response is shown in Figure 7.10(b). It can be seen that the bus voltage is now overdamped. It should be noted that these two techniques are not the only methods available for stabilising the system. Section 8.4 explains a number of techniques that can be applied to a practical system. However, input filters and a bus capacitor were used in the experimental system since these methods were the most simple means of ensuring stable operation. It must be noted that the purpose of stabilising the system was simply to allow stable results to be obtained from the system in order to verify the operation of DBS in a practical system, not to provide an optimal solution to the issue of small signal stability.

7.5 IMPLEMENTATION OF DBS CONTROL LAWS

Before experimental results could be obtained from the system, the control laws governing its operation were implemented. The supply and demand-side control laws implemented in the experimental system were the same as those used for the simulation model. These control laws were presented in Section 6.3.3.

With the simulation model, the supply-side control law was implemented by prioritising the voltage thresholds for the converters that supply power to the system. Similarly, the demand-side control law was implemented by prioritising the shutdown thresholds of the load-side converters. The spacing between all thresholds was then calculated to ensure correct operation of the supply and demand-side control laws.

In the experimental system, the same prioritisation of the voltage thresholds was used since its control laws are identical to those used in the simulation model. However, the voltage thresholds were recalculated since the experimental system is one-tenth the scale of the simulation model, operating at 70 V rather than 700 V. Using the procedure outlined in Section 5.4, the voltage thresholds for implementing the supply-side control law and the shutdown thresholds for implementing the demand-side control law were calculated. The results are portrayed in Table 7.2. The thresholds were then programmed into the source and load interface controllers, allowing the supply and demand-side control laws to function in the experimental system.

It should be noted that in the experimental system, because the resistance of the transmission network was scaled down in addition to the power and voltage rating of the system, similar per-unit values for the worst-case voltage drop calculations in each state were obtained compared with the simulation model. However a greater margin of error was used compared to the simulation model. A margin of error of up to 3 V was used to prevent voltage measurement discrepancies between control modules and voltage ripple on the dc bus from preventing correct operation of the control law. Consequently the per-unit values for the voltage thresholds in the experimental system are lower than those used in the simulation model.

7.6 RESULTS

In this section, the results obtained from the experimental system are presented to demonstrate the operation of the supply and demand-side control laws and to verify the sim-

Table 7.2 Thresholds for implementing supply and demand-side control laws

	Threshold	Value (V)
Voltage Thresholds	V_0	70
	V_1	66
	V_2	62
	V_3	60
Shutdown Thresholds	V_{s1}	58
	V_{s2}	56
	V_{s3}	54

ulation results. As with the simulation model, the supply-side control law is verified by monitoring the response of the supplies to changes in the MPP of the renewable sources and fluctuations in the load demand. The demand-side control law is tested by creating overload conditions where the total load demand exceeds the available generation. The response of the loads is monitored to ensure that they are shed according to their utilisation priority under overload conditions. It should be noted that the experimental results portray the output current of each converter rather than the output power. The reason for this is that current measurements are simpler to obtain from the experimental system.

7.6.1 Verification of Supply-Side Control Law

System Response to Load Changes

Since the supply-side control law attempts to maintain the power balance in the system by scheduling sources in the presence of load and supply changes, this control law is tested by first applying load changes to the system. Figure 7.12 demonstrates the effect that load changes have on the bus voltage. The load currents drawn from the 70 V bus by the load interface converters are shown in Figure 7.12(a). The currents supplied to the 70 V bus by the storage and generator interface converters are shown in Figure 7.12(b). The output currents of the wind turbine and photovoltaic interface converters are not shown since they are constant in this experiment. For the duration of the experiment, these converters operate at their peak output of 70 W.

Initially, load 1 is 50 W and load 2 is 25 W. Since there is an excess of power, the system operates in state 1, with the storage charging from the excess power. The storage node regulates the bus voltage at its voltage threshold for charging, V_1, by drawing a current of -0.9 A from the system as shown in Figure 7.12(b). The generator remains off during

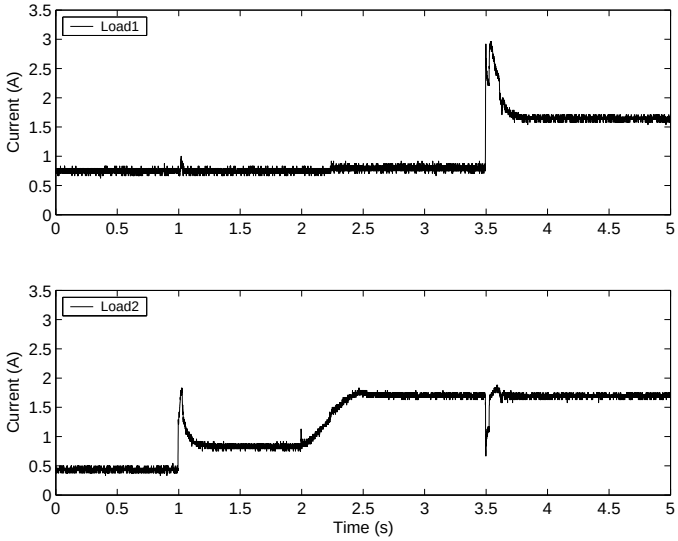

(a) Load interface converter currents

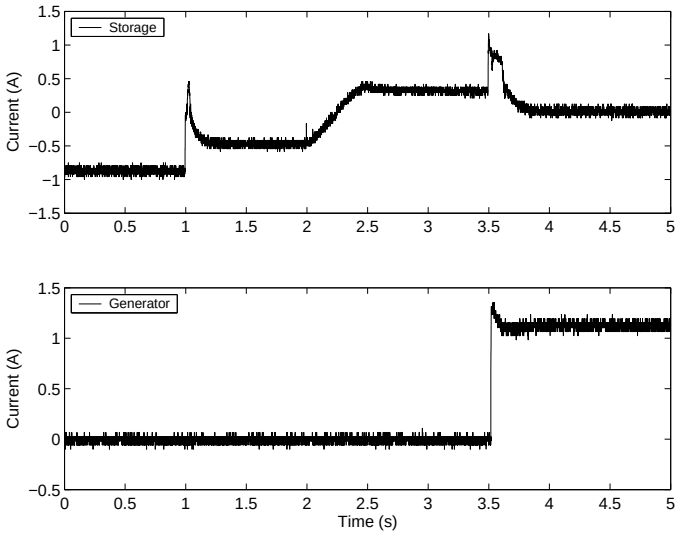

(b) Generator and storage currents

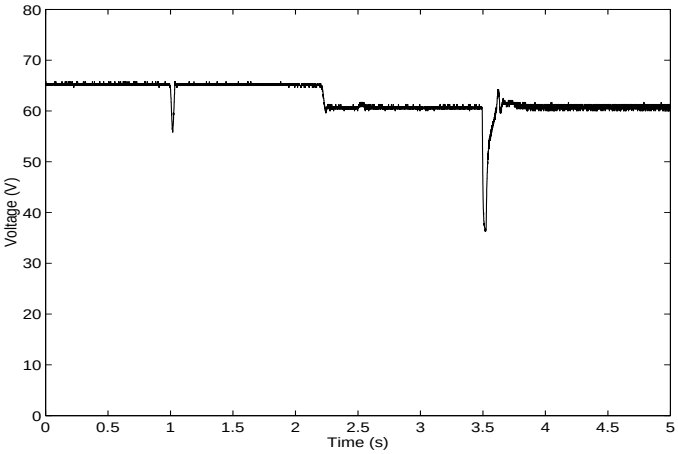

(c) Voltage at bus V1

Figure 7.12 Effect of load changes

this interval.

At 1 s, load 2 increases to 50 W, reducing the excess renewable power. Consequently the charge current is diminished to approximately -0.4 A. The system still operates in state 1 with the storage node regulating the bus voltage to its voltage threshold for charging.

Load 2 is increased to 100 W at 2 s, forcing the storage node to begin discharging. This load increase creates a power shortfall, forcing the bus voltage to collapse. When the bus voltage decreases to the discharge threshold of the storage node, the storage node begins discharging, supplying approximately 0.4 A to maintain the power balance. It can be seen from Figure 7.12(c) that the dc bus is now regulated at the storage node's voltage threshold for discharging, V_2. This operating condition corresponds to state 2.

At 3.5 s, load 1 is also increased to 100 W. With this load increase, the storage is unable to maintain the balance of power alone. Figure 7.12(b) shows that the storage briefly supplies its peak current to the system. This increase in output however, is insufficient to balance the load, as indicated by a sharp decrease in the bus voltage shown in Figure 7.12(c). Once the generator node has detected the decrease in bus voltage below its voltage threshold, V_3, it comes online. It should be noted that a startup delay of 100 ms is imposed on the generator node to demonstrate the adverse effect of startup delay in a practical system. During the startup period of the generator node, a power shortfall exists in the system, causing the bus voltage to decrease below the designed the voltage window. The load interface converters in turn lose regulation of their output since they are designed to maintain a regulated output of 12 V at full load within this voltage window. This problem of a temporary power shortfall can be addressed with the use of additional storage or by using load shedding.

Once the generator has come online, it takes the same discharge priority as the renewable sources and supplies its maximum power to the system in a bid to balance the load. Since this is insufficient to balance the load, the storage discharges at a reduced rate of 0.1 A to supply the balance of power required by the system.

System Response to Supply Changes

Figure 7.13 demonstrates the effect that changes in the MPP of the renewable sources have on the supply-side control law. For this experiment, the MPP of the renewable sources is varied, and the resultant changes in the dc bus and storage and generator output currents are monitored. Figure 7.13(a) shows the variations in the renewable source

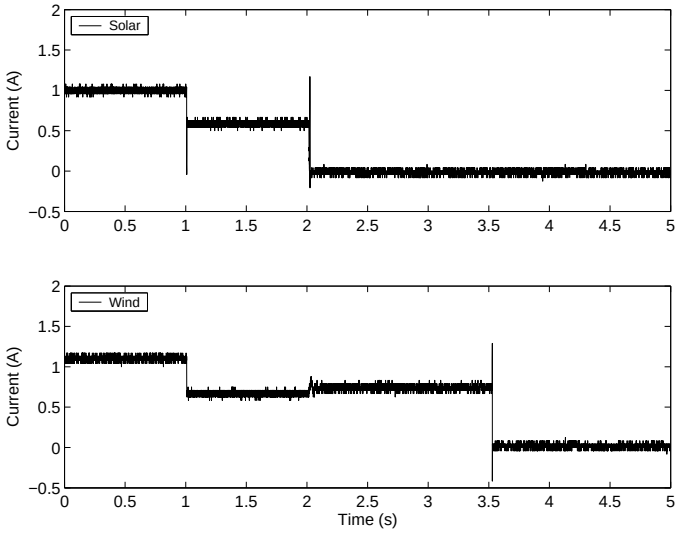

(a) Source interface converter currents

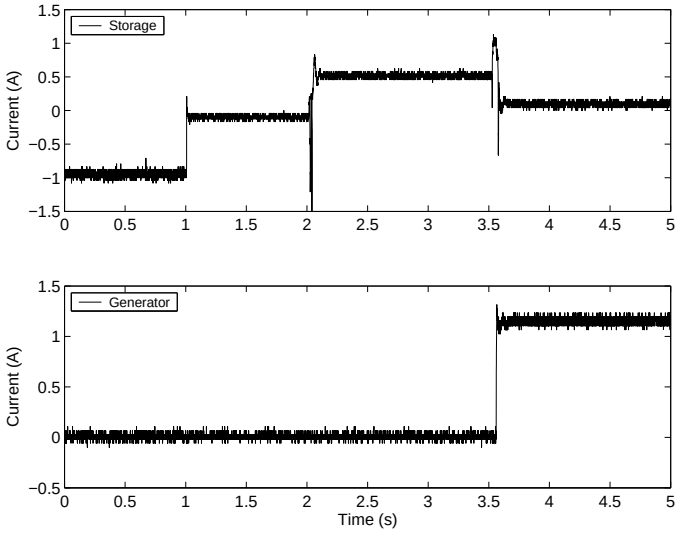

(b) Generator and storage currents

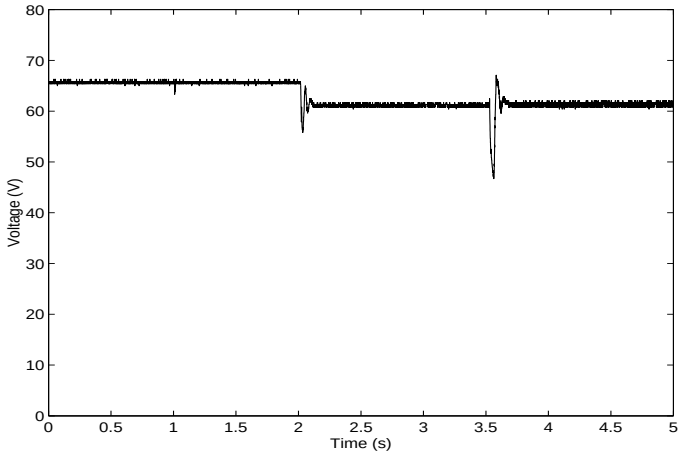

(c) Voltage at bus V1

Figure 7.13 Effect of renewable supply changes

supply currents, and Figure 7.13(b) shows the current supplied by the the generator and storage nodes to maintain the power balance. The voltage level at bus V1 is portrayed in Figure 7.13(c). The load currents are omitted for simplicity as the loads remain constant for the duration of the experiment. In this experiment, load 1 is set to 25 W, and load 2 is set to 50 W.

Initially the MPP of the wind turbine and photovoltaic array are both 75 W. An excess of renewable power exists in this operating condition, therefore the storage charges at a rate of -1 A to take up the power slack. The bus voltage is therefore regulated by the storage node to its voltage threshold for charging, V_1.

At 1 s, the MPP of both the wind turbine and photovoltaic array are reduced to 50 W. This supply change impinges on the excess power available to the storage. The storage node therefore charges at a reduced rate of -0.1 A.

At 2 s, another reduction in the power available from the renewable sources forces the storage node to begin discharging. The MPP of the photovoltaic array is reduced to zero, effectively bringing this source offline. The storage node begins discharging at a rate of 0.5 A to maintain the power balance. It should be noted that at this point, the bus voltage decreases to the storage node's discharge voltage threshold, V_2.

The wind turbine is also brought offline at 3.5 s, requiring the storage to balance the load alone. The output of the storage node briefly spikes to a peak value of 1.2 A as indicated in Figure 7.13(b). However, since the total load current still exceeds the peak storage output, the bus voltage collapses, signalling the generator node to begin discharging. After a brief startup delay, the generator comes online, supplying its maximum current of 1.2 A to the system. The storage remains discharging since it is still needed to supply power in order to balance the load.

7.6.2 Verification of Demand-Side Control Law

To verify the operation of the demand-side control law, the experimental setup shown in Figure 7.1 is first modified to permit the operation of load shedding. The modified system, shown in Figure 7.14, has loads that are divided into three different priorities: low, medium, and high. Load shedding is facilitated in the system by extending the control capabilities of the load controller. The software in the load controller is redesigned such that it can deactivate the loads when the system is in danger of an overload. Two separate load shedding functions, Load Shedding 1 and Load Shedding 2, are written to ensure that

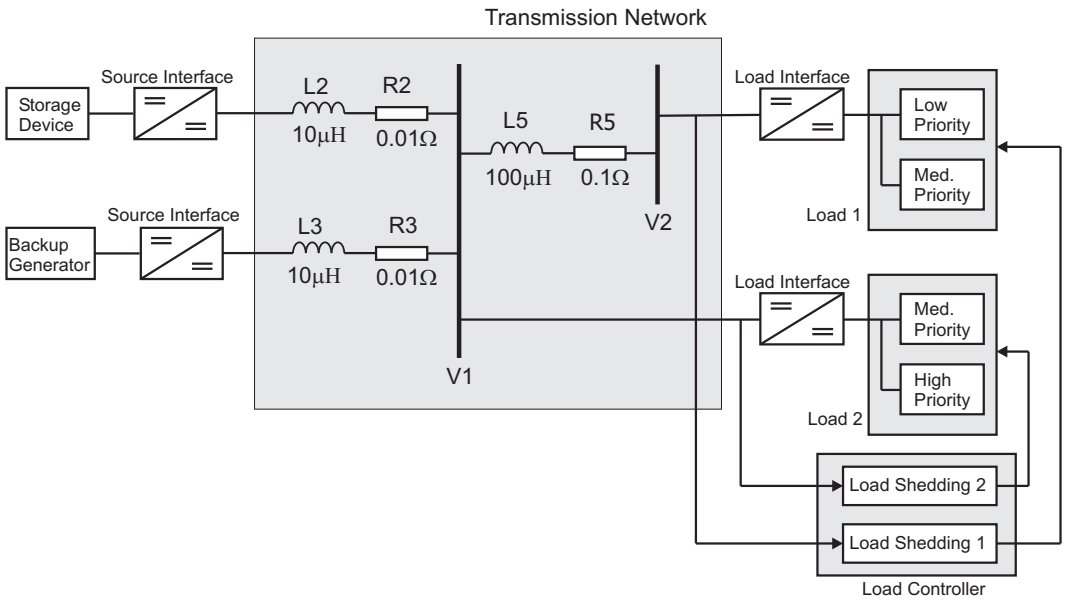

Figure 7.14 Experimental setup for load shedding

the load shedding is performed based on the voltage at each load's point of connection with the system. Load 1 is controlled based on the voltage level at bus V2, and load 2 based on the voltage level at bus V1.

With the test setup modified, the demand-side control law is verified in the experimental system by monitoring the response of the loads to overload conditions. As with the simulation model, overload conditions are created by reducing the available supply or increasing the load such that the total load demand exceeds the available generation. These operating conditions cause load shedding to occur as shown in Figure 7.15.

Initially the system operates in state 3, with the renewable sources inactive. The total load on the system is 125 W. Load 1, comprising 25 W of both low and medium-priority load, contributes 50 W to this total. Load 2 contributes 75 W to the total load in the form of 50 W of medium-priority load and 25 W of high-priority load. The supply currents of loads 1 and 2 are shown in Figures 7.15(a) and 7.15(b) respectively. It should be noted that the load currents are monitored at the 12 V output side of the load interface converter rather than the 70 V input side to allow the portion of current the load interface converter supplies to each load to be distinguished. Consequently, the load current response has a larger magnitude than that portrayed in the supply-side control law load currents, which are monitored at the 70 V side.

In order to supply power to the loads, the storage node supplies its peak output of 75 W to the system and the generator acts as a slack bus, providing power to supply the remaining load demand and compensate for the power losses in the system. The supply currents

are shown in Figure 7.15(c). Because the generator acts as a slack bus, the bus voltage is regulated at the generator's discharge voltage threshold, V_3, as shown in Figure 7.15(d).

The first overload condition is created at 1.75 s by increasing the high-priority portion of load 2 from 25 W to 50 W. As shown in Figure 7.15(b), the current drawn by the high-priority load peaks before settling to its new value due to the startup current surge of the incandescent lamp used as the load. The output of the generator interface briefly increases to its peak value in a bid balance the increased load. However, since this supply increase is insufficient to maintain the power balance in the system, the bus voltage collapses. The load controller therefore sheds the low-priority load to restore the power balance. Power is therefore maintained to the medium and high-priority loads during the overload. It should be noted that because the bus voltage briefly deviates outside the designed operating window, decreasing to 40 V during the overload. This causes the load interface converters to briefly lose regulation of their output, as can be seen by the glitch in the current drawn by the medium-priority load.

The second overload condition is created by removing the storage from the system at 3.25 s as shown in Figure 7.15(c). The load once again exceeds the maximum generation and consequently the bus voltage decreases. When the load controller has detected that the voltage at each load bus has decreased below the shutdown threshold of the medium-priority loads, V_{s2}, the medium-priority loads are shed, restoring the power balance in the system. Thus the power to the high-priority loads remains uninterrupted aside from a brief transient glitch.

7.6.3 Discussion

The experimental results demonstrating the operation of the supply and demand-side control laws compare well with the simulation results presented in Chapter 6. Although the rating of the experimental system is one-tenth that of the simulation model, the results show that similar changes to the loads and renewable sources cause the same transitions in operating states. However, there are some notable differences to be seen in the transient response. The most apparent of these are the current spikes that occur during step change increases in the load. These load transients are not seen in the simulation results. This anomaly can be attributed to the use of incandescent lamps for the loads. During a cold start, the filament draws a peak current that is three times its nominal operating current for 150 ms. The simulation results do not depict this startup transient since the load

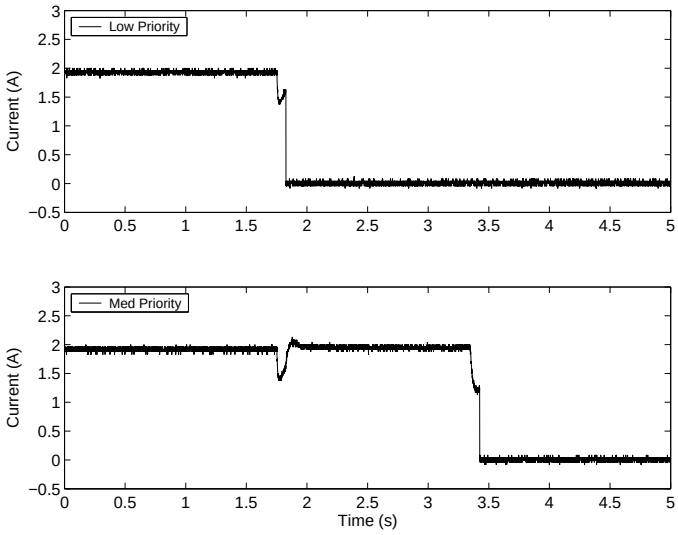

(a) Load 1 currents

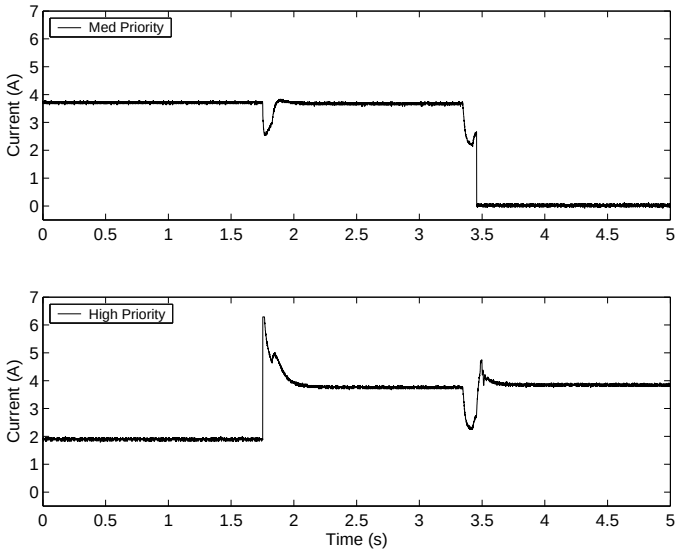

(b) Load 2 currents

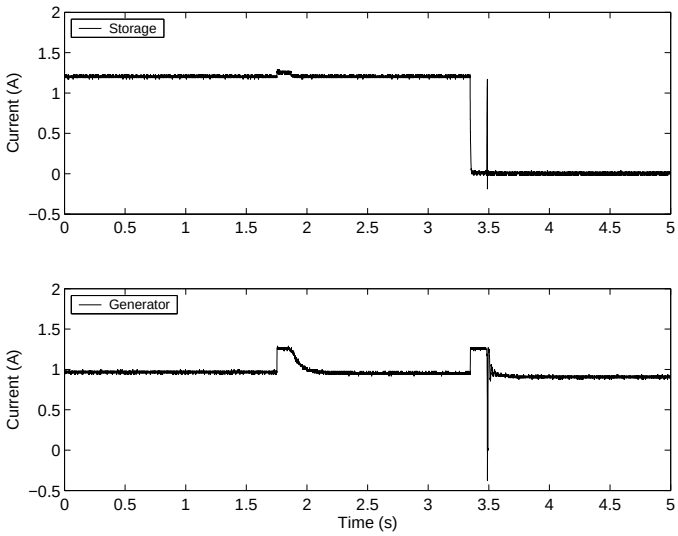

(c) Generator and storage currents

Figure 7.15 Load shedding results

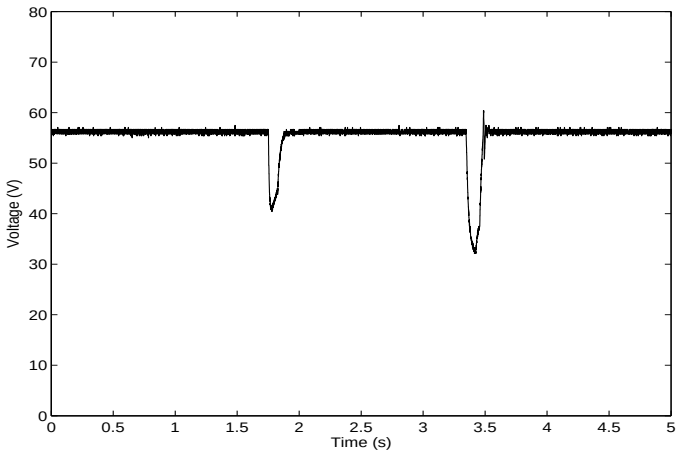

(d) Voltage at bus V1

Figure 7.15 Load shedding results continued

model does not account for this low startup resistance.

The results depicting the operation of the supply-side control law highlight the need for short-term storage in a practical system. For example, the temporary power imbalance caused by the startup delay of the generator causes the bus voltage to deviate outside the nominal operating window. In a practical system, this may cause sensitive electronic equipment to malfunction. This problem can be addressed with the use of short-term storage, as explained in Section 8.6. The short-term storage would idealise the startup response of the generator node, preventing any startup delay from affecting the performance of the system.

As with the simulation results, the load shedding results show that under overload conditions, the demand-side control law prevents the dc bus from a complete collapse by shedding loads, beginning with those having the lowest priority. Again, the only real difference between the two sets of results is the transient response. Under overload conditions, the bus voltage in the experimental system briefly decreases to approximately 50% of its nominal value, whereas the bus voltage in the simulation model drops by only 5%. Since this deviation is well outside the designed voltage window of the system, the load interface converters are briefly unable to maintain regulation of the loads. A main reason for this anomaly is the time delay added to the load controller to prevent very brief glitches in the supply voltage from causing loads to be shed.

This brief collapse of the supply voltage is unlikely to pose any problems for loads such as heating and lighting. However, for sensitive electronic equipment, this brief decrease in the bus voltage may be an issue since these loads require a constant supply voltage.

To circumvent this problem, the load converters could be redesigned to regulate the output voltage over a wider operating window. Alternatively, additional storage could be combined with sensitive critical loads to ensure they enjoy a constant supply of power.

Overall, the experimental results have verified the viability of using DBS to schedule sources in a practical power electronic based system. Even in the presence of transmission line impedance, information was successfully conveyed in the form of voltage level changes to the source and load interface converters, allowing the supply and demand-side control laws to operate successfully. The experimental results compared well with the simulation results in terms of the steady-state response. With the same supply and load changes applied to the system, the supply and demand-side control laws responded in the same manner in order to restore the power balance in the system. However there were anomalies present in the transient response, which were the result of differences between the simulation model and experimental system.

Chapter 8

PRACTICAL ISSUES

8.1 INTRODUCTION

The previous chapter has verified the practicality of DBS by implementing the strategy in an experimental system that was built in the laboratory. In a real-life system however, a number of practical issues must be addressed in order to ensure the successful operation of a nanogrid. This chapter deals with the main issues related to the operation of a dc system that is based on power electronics, namely operation under fault conditions, the impact of the operating voltage on the interface converter design, and small-signal stability. Since dc systems based on power electronics have previously been examined for practical applications, these issues are addressed by highlighting solutions that have been proposed for existing systems. In addition, issues related to the impact of DBS on the design of the system are examined in this chapter. One of these issues is sizing the range over which voltage level changes on the dc bus are permitted. Known as the voltage window, this voltage range must be minimised to maximise transmission efficiency. Lastly, the need for including short-term storage in the system to idealise the startup response of backup generation is explained.

8.2 OPERATION UNDER FAULT CONDITIONS

8.2.1 Source Interface Converter Current Limiting

Under normal operating conditions, a significant decrease in load resistance causes the source interface converters to enter a constant power limit mode. When the source interface converters enter this mode of operation, the bus voltage decreases, bringing additional sources online. The constant power characteristic of the source interface converters is nor-

mally acceptable since the source interface converters should supply their maximum power to the system despite small decreases in the bus voltage. However, when the bus voltage collapses due to fault conditions, the constant power characteristic potentially causes large fault currents to flow.

The output current of each source interface when operating in constant power mode is given by $I_o = P_{max}/V_o$, where P_{max} is the MPP of the renewable source or the peak power rating of the converter and V_o is the bus voltage. As a fault reduces the bus voltage towards zero, the output current of each source interface converter becomes very large. In the same way that an additional mode of operation is added to the load interface converters to shut them down in a prioritised fashion in the event of an overload, a current-limiting mode of operation is added to the source interface converters to protect the nanogrid in the event of a fault.

To prevent excessive fault currents from flowing, the source interface converters are designed to exhibit a current limit mode when the bus voltage decreases below the voltage window. There are two possible types of fault current limit that can be implemented in the source interface, a current foldback limit or a constant current limit. With current foldback, the current limit is decreased as the bus voltage decreases. With a constant current limit however, the current limit remains unchanged when the bus voltage collapses.

A constant current limit, shown in Figure 8.1, is used for the source interface converters since this current limit is simpler to implement than a current foldback limit. Current foldback is primarily used in linear power supplies to prevent the power dissipation in the supply from increasing when the output voltage decreases to zero [58]. However current foldback does not provide any significant advantages for switching converters, which are non-dissipative regulators. Adopting current foldback for switched mode converters may also introduce problems such as startup lockout of nonlinear loads [58].

8.2.2 DC circuit breakers

Although the constant current limit feature of the source interface converters acts to limit the fault current, dc circuit breakers must be included in the system to provide rapid detection and electrical isolation of any fault. DC circuit breakers are generally more complicated than their ac counterparts since dc arcs are inherently non-self extinguishing. When a dc switch begins arcing, the arc is maintained until the switch voltage decreases below a certain level. In the ac system, arcing is not as great a problem since the zero

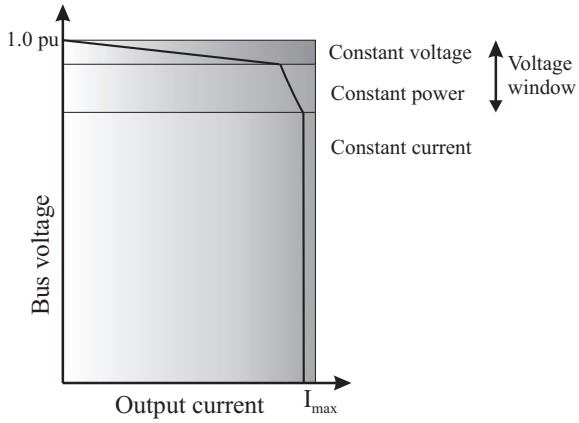

Figure 8.1 Constant current limit for source interface converter

crossings in the ac waveform make it difficult for an arc to be sustained.

There are three different types of circuit breakers that can be used in dc systems: mechanical, solid-state, and hybrid. Mechanical circuit breakers are the most basic variety. Simple in construction, they are robust and provide electrical isolation. However, they have a limited lifetime due to mechanical degradation of the contacts under switching. For low voltage dc applications, mechanical ac circuit breakers can be employed, provided the ratings are adjusted according to the manufacturers specifications [59]. To adjust the ac trip curves for dc applications, a multiplying factor of $1.1 - 1.4$ is typically used. The molded-case circuit breaker is commonly used for low voltage dc applications [60]. This circuit breaker is typically rated from 10 to 2500 A at 600 V dc.

Solid-state circuit breakers on the other hand consist of no moving parts and can provide millions of operating cycles without degradation since no arcing is generated during switching. Solid-state circuit breakers offer advanced features such as programmable trip times and current ratings, Typically controlled with a microcontroller, solid-state circuit breakers can be programmed to respond to trip at small overloads, provide transient overload and I^2t protection, and not react to inrush currents [34, 61]. Due its control flexibility, the solid-state circuit breaker has been proposed for use in spacecraft applications that operate at 120 V dc [61].

Solid-state circuit breakers also provide faster interruption of fault currents than mechanical circuit breakers. For example, a solid-state circuit breaker that is based on an emitter turn-off thyristor can interrupt fault currents of 1.5 kA in 5 μs [62]. The main drawback with solid-state circuit breakers is their inability to provide electrical isolation, and their higher power dissipation than mechanical circuit breakers. Solid-state circuit breakers have a higher forward voltage drop than mechanical circuit breakers and therefore need a

heatsink to dissipate the extra power. However it should be noted that the losses in the circuit breaker are insignificant compared with the total load demand. For example, an IGBT-based circuit breaker with a forward voltage drop of 2 V only dissipates 6 W in a 700 V, 2 kW nanogrid. This loss is equal to 0.3 % of the total load demand.

To combine the advantages of solid-state and mechanical circuit breakers, hybrid topologies must be used. A common hybrid design includes mechanical contacts in series with a solid-state circuit breaker to provide electrical isolation [34]. Under fault conditions, the solid-state circuit breaker first interrupts the fault current. The mechanical contacts are then opened to provide electrical isolation. This arrangement minimises wear on the metal contacts since the contacts essentially switch at zero current, producing no arcing.

Although all three circuit breaker topologies can potentially interrupt fault currents in a nanogrid, only the mechanical and hybrid circuit breakers are suitable candidates since they provide electrical isolation of the fault. The hybrid circuit breaker is better-suited to a nanogrid since it provides faster operation than a mechanical circuit breaker and has programmable features, while not presenting significant losses. In a nanogrid, the mechanical circuit breaker will not respond as quickly to faults as the hybrid circuit breaker since the fault current is kept at a small value by the current limiting feature of the source interface converters. Furthermore, the programmable features of hybrid circuit breakers are an advantage since they can be designed to ignore normal transient current spikes, preventing nuisance tripping.

8.3 IMPACT OF TRANSMISSION VOLTAGE ON CONVERTER DESIGN

Another practical issue of importance in a nanogrid is the selection of the operating voltage. The operating voltage not only affects the transmission line efficiency as explained in Section 3.6, but also has a major effect on the design of the interface converters. With a full-bridge converter topology, the operating voltage dictates the voltage rating of the input switches in the load interface converter and the voltage rating of the output diodes in the source interface converter. Ideally, MOSFET switches should be used in the load interface converter to permit a high switching frequency and thus reduce the size and cost of the magnetic components. However, the peak voltage rating in silicon MOSFETs is currently limited to approximately 1000 V. This limits the admissible bus voltage.

To permit the nanogrid to operate at a higher voltage, different switches or converter topologies must be used. The use of silicon carbide (SiC) MOSFETs will allow a higher

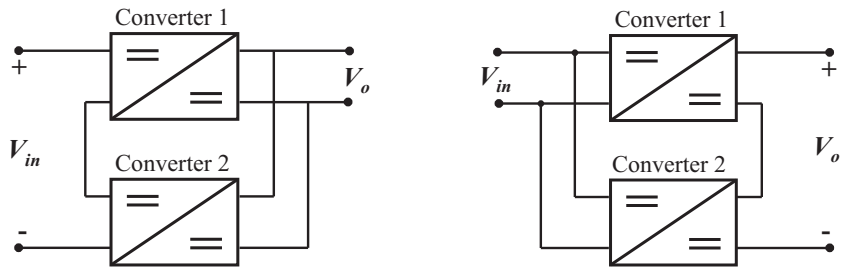

(a) Series-input, parallel-output (b) Parallel-input, series-output

Figure 8.2 Converter configurations

operating voltage. The breakdown voltage of SiC MOSFETs is 1800 V, roughly twice that of their silicon counterparts [63]. Similarly, the use of insulated gate bipolar transistor (IGBT) switches will allow a higher operating voltage. IGBTs have voltage ratings in the order of 1500-2000 V; however, they cannot switch as fast as MOSFETs due to their higher turn-off losses. Multi-level or multi-stage converters may also be used to reduce the voltage or current rating on each individual switch.

Connecting multiple converters in different configurations as shown in Figure 8.2 eases the voltage or current rating on the semiconductor switches by distributing the total voltage or current between the converter modules. The series-input, parallel-output configuration allows the converters to share the input voltage [64], and the parallel-input, series-output configuration reduces the current stress on the input switches of MOSFET-based step-up converters with a high voltage transformation ratio [65].

The main advantage of using converter modules connected in series/parallel to increase the effective voltage/current rating of the converter is that this approach lends itself well to the mass production of a universal converter module that can be used as the building block for a nanogrid. This modular configuration will simplify the converter design requirements for systems with different voltage and power ratings. Using these modular building blocks, converters with higher power or voltage requirements can be formed by simply connecting additional converter modules in series or parallel.

8.4 SMALL SIGNAL STABILITY

Another major issue that must be addressed in a power electronic system is small signal stability. A power electronic system can become unstable when the source interface converters, designed using conventional techniques, are connected to load converters rather than resistive loads. Interaction can occur between the source and load interface convert-

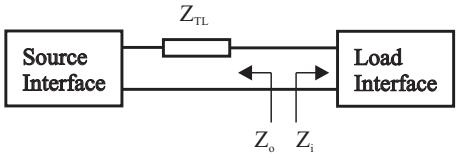

Figure 8.3 Small signal impedances in a power electronic system

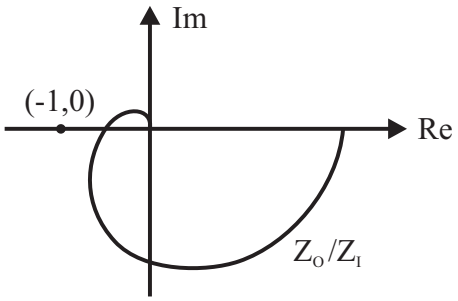

Figure 8.4 Nyquist plot for a stable power electronic system

ers [56, 57]. If the system is not designed correctly, the interaction between the converters can result in an underdamped or unstable system in the small signal sense. This issue was addressed in a simple manner in Section 7.4 for the experimental system. This section delves into the issue of small signal stability in more detail, presenting solutions that are well-suited for deployment in a real-life system.

8.4.1 Definition

The system stability is determined by the ratio of the small signal output impedance to input impedance, Z_o/Z_i, where Z_o is the output impedance of the source interface converter in conjunction with the effective transmission line impedance, Z_{TL}, and Z_i is the cumulative input impedance of the load interface converters. These parameters are shown for a simple system in Figure 8.3. The Nyquist plot for a stable system is shown in Figure 8.4. The system becomes unstable if Z_o/Z_i encircles (-1,0) on the Nyquist plot.

8.4.2 Forbidden Region

The issue of small signal stability was first examined by Middlebrook in 1976 [66] when he examined the interaction between a converter and its input filter. The solution proposed to ensure stability of this small system was to ensure the output impedance of the filter Z_o was much smaller than the input impedance of the converter over the entire frequency range, i.e. $|Z_o| << |Z_i|$. In a distributed power system, adopting this approach is impractical as

it results in a conservative, costly design [67].

A more recent contribution that proposes a less conservative design requirement for a distributed power electronic system is given in [68]. An alternative forbidden region is proposed to ensure stability of the system:

$$\mathrm{Re}\left(\frac{Z_o}{Z_i}\right) \geq -1/2 \tag{8.1}$$

By designing the system such that Z_o/Z_i stays out of the forbidden region, stable operation of the system is ensured. The system exhibits a gain margin of 6 dB and a phase margin of 60°.

8.4.3 Solutions

In order to address the problem of small signal stability for a nanogrid, a number of solutions that have been proposed for power electronic dc systems are first examined. The issue of small signal stability can be addressed using a variety of techniques. In general these methods fall into two categories. They either shape Z_o or Z_i to ensure the system is stable according to Equation (8.1).

Shaping Z_i

Shaping the input impedance of the load subsystem, Z_i, is the most common approach outlined in literature. The input impedance is modified at the modular or system level to make the load appear more resistive.

One approach that tackles the issue at the system level is to use an active bus conditioner [69]. Behaving in a similar manner to an active filter, the bus conditioner effectively increases the input impedance of the load interface converters by compensating for the ac component on the dc bus.

Another approach is to increase the dc bus capacitance [57]. This increases the phase margin of the system, but results in a large inrush current and a poor dynamic response. Another solution proposed in [57] is to reduce the bandwidth of the voltage control loop of the load interface converters. This effectively increases Z_i at all but frequencies below the bandwidth of the load interface converters' voltage loop.

A solution that addresses the issue of small signal stability at the modular level is to use input filters to shape the input impedance of each load converter [70]. With this

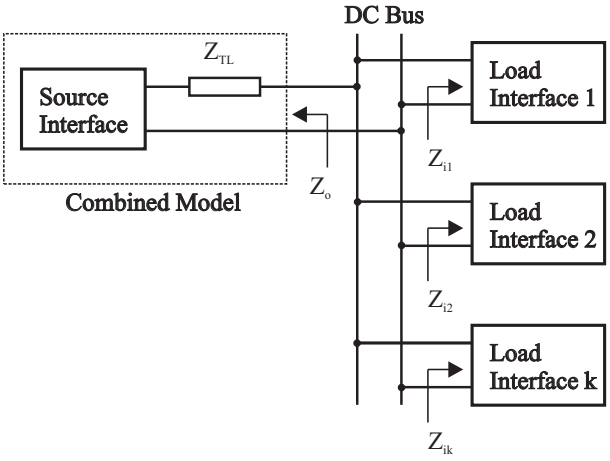

Figure 8.5 Impedances in a multi-converter system

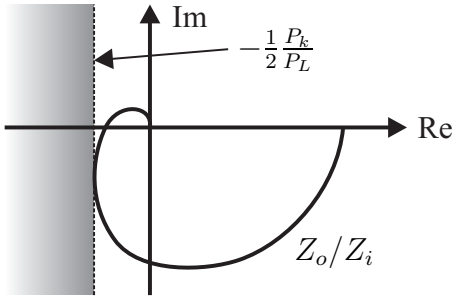

Figure 8.6 Forbidden region for individual load interface converters

approach, the system-wide impedance specification in Equation (8.1) is modified to obtain an impedance requirement for each converter a multi-module system such as that shown in Figure 8.5. The individual impedance specification for each load converter is obtained by adjusting the impedance specification according to the power level of each load. The forbidden region for each module is thus defined as

$$\mathrm{Re}\left(\frac{Z_o}{Z_{ik}}\right) \geq -1/2\left(\frac{P_k}{P_L}\right) \tag{8.2}$$

where P_k/P_L is the proportion of the total load the module supplies, and Z_{ik} is the input impedance of the module under consideration. This new forbidden region is portrayed in Figure 8.6.

The input filter is designed to shape Z_{ik} such that the individual impedance specification in Equation (8.2) is satisfied. With this approach, the interaction between the input filter and the load interface converter itself must also be considered to ensure the load interface converter does not interact with the input filter.

Shaping Z_o

The output impedance of each source interface converter can also be modified to ensure the system operates in a stable fashion. For example, it has been shown that a non-linear stabilising controller is capable of stabilising the source converter present in a multi-converter system [56]. In [71], it is also shown that when the control loop for the source converter is designed correctly, stable operation of a multi-converter system can be ensured. For example, a current controlled buck type converter can be stabilised by selecting a sufficiently large integrator gain. This technique compensates for the RHP pole present in the control transfer function when the converter is supplying a constant power load.

8.4.4 Application to a Nanogrid

Although a number of techniques are available for maintaining the small signal stability in a power electronic system, not all techniques are well-suited to a nanogrid. Ideally, the chosen method should solve the problem at the modular level in order to maintain the modularity inherent in the structure of the system. Therefore employing input filters and stabilising controllers are the two techniques that should be adopted for a nanogrid.

It should be noted that using input filters and stabilising controllers to maintain stability is not as simple in a nanogrid compared to systems based on controllable sources. In a nanogrid, the structure of the system changes as additional sources come online to meet the fluctuating load demand. The effective transmission line impedance changes, in turn affecting Z_o. To ensure stability under all operating conditions, the operating condition that creates the largest output impedance must be accounted for.

8.5 SIZING THE VOLTAGE WINDOW

One of the main differences between a nanogrid and the ac system is that the voltage regulation of the ac system is maintained within strict standards, whereas the bus voltage in a nanogrid varies as the operating state changes. As the operating state changes, the voltage threshold to which the dc bus is regulated alters as additional source/storage interface converters come online. The nanogrid operates over a range of voltages, known as the voltage window. A large voltage window prevents optimal design of the system, as the interface converters must be designed to operate over a range of bus voltages.

However, the voltage window can be minimised by reducing the voltage drop that occurs in each operating state.

8.5.1 Need for a Voltage Window

A voltage window is necessary with the use of DBS since the transmission line impedance and voltage droop of the converters introduce voltage drop into the system. This affects the discrimination of the voltage threshold to which the dc bus is being regulated by converters assigned to lower voltage thresholds. The extra voltage drop in the system causes unequal propagation of the dc bus voltage throughout the transmission network, causing the converters to experience different voltages at the same operating point.

As explained in Section 5.4, this problem is alleviated by spacing the voltage thresholds apart to allow each converter to discriminate the existing voltage threshold in spite of these disturbances. The gap between voltage thresholds is calculated to ensure that the parasitic voltage drop in the system does not prematurely activate converters assigned to lower voltage thresholds. However this increases the size of the voltage window.

8.5.2 Impact of Voltage Window on System Design

Although a voltage window is necessary to allow the implementation of DBS in a practical system, a large voltage window is detrimental to the efficiency and cost of the system. A large voltage window reduces the transmission line efficiency when the system operates at the lower end of the window. For example, the conduction losses in a transmission line increase by approximately 56% when the operating voltage is reduced to 80% of its nominal value. This is illustrated with the lumped nanogrid model shown in Figure 8.7.

In the lumped nanogrid model, the sources are grouped as V_S', and the total load on the nanogrid is P_L'. The equivalent transmission line resistance is denoted as R_{TL}'. With $V_S' =$ 1.0 pu, the line current is approximately given by V_S'/P_L'. In practice, the line current is slightly higher because the constant power load draws additional current to compensate for the line losses. With a load of 1.0 pu, the line losses are $1.0 \times R_{TL}'$. When the nanogrid bus voltage decreases to 0.8 pu, the line current increases to 1.25 pu and the line losses are equivalent to $1.56 \times R_{TL}'$, an increase of 56%.

A large voltage window also increases the current stress in the load interface converters when they operate at the lower limit of the window. Since the converters act as constant

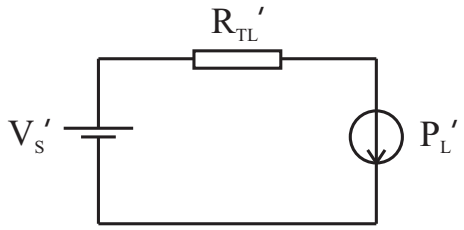

Figure 8.7 Lumped nanogrid model

power loads, the current drawn from the system increases as the bus voltage drops. With a significant voltage window, the increased current creates higher conduction losses in the converter switches, which may result in the need for larger heatsinking. In addition, the current rating of the switches in the load interface may need to be increased to cope with the increased current that occurs at the lowest bus voltage.

8.5.3 Minimising the Voltage Window

The voltage window is shown in Figure 8.8. It can be seen that the voltage window, V_w, is the difference between the upper voltage threshold, V_0, and the lowest voltage present in the system when converters assigned to the lowest voltage threshold are online. This is denoted as V_{min}. The voltage window can also be calculated using

$$V_w = V_0 - V_n - Vd_n - V_e \tag{8.3}$$

where V_n is the lowest voltage threshold, Vd_n is the worst case voltage drop in operating state n, and V_e is the margin of error. The margin of error is usually fixed; however, the voltage drop is dependent on the design of the system and the peak loading. Assuming that V_e is the same for all states, the voltage window in (8.3) is also given by

$$V_w = \sum_{i=1}^{n} Vd_i + n \cdot V_e \tag{8.4}$$

It can be seen that the voltage window can be minimised by reducing the voltage drop, Vd_i. The voltage drop is caused by the potential difference across the transmission line resistance and the steady-state error caused by the use of voltage drop.

The best method of minimising the voltage window is to increase the nominal operating voltage of the system, V_0. A high nominal operating voltage reduces the voltage drop across the transmission line resistance since the line current is reduced at a higher voltage

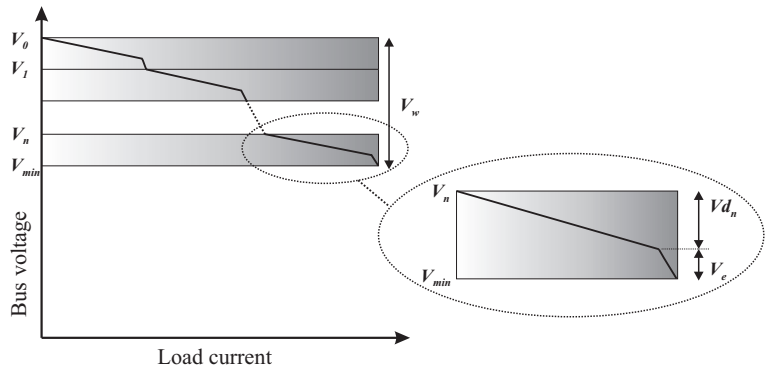

Figure 8.8 Voltage window

level. It must be noted that increasing V_0 impacts the design of the interface converters as explained in Section 8.3.

The other possible method of minimising the voltage window is to reduce the resistance of the transmission lines since this reduces the voltage drop across the lines. Because this is usually a costly exercise, increasing the operating voltage of the system should be used in preference to this method.

8.6 VOLTAGE COLLAPSE AND SHORT-TERM STORAGE

Another practical issue that must be given consideration is the need for short-term storage to compensate for temporary power shortfalls in the system. Power shortfalls cause the dc bus to collapse, adversely affect the operation of the loads. A major cause of power shortfalls in a practical system is the startup delay of backup generation. The experimental results given in Figure 7.13 showed that with a 100 ms generator startup delay, the voltage on the 70 V bus fell below the operating window of the load interface converters, causing them to lose regulation. In practice, this issue is likely to be exacerbated since the startup time of a generator is typically in the order of seconds rather than milliseconds.

One possible solution to this problem is to design the storage interface converter with a transient overload capability such that it can supply the temporary power shortfall. The transient overload mode of operation would become active at a threshold below the generator's threshold, supporting the bus yet allowing the generator to be triggered online. The major benefit with this solution is that additional hardware is not required.

Further measures may be needed if the transient overload capability of the storage interface is not sufficient to supply the necessary power shortfall. One means of achieving this is to combine short-term storage at the low voltage side of the generator node to prevent

stability problems from arising. A multi input converter topology is required for this solution to allow the interface converter to supply power to the system from either the backup generator or the storage. An example of such a topology is given in [72] to allow battery storage to buffer power shortfalls in a fuel cell system. The main requirement with this solution is that the storage is sized such that it can provide the worst-case energy shortfall in the system while the generator is starting.

8.7 SUMMARY

A number of practical issues pertaining to the operation of a dc system based on power electronics have been addressed in this chapter. Firstly, the issue of operation under fault conditions has been examined. By designing the source interface converters with a constant current limit, the fault current can be limited. Electrical isolation of the fault can be achieved using a mechanical or hybrid circuit breaker, with the latter providing a faster response and greater operational flexibility. The impact of the operating voltage on the design of the interface converters has been discussed. The operating voltage is limited by the voltage rating of the switches in the load interface converter. However, this problem can be alleviated by connecting converter modules in series to share the total bus voltage. In addition, the issue of small-signal stability in a modular power electronic system has been addressed. The small-signal stability of a nanogrid can be maintained in a modular fashion by using input filters for the load interface converters and stabilising controllers for the source interface converters.

Practical issues specifically related to the use of DBS in a nanogrid have also been examined. To permit the operation of DBS in a nanogrid, a voltage window is necessary, although this reduces the efficiency of the transmission line at the lower bound of the window. The voltage window can be minimised by reducing the resistance of the line or selecting a higher operating voltage. Another practical requirement required to permit the operation of DBS in a nanogrid is short-term storage. Short-term storage must be used in parallel with sources in a nanogrid that have a non-ideal startup response to prevent the dc bus from a total collapse during the startup period of the source.

Chapter 9

CONCLUSION

9.1 FUTURE WORK

This thesis has presented a novel control strategy, DBS, as a means of implementing a supply and demand-side management scheme in a nanogrid. The theory behind the operation of DBS has been explained, and the procedure by which supply and demand-side control laws are implemented in a nanogrid using DBS has been detailed. Although the key issues related to the operation of this control strategy in a nanogrid have been addressed, there is still scope for additional work to be carried out in this field of research.

Firstly, there are many opportunities for further research to be conducted in the area of analysing system design tradeoffs. For example, scope exists for investigating the relationships between efficiency, operating voltage and cost for the transmission lines and interface converters.

Another area of future work is to design soft-switching or resonant converters for the source and load interface converters. The experimental results were obtained from a system based on full-bridge, hard switched converters. While these converters are simple to construct, they do not provide the necessary efficiency demanded by a renewable energy system. The converters should ideally function as modular building blocks, allowing series/parallel connection with other converters. This modular configuration will simplify the converter design requirements for systems with different voltage and power ratings. Using these modular building blocks, converters with higher power or voltage requirements can be formed by simply connecting additional converter modules in series or parallel.

Another area of possible future work is to develop an algorithm that automatically calculates the voltage thresholds for the supply-side interface converters, and the shutdown thresholds for the load-side interface converters. To implement DBS in the simulation and

experimental systems, these thresholds were calculated manually by performing a dc load flow for each loading permutation. While this approach is adequate for small systems, it will not suffice for larger systems containing many loads due to the number of permutations. Therefore a fully-automated program that calculates each voltage or shutdown threshold would be beneficial for larger systems.

Lastly, the opportunity for the storage interface to double as an active bus conditioner could be examined. It was explained in Section 8.4.3 that one method of dealing with the issue of small signal stability is to compensate for the ripple on the dc bus, making the load appear more resistive. Because the storage device is capable of injecting and absorbing power from the system, it could also provide this high-frequency damping function. An investigation into the control design required for the storage device to perform this function could therefore be carried out.

9.2 CONCLUSION

Advances in power electronics have created new opportunities for harnessing renewable resources. With the use of switching converters, renewable sources can be connected directly to the central ac system. Another option is to combine renewable sources with local loads to form an independent power system such as a nanogrid.

A nanogrid is completely power electronic based. Power electronic interface converters connect both sources and loads to the system. Consequently, a nanogrid is not restricted to operation at 50/60 Hz. This thesis has evaluated a number of possible transmission frequencies to determine the frequency that provides most benefits to a nanogrid. The final choice was made between dc and 50 Hz since both operating frequencies have their advantages. DC was chosen largely because it has simpler requirements for interfacing asynchronous ac sources or variable voltage dc sources to the system. DC also presents less risk of fibrillation and has the best transmission efficiency. In addition, the choice of dc necessitates the use of load interface converters to connect loads to the system as opposed to 50 Hz transformers. The load interface converters can be controlled to provide better power quality to the loads than transformers in an ac system, and voltage deviations on the system bus can be used to convey control information without adversely affecting the operation of the system.

A number of different control topologies were evaluated for implementing a supply-side management scheme in a nanogrid. Hybrid distributed control was identified as a suitable

control topology since it allows the implementation of a supply-side control law with the same reliability and implementation cost as a decentralised control strategy. A novel control strategy, DBS, was proposed as a method for implementing a supply-side control law using this control topology.

The main attraction with DBS is its simplicity and reliability. Compared with the conventional hybrid central control technique, a central controller and communications link are not required, and the control strategy maintains the modularity and reliability inherent in the structure of the distributed system. The system can still operate according to the supply-side control law if supply modules fail, and additional modules can be added with the ease of a plug-and-play system.

The principal contribution of this thesis was the development of DBS for implementing a supply-side management scheme in a nanogrid. A supply-side control law is implemented using DBS by controlling the source and storage interface converters based on the voltage level of the dc bus. Each converter is assigned a voltage threshold to trigger the point at which it begins discharging into or charging from the system. The converters not only respond to the level of the dc bus, but they also change the level of the dc bus when their maximum power output is exceeded. Thus other converters in the system are automatically controlled.

A procedure for implementing a supply-side control law was presented. To achieve this, the voltage thresholds of the interface converters are prioritised according to their utilisation priority. The voltage threshold values are then calculated to prevent additional voltage drop in the system, caused by transmission line impedance, from prematurely activating sources with a lower utilisation priority. A dc load flow is used to determine the worst-case voltage drop in the system. This same technique was also applied to a demand-side control law to allow its implementation in a practical system with non-ideal transmission line impedance.

Practical issues pertaining to the implementation of DBS in power electronic dc systems were also considered. Although operation of a power electronic dc system poses practical challenges, these issues are by no means insurmountable. Practical issues such as operation under fault conditions and small-signal stability were addressed by pointing to applicable solutions from existing research. In addition, the detrimental effect of an operating window was explained, and methods of minimising the operating window were outlined to allow a reduction of transmission line losses and optimal design of the load interface converters.

The feasibility of DBS was demonstrated with the aid of a simulation model and an experimental system. A simplified simulation model of a nanogrid suitable for steady state analysis was developed, and results were obtained to demonstrate the operation of DBS. The simulation results demonstrated that the supply-side control law maintained the power balance in the system in the presence of of supply and load changes. Under overload conditions, the demand-side control law maintained a constant supply of power to the high-priority loads by shutting down loads with a lower priority. The practicality of DBS was then tested with the aid of an experimental system. The experimental system was designed and constructed in the laboratory to be a scale model of a nanogrid comprising renewable sources, storage and backup generation, and variable loads. The experimental results obtained were consistent with the simulation results, demonstrating that supply and demand-side control laws can be successfully implemented in a practical power electronic based dc system using DBS.

REFERENCES

[1] R Lasseter. Microgrids [distributed power generation]. *IEEE Power Engineering Society Winter Meeting*, 1:146–149, 2001.

[2] Allen J. Wood and Bruce F. Wollenberg. *Power generation operation and control*. John Wiley and Sons, New York, 2 edition, 1986.

[3] J. Gutierrez-Vera. Use of renewable sources of energy in mexico case: San antonio agua bendita. *IEEE Transactions on Energy Conversion*, 9(3):442–450, September 1994.

[4] W. Dalbon, M. Roscia, and D. Zaninelli. Hybrid photovoltaic system control for enhancing sustainable energy. *IEEE Power Engineering Society Summer Meeting*, 1:134–139, 2002.

[5] Riad Chedid and Saifur Rahman. Unit sizing and control of hybrid wind-solar power systems. *IEEE Transactions on Energy Conversion*, 12(1):79–85, March 1997.

[6] B. K. Johnson and R. Lasseter. An industrial power distribution system featuring ups properties. *Power Electronics Specialists Conference*, pages 759–765, June 1993.

[7] Weizhong Tang and R. H. Lasseter. An lvdc industrial power supply system without central control unit. *Power Electronic Specialists Conference*, 2:979–984, 2000.

[8] R. Swisher, C. R. De Azua, and J. Clendenin. Strong winds on the horizon: Wind power comes of age. *IEEE Proceedings*, 89(12):1757–1764, December 2001.

[9] S Dunn. Micropower - the next electrical era. *Worldwatch Paper 151*, July 2000.

[10] A. I. Gardiner and I. A. Sanders. Are microgrids the answer for post 2013? In *Electrical Engineers Association (NZ) Conference*, June 2002.

[11] R. Gasch and J. Twele. *Wind Power Plants*. Solarpraxis AG, Germany, 2002.

[12] F. Blaabjerg, Z. Chen, and S.B. Kjaer. Power electronics as efficient interface in dispersed power generation systems. *IEEE Transactions on Power Electronics*, 19:1184–1194, Sept 2004.

[13] E. Spooner and A. Williamson. Direct coupled, permanent magnet generators for wind turbine applications. *IEE Proceedings Electric Power Applications*, 143(1):1–8, Jan 1996.

[14] Gilbert M. Masters. *Renewable and efficient electric power systems*. Wiley, New Jersey, 2004.

[15] T. Peterson and B. Fies. Solar power to the people. *Physics World*, pages 35–36, July 2002.

[16] James Larminie and Andrew Dicks. *Fuel Cell Systems Explained*. John Wiley and Sons, 2003.

[17] J. Wang, F.Z. Peng, J. Anderson, A. Joseph, and R. Buffenbarger. Low cost fuel cell converter system for residential power generation. *IEEE Transactions on Power Electronics*, 19:1315–1322, September 2004.

[18] *http://www.cfcl.com.au*.

[19] S. Kato, N. Hoshi, and K. Oguchi. A low-cost system of variable-speed cascaded induction generators for small-scale hydroelectricity. *IEEE Industry Applications Conference*, 2:1419–1424, October 2001.

[20] Simon Heng. The design of a 5 kw microhydro generating set. Master's thesis, University of Canterbury, February 1992.

[21] H. L. Willis and W. G. Scott. *Distributed power generation*. Marcel Dekker, New York, 2000.

[22] J.B. Ekanayake. Induction generators for small hydro schemes. *Power Engineering Journal*, 16(2):61–67, April 2002.

[23] John P. Barton and David G. Infield. Energy storage and its use with intermittent renewable energy. *IEEE Transactions on Energy Conversion*, 19(2):441–448, June 2004.

[24] R. Billinton and R. Karki. Maintaining supply reliability of small isolated power systems using renewable energy. *IEE Proceedings Generation, Transmission and Distribution*, 148(6):530–534, November 2001.

[25] *http://www.daws.com.au*.

[26] L.M. Tolbert, W.A. Peterson, M.B. Scudiere, C.P. White, T.J. Theiss, J.B. Andriulli, C.W. Ayers, G. Farquharson, G.W. Ott, and L.E. Seiber. Electronic power conversion system for an advanced mobile generator set. *IEEE Industry Applications Conference*, 3:1763–1768, Oct 2001.

[27] *http://www.whispergen.com*.

[28] L. Weimers. Hvdc light: a new technology for a better environment. *IEEE Power Engineering Review*, 18(8):19–20, Aug 1998.

[29] Weixing Lu and Boon-Teck Ooi. Optimal acquisition and aggregation of offshore wind power by multiterminal voltage-source hvdc. *IEEE Transactions on Power Delivery*, 18(1):201–206, Jan 2003.

[30] Hongbo Jiang and A. Ekstrom. Multiterminal hvdc systems in urban areas of large cities. *IEEE Transactions on Power Delivery*, 13(4):1278–1284, Oct 1998.

[31] T. M. Gruzs and J. Hall. Ac, dc or hybrid power solutions for today's telecommunications facilities. *International Telecommunications Energy Conference*, pages 361–368, September 2000.

[32] J. G. Ciezki and R. W. Ashton. Selection and stability issues associated with a navy shipboard dc zonal electric distribution system. *IEEE Transactions on Power Delivery*, 15(2):665–669, April 2000.

[33] Walter L. Weeks. *Transmission and Distribution of Electrical Energy*. Harper and Row, 1981.

[34] P. Meckler and W. Ho. Does an electronic circuit breaker need electrical contacts? *IEEE Holm Conference on Electrical Contacts*, pages 480–487, 2004 September.

[35] I. Takahashi and G. J. Su. A 500 hz power system - applications. *IEEE Industry Applications Society Annual Meeting*, 1:996–1002, 1989.

[36] J. A. Ferreira and H. W. van der Broeck. Alternative power distribution in residential and commercial buildings. *Fifth European Conference on Power Electronics and Applications*, 7:188–193, 1993.

[37] Prabha Kundur. *Power System Stability and Control*. McGraw-Hill, 1993.

[38] G. Andersen, C. Klumpner, S. Kjaer, and F. Blaabjerg. A new green power inverter for fuel cells. *Power Electronic Specialists Conference*, 2:727–733, June 2002.

[39] P. Krein, R. Balog, and X. Geng. High-frequency link inverter for fuel cells based on multiple-carrier pwm. *IEEE Transaction on Power Electronics*, 19(5):1279–1288, September 2004.

[40] G.R. Walker and P.C. Sernia. Cascaded dc-dc converter connection of photovoltaic modules. *IEEE Transactions on Power Electronics*, 19:1130–1139, July 2004.

[41] R. Teodorescu and F. Blaabjerg. Flexible control of small wind turbines with grid failure detection operating in stand-alone and grid-connected mode. *IEEE Transactions on Power Electronics*, 19(5):1323–1332, September 2004.

[42] Z. Chen and E. Spooner. Voltage source inverters for high-power, variable-voltage dc power sources. *IEE Proceedings Generation, Transmission and Distribution*, 148:439–447, Sept 2001.

[43] E. Acha, V. G. Agelidis, O. Anaya-Lara, and T. J. E. Miller. *Power Electronic Control in Electrical Systems*. Newnes, 2002.

[44] B. Fardanesh. Future trends in power system control. *IEEE Computer Applications in Power*, 15:24–31, July 2002.

[45] S. Luo, Z. Ye, R. L. Lin, and F. C. Lee. A classification and evaluation of paralleling methods for power supply modules. *Power Electronics Specialists Conference*, 2:901–908, 1999.

[46] Weizhong Tang and R. H. Lasseter. An lvdc industrial power distribution system without central control unit. *Power Electronics Specialists Conference*, 2:979–984, June 2000.

[47] P. Karlsson and J. Svensson. Dc bus voltage control for a distributed power system. *IEEE Transactions on Power Electronics*, 18:1405–1412, November, 2003.

[48] A. Tuladhar, H. Jin, T. Unger, and K. Mauch. Parallel operation of single phase inverter modules with no control interconnections. *Applied Power Electronics Conference and Exposition*, 1:94–100, Feb 1997.

[49] Zhihong Ye, Dushan Boroyevich, Kun Xing, and Fred. C. Lee. Design of parallel sources in dc distributed power systems by using gain scheduling technique. *Power Electronics Specialists Conference*, 1:161–165, July 1999.

[50] R. Sebastian, M. Castro, E.; Sancristobal, F. Yeves, J. Peire, and J. Quesada. Approaching hybrid wind-diesel systems and controller area network. *IECON*, 3:2300–2305, Nov 2002.

[51] E. Nogaret, G. Stavrakakis, G. Kariniotakis, M. Papadopoulos, N. Hatziargyriou, A. Androutsos, S. Papathanassiou, J.A. Pecas Lopes, J. Halliday, G. Dutton, J. Gatopoulos, and V. Karagounis. An advanced control system for the optimal operation and management of medium size power systems with a large penetration from renewable power sources. *Renewable Energy*, pages 137–149, October 1997.

[52] K. Agbossou, M. Kolhe, J. Hamelin, and T. Bose. Performance of a stand-alone renewable energy system based on energy storage as hydrogen. *IEEE Transactions on Energy Conversion*, 19(3):633–640, September 2004.

[53] J. E. Newbury and K. J. Morris. Power line carrier systems for industrial control applications. *IEEE Transactions on Power Delivery*, 14(4):1191–1196, October 1999.

[54] G. Schickhuber and O. McCarthy. Control using power lines. *IEE Computing and Control Engineering Journal*, 8(4):180–184, August 1997.

[55] Lloyd Dixon. Average current mode control of switching power supplies. In *Unitrode Application Note*, pages 3.356–3.369. Unitrode Corp. Merrimack, 1990.

[56] A. Emadi and M. Ehsani. Dynamics and control of multi-converter dc power electronic systems. *Power Electronics Specialists Conference*, 1:248–253, June 2001.

[57] G. S. Thandi, R. Zhang, K. Xing, F. C. Lee, and D. Boroyevich. Modeling, control and stability analysis of a pebb based dc dps. *IEEE Transactions on Power Delivery*, 14(2):497–505, April, 1999.

[58] Keith Billings. *Switchmode Power Supply Handbook*. McGraw-Hill, 2 edition, 1999.

[59] A. Sannino, G Postiglione, and M. Bollen. Feasibility of a dc network for commercial facilities. *IEEE Transactions on Industry Applications*, 39(5):1499–1507, September 2003.

[60] G. D. Gregory. Applying low-voltage circuit breakers in direct current systems. *IEEE Transactions on Industry Applications*, 31(4):650–657, July 1995.

[61] C. B. Henze, N. Mohan, C. P. Henze, and R. Button. A programmable solid-state active current limiting circuit breaker for space applications. *IEEE Annual Conference of the Industrial Electronics Society*, 4:2849–2854, November 2002.

[62] Z. Xu, Zhang B, S. Sirisukprasert, X. Zhou, and A. Q. Huang. The emitter turn-off thyristor-based dc circuit breaker. *IEEE Power Engineering Society Winter Meeting*, pages 288–293, 2002.

[63] L. Lorenz. New power semiconductor components for future innovative high frequency power converters. *IEEE International Conference on Industrial Technology*, 2:1173–1177, December 2003.

[64] J. Kim, J. You, and B. H. Cho. Modeling, control, and design of input-series output-parallel-connected converter for high-speed-train power system. *IEEE Transactions on Industrial Electronics*, 48(3):536–544, June 2001.

[65] Jeong il Kang, Chung-Wook Roh, Gun-Woo Moon, and Myung-Joong Youn;. Phase-shifted parallel-input/series-output dual converter for high-power step-up applications. *IEEE Transactions on Industrial Electronics*, 49(3):649–652, June 2002.

[66] R. D. Middlebrook. Input filter consideration in design and application of switching regulators. *Proc. IEEE Industrial Applications Society Annual Meeting*, 1976.

[67] C. M. Wildrick, F. C. Lee, B. H. Cho, and B. Choi. A method of defining the load impedance specification for a stable distributed power system. *IEEE Transactions on Power Electronics*, 10(3):280–285, May 1995.

[68] Xiaogang Feng, Jinjun Liu, and F. C. Lee. Impedance specifications for stable dc distributed power systems. *IEEE Transactions on Power Electronics*, 17(2):157–162, March, 2002.

[69] Kun Xing, Jinghong Guo, Wenkang Huang, Dengming Peng, Fred C. Lee, and Dusan Borojevic. An active bus conditioner for a distributed power system. *Power Electronics Specialists Conference*, 2:895–900, June 1999.

[70] Xiaogang Feng, Zhihong Ye, Kun Xing, F. C. Lee, and D. Borojevic. Impedance specification and impedance improvement for dc distributed power system. *Power Electronics Specialists Conference*, 2:889–894, June 1999.

[71] B. Choi, B. H. Choi, and S. Hong. Dynamics and control of dc-to-dc converters driving other converters downstream. *IEEE Transactions on Circuits and Systems*, 46(10):1240–1248, October 1999.

[72] L. Solero, A. Lidozzi, and J. A. Pomilio. Design of multiple-input power converter for hybrid vehicles. *IEEE Transactions on Power Electronics*, 20(5):1007–1016, September 2005.

Appendix A

DESIGN OF STORAGE CHARGER

The simplified model of the storage charger is shown in Figure A.1. The main difference between this model and that presented in Section 7.3.1 is that the control transfer function is v_i/i_{ref} rather than v_o/i_{ref}. Consequently, the dynamics of the source interface and transmission line are included in the model since these impact the input voltage.

The open loop transfer function is given by:

$$\frac{v_i}{i_{ref}} = \frac{kDn(-smL + (1 - mR))}{s^2mLC + s(mRC - C) + m} \tag{A.1}$$

where

- D is the steady state duty cycle of the converter at the operating point
- n is the turns ratio of the transformer
- k is the gain of the current loop
- m is the slope of the constant power characteristic of the source interface converter

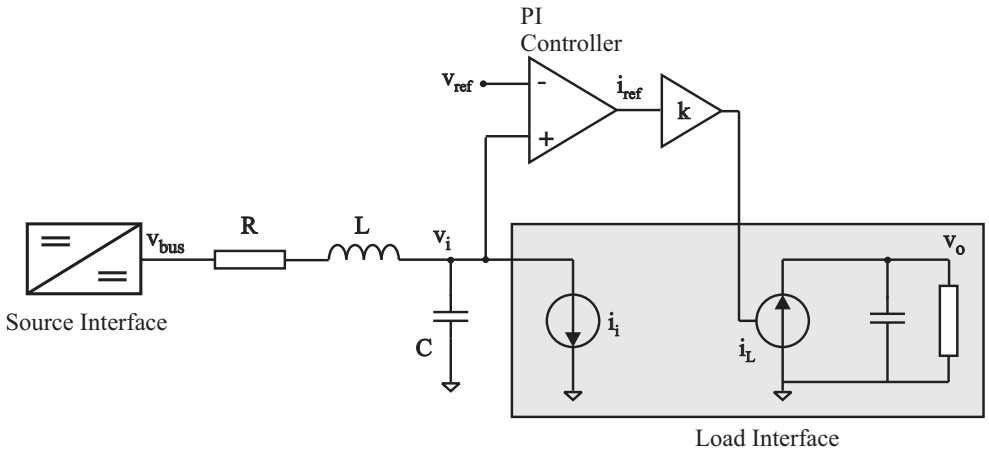

Figure A.1 Simplified model of storage charger

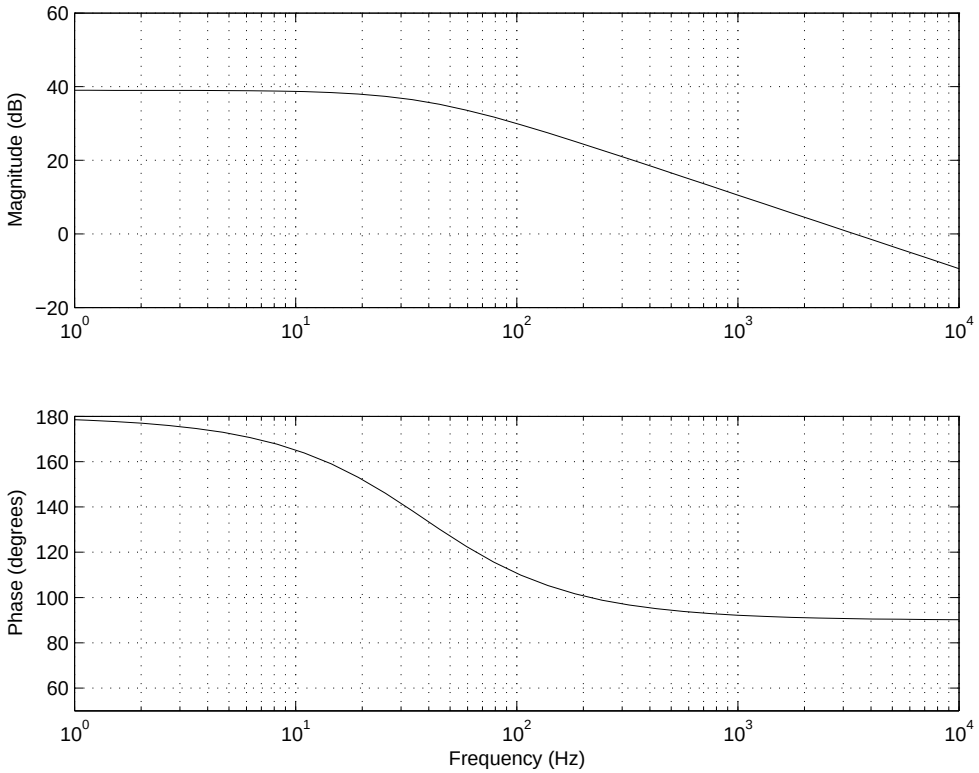

Figure A.2 Open loop bode plot of voltage loop

The corresponding bode plot of the system is portrayed in Figure A.2. The parameters used to obtain the bode plot were: R = 0.01 Ω, L = 100 μH, C = 100 μF, m = -0.0238, D = 0.9, n = 4/17, and k = 10. It can be seen that under open loop operation, the system is potentially unstable. At low frequencies, the phase approaches 180° while the open loop gain is greater than 1.

A PI controller is sufficient to control the system in a stable fashion as it introduces 90° of phase lag at low frequencies. The PI controller is designed such that crossover frequency of the closed loop system is approximately 300 Hz, and the loop gain at dc is 40 dB. Based on these parameters, the proportional and integral gains were calculated to be 0.01 and 6.28 respectively.

Appendix B

PAPER ACCEPTED FOR PUBLICATION IN IEEE TRANSACTIONS ON INDUSTRIAL ELECTRONICS JOURNAL